2009

Characterization And Aqueous Colloidal Processing Of Tungsten Nano-powders

Zhengtao Yang
University of Central Florida

CHARACTERIZATION AND AQUEOUS COLLOIDAL PROCESSING OF TUNGSTEN NANO-POWDERS

by

ZHENGTAO YANG

B.S. Southwest Jiaotong University, 1995
M.S. University of North Texas, 2005

A thesis submitted in partial fulfillment of the requirements
for the degree of Master of Science
in the Department of Mechanical, Materials and Aerospace Engineering
in the College of Engineering and Computer Science
at the University of Central Florida
Orlando, Florida

Summer Term

2009

ABSTRACT

Extensive attention has been paid to consolidate nanoparticles into nanocrystalline components that possess better properties than their coarse-grained counterparts. Nanocrystalline monolithic tungsten (W) has been envisaged to possess better properties than coarse-grained tungsten and to improve the performance of many military components. Commercially available nano-W powders were characterized via X-ray diffraction (XRD), scanning electron microscopy (SEM), transmission electron microscopy (TEM), X-ray photoelectron spectroscopy (XPS), Auger electron spectroscopy (AES) and Brunauer, Emmett, and Teller (BET) measurement. While the bulk of nano-W powders consisted of bcc-W as confirmed by XRD and TEM, much of their surface consisted of WO_3 with traces of WO_2 and WC. Despite the irregular morphology and agglomerates greater than 1 μm in size, the diameter of individual nano-W powders ranged from 30 to 100 nm with a surface area of 10.4 m^2/g. To obtain green bodies of higher densities and more homogeneous microstructures after consolidation, W nanopowders were de-agglomerated in water and slip cast in plaster molds. De-agglomeration in water was conducted by repeated ultrasonication, washing, centrifuge and pH adjustment. The change in particle size and morphology was examined via SEM. After the initial surface oxide was removed by repeated washing, the reactivity of W nanoparticles to water was somewhat inhibited. Increasing the number of cycles for ultrasonication and washing increased the pH, the degree of de-agglomeration and the stability of W suspension. The zeta potential was more negative with increasing pH and most negative at pH values close to 5.

Viscosity also decreased with increasing pH and reached a minimum at a pH 5.

To obtain the highest solid loading with the lowest viscosity, the pH value of W suspension was adjusted to 5 using aqueous tetramethylammonium hydroxide solutions. The relative density of the slip cast increased with longer ultrasonic time, increasing slurry pH up to 5, and consequent increase in solids loading. Smaller particles were separated from larger ones by ultrasonication, washing with water and centrifugation. At a 27.8 vol.% solids loading, the size-separated fine W slurry was slip cast into pellets with relative green densities up to 41.3 % and approximate particle sizes of 100 nm. W powders were also ultrasonicated in aqueous poly (ethyleneimine) (PEI) solutions with various concentrations. SEM examinations of particle sizes showed that 1 wt.% PEI led to the optimum dispersion and ultrasonication for longer time with a low power resulted in better dispersion. 0.5 g of W powders were ultrasonicated in 10 ml aqueous poly (allylamine hydrochloride) (PAH) solutions with molar concentrations ranging from 0.01 to 0.05 M. W suspensions with 0.03 M and 0.04 M PAH after two washing cycles showed improved dispersion. Cold isostatic pressing can further increase the green density following slip casting. Sintered slip casts made from de-agglomerated nanoparticle W showed a lower density, more uniform microstructure, smaller grains and smaller pores than the sintered dry pressed pellets.

ACKNOWLEDGMENTS

I would like to thank Dr. Yongho Sohn, Dr. Weifeng Fei, Dr. Lei Zhai, and Dr. Hyunju Choi for advising me in this project so that I can complete my master's work. I would like to thank Dr. Helge Heinrich for being a committee member and giving me valuable comments on my thesis. I would also like to thank Mr. Kyu Cho and Mr. Eric Klier from Army Research Laboratory for providing necessary financial support and valuable technical collaboration. I would like to thank Dr. Jing Liu and Mr. Biao Yuan for their contribution of TEM work to my thesis and this research project.

TABLE OF CONTENTS

LIST OF FIGURES

LIST OF TABLES

LIST OF ACRONYMS/ABBREVIATIONS

BF	Bright Field
DBTT	Ductile-to-brittle Transition Temperature
KE	Kinetic Energy
PAH	Poly (allylamine hydrochloride)
PEI	Polyethyleneimine
SAD	Selected Area Diffraction
SEM	Scanning Electron Microscopy
TEM	Transmission Electron Microscopy
TMAH	Tetramethylammonium dydroxide
XPS	X-ray Photoelectron Spectroscopy
XRD	X-ray Diffraction
W	Tungsten
WHAs	Tungsten Heavy Alloys (WHAs)

1. INTRODUCTION

Tungsten (W) and W alloys have been widely used for a variety of applications due to their high melting points, high densities, hardness, and elastic modulus. In particular, W-based materials have been used for Kinetic Energy (KE) Penetrator materials applications [1-2] and can replace depleted uranium (DU) KE penetrators. Cho *et* al. [3] realized that monolithic W has higher density, therefore would perform better than tungsten heavy alloys (WHAs). Nanoscale W powders are expected to improve strength, hardness and wear resistance according to Hall-Petch effect (hardness is proportional to the inverse square root of grain size) if they could be consolidated to fully dense products while maintaining their nanoscale sizes. However, processing of nanoscale W powders is challenging. Nanoscale powders tend to agglomerate and agglomeration generally decreases the densities of green bodies. Such agglomeration is correlated with increasing attraction between particles with decreasing particle size due to van der Waals interaction. Packing density decreases with decreasing particle size because smaller particles have a larger surface area, higher surface energy and greater friction between particles than coarse ones. Green density depends on the applied compaction pressure, particle size, and size distribution of the powders. The green density increases with increasing compacting pressure. The green density is low when the particle size is fine and increases with increasing average particle size of the powders. Smaller particles resist compression and result

in a low green density and green strength. Ultra-high compaction pressures for adequate green strength are predicted for fine particles [4]. It is difficult to consolidate nanopowders with a low apparent density and agglomeration. Agglomerated powders contain inter-agglomerate pores, which are much larger than intra-agglomerate ones. The removal of these pores requires higher temperatures and longer sintering time, leading to significant grain growth. Mayo *et* al. [5] observed higher sintering temperatures for larger agglomerates consisting of nanometer TiO_2 powders and demonstrated agglomerate size instead of individual particle size, controlled sintering behavior. They also found the non-agglomerated powders with the largest particle size sintered at the lowest temperature.

In order to overcome the problematic agglomeration and low green density, colloidal processing is a preferred approach for nanoparticles. A colloidal system consists of two distinct phases: a continuous phase (the dispersion medium) and a fine dispersed particulate phase (the dispersed phase). In a colloid, the dispersed phase is made of tiny particles or droplets that are distributed evenly throughout the continuous phase. The size of the dispersed phase particles are between 1 nm and 1000 nm in at least one dimension. Colloidal processing is widely used for forming ceramics. In ceramic processing, a colloid suspension consists of a dispersion of solid particles in a liquid and is being used increasingly in the consolidation of ceramic powders to produce the green body. Colloidal processing of ceramics has been widely investigated because it produces green bodies with higher densities and more homogeneous microstructures. Compared to powder consolidation by dry or semidry pressing in a die, the colloidal approach

can produce more homogeneous particle packing of the green body and lead to better control of microstructure during sintering. The colloidal approach prepares stable suspensions with repulsive forces between particles. The stability of colloid suspensions is very important to the packing homogeneity of the consolidated body. A stable colloid suspension can be consolidated into a densely packed structure whereas an unstable suspension may result in a loosely packed body. Attractive van der Waals forces exist between the particles. If the attractive force is large, the particles will stick together, leading to rapid sedimentation of particle clusters, namely, flocculation or coagulation. Introducing repulsive forces between the particles can be used to prevent flocculation. Repulsion between electrostatic charges (electrostatic stabilization), between adsorbed polymer molecules (steric stabilization) and the combination of the two (electrosteric stabilization) are the main mechanisms for colloid stabilization. Electrostatic stabilization is based on the mutual repulsion of like electrical charges. An electrical double layer of charge is produced around every particle and the repulsion occurs due to the interaction of the double layers. Polymers are commonly used as dispersing agents for fine particles. Adsorption of polymers can induce repulsive interparticle forces that prevent particles from aggregating. The steric repulsion has its origin in the positive free energy of mixing when two adsorbed polymer layers interpenetrate. Polymers with chargeable functional groups, called polyelectrolytes, can induce an electrostatic repulsion between charged surfaces. Hence, their stabilizing mechanism is a combination of electrostatic and steric repulsion, commonly called electrosteric stabilization.

There are several processes by which particles dispersed in a liquid can acquire a surface charge: (1) preferential adsorption of ions, (2) dissociation of surface groups, (3) adsorption of charged polymers (polyelectrolytes). Preferential adsorption of ions from solutions is the most common process for oxide particles in water and the adsorption of polyelectrolytes is the main charging mechanism in electrosteric stabilization. In the process of preferential adsorption of ions from solution, an electrolyte such as a metal salt, an acid or a base is added to the aqueous solution. Ions are preferentially adsorbed to the surface of the dispersed particles, resulting in charges on the particle surface. Most oxide surfaces are hydrated with MOH groups on the surface for an oxide of a metal M. In acidic solutions, adsorption of H^+ ions leads to a positively charged surface while in basic solutions, adsorptions of OH^- ions produce a negatively charged surface. Therefore, oxide surfaces are positively charged at low pH and negatively charged at high pH. At a pH, the adsorption of H^+ and OH^- ions will balance and the particle surface will be neutral. The pH at which the particle surface has zero net charge is the point of zero charge (PZC).

Slip casting is a widely-used forming process in which particles in a suspension are consolidated by a filtration process and complicated shapes can be obtained. In slip casting, a suspension is poured into a permeable "Plaster of Paris" mold commonly made from gypsum. The microporous mold provides a capillary pressure, on the order of 0.1 to 0.2 MPa, which draws the liquid (the filtrate) from the suspension into the mold [6]. A consolidated layer of solids, referred to as a cast, form on the wall of the mold. After a sufficient thickness of the cast

has formed, the surplus slip is poured out, and the cast along with the mold is allowed to dry. To achieve a high green density, the suspension pH must be well controlled. An inappropriate pH will result in particle flocculation, which leads to a high viscosity of the slip. The slip must have a relatively low viscosity to flow well into the cavities of the mold. Intuitively, the higher the solids loading, the more viscous the slip will be. However, a high solids loading is essential to obtain a dense part. A balance must be achieved to meet these contrary requirements [7].

Colloidal processing is less widely used for metal powders than for ceramic powders. One reason is the high reactivity of metal particles with water. Although green compacts for W, molybdenum (Mo), and other powders are made by slip casting, the process is used to a limited extent for metals and not suited to high production rates. For metal powders it is assumed that deflocculation is caused by the oxide layer on these powders which behaves as a ceramic oxide towards the liquid vehicle. Dobrovol'skii *et* al. [8] prepared molybdenum (Mo) slurries by mixing milled micron-sized powders with water and slip cast dense Mo blanks. The density of casts from the Mo slurries was high and could be obtained by compacting Mo powders in steel dies at optimum compaction pressures. Hernández *et* al. [9] dispersed concentrated nickel powders in water with an acrylic-based polyelectrolyte and tetramethylammonium dydroxide (TMAH) at alkaline pH. They optimized the suspensions by rheological measurements as a function of pH and solids volume fraction, slip cast the optimized suspensions, and obtained relative green densities higher than 50%. The good stability and homogeneous packing led to a reduced sintering temperature and dense products.

Nanoscale tungsten powders undergo rapid grain growth during sintering. Ultra-fine W powder can be sintered to 94% theoretical density at 1550°C for 30 min [10]. Grain growth inhibitors such as Y_2O_3 dispersoids resulted in smaller tungsten grain size at the same sintering time and reduced grain growth during sintering [11]. Based on the processing model by Randall *et* al. [12], high compaction pressures, low sintering temperature and short sintering time are required to obtain dense products with small grain sizes.

Ultrasonication of powder suspensions is an effective dispersion technique and has been extensively used to disperse ceramic powders, especially sub-micrometer-sized powders [13-14]. Ultrasonic dispersion was utilized to prepare concentrated and well-dispersed TiO_2 nanoparticle suspensions [15]. Turbulent flow and shock waves produced by acoustic cavitation were found to cause interparticle collisions of metal powders in hydrocarbon liquids at roughly half the speed of sound and generate localized high temperatures at the impact points [16]. The agglomerates can be eroded and split by the collisions.

So far, de-agglomeration and slip casting of W nanopowders through aqueous colloid processing has not been reported in the literature. The aim of this study is to investigate the de-agglomeration of W nanopowders and slip casting of the W slurries. De-agglomeration was carried out by repeated ultrasonication in water, washing with water, centrifugation and pH adjustment. Water was chosen as the dispersing medium and has the advantage to be

environmentally benign. The zeta potential and viscosity were measured as a function of W suspension pH and the optimum pH was determined. The optimum pH was adjusted before slip casting to increase the solids loading and green density. W nanopowders were also ultrasonicated in aqueous poly (ethyleneimine) (PEI) and poly (allylamine hydrochloride) (PAH) solutions to study the effects of PEI and PAH concentrations on the dispersion of W powders. In addition, W nanopowders were ultrasonicated in (oleic acid and ethanol) and (fish oil and ethanol) to determine the optimum concentration of oleic acid and fish oil for dispersion of W powders. The microstructures of sintered slip cast and dry-pressed compacts were examined.

2. LITERATURE REVIEW

2.1 W-Based Materials as Kinetic Energy (KE) Penetrator

KE penetrators are long rods fired from smooth bore, large caliber guns in tanks. Muzzle velocities as high as 2000 m/s are achieved, and rolled homogeneous armor thicknesses exceeding 1 m can be pierced. Excellent penetration performance and high density is required for THAs to be employed as penetrators. The denser the penetrator material, the higher the energy can be delivered to the impacted area. The penetration performance is usually evaluated by the diameter of the tunnel formed upon penetration through the armor plate. It is often deteriorated due to the increasing diameter of the penetration tunnel resulting from the mushrooming effect caused by the heavy plastic deformation at the penetrator head. The past generation of kinetic energy penetrators was made of depleted uranium, which has the desired density (ρ=19.05) and ductility, but it posed serious environmental problems due to the heavy dust production after penetration. It is pyrophoric and highly toxic after impact. The high density, high strength, and high melting point make tungsten an attractive candidate material for KE penetrators. Tungsten is cheaper than uranium.

Depleted uranium alloys were reported to have the improved penetration performance owing to the ‘self-sharpening' effect, which causes easy fracture at edges of the penetrator head

and reduced the diameter of the penetration tunnel during penetration. A new generation of kinetic energy penetrators utilized tungsten alloys that have an equally high density. One requirement of using tungsten or tungsten heavy alloys (WHA) to make high-density KE anti-armor penetrators is that the materials show self-sharpening behavior. To meet this requirement, plastic flow should be localized so that cracks form at desired strain levels only in heavily deformed shear bands to discard pieces of the material along the penetration path. Magness and Farrand [17] explained this self-sharpening effect in terms of the forming frequency of adiabatic shear bands. The adiabatic shear bands are formed during dynamic deformation at a high strain rate and heat generated by the localized shear plastic deformation is hardly emitted outside due to short time, causing an abrupt temperature rise in the localized deformation region. This local temperature rise and the accelerated plastic instability are the major factors for the band formation, leading to rapid deterioration of load carrying capacity. If adiabatic shear bands are produced with control only at the penetrator head and cracks are readily propagated along them, the fall-off of the edge of the penetrator head occurs easily. This can effectively reduce the diameter of the penetration tunnel and result in improved penetration performance.

W is resistant to adiabatic shear banding due to its strong rate sensitivity and high ductile-to-brittle transition temperature (DBTT), which leads to cracking at many sites before the accumulation of the plastic dissipation required to trigger plastic instabilities. W is a Group VIa body centered cubic (bcc) refractory metal with a melting temperature of 3410±20°C. W is

intrinsically brittle because the dislocation nucleation at crack tips is very difficult in comparison to cleavage at very low temperatures. The yield stress of W is strongly temperature-dependent and the flow stress is rate dependent. Polycrystalline W is generally brittle at room temperature. The DBTT for polycrystalline tungsten is a function of grain size, impurity concentration, and tensile strain rate. Orientation of the grain structure of pure polycrystalline W is important because most KE penetrators made of WHAS are either extruded or swaged into their final shape, resulting in a grain structure that is elongated in the direction of the penetrator axis. It was shown that the behavior of the pure W component dominated the performance of the WHAs at high strain rates. The mechanical properties of the KE penetrators at high strain rates are very important and investigated by many researchers. Dümmer *et* al. [18] investigated the effect of strain rate on plastic flow and failure in polycrystalline tungsten. They tested polycrystalline tungsten at quasi-static (3×10^{-3}) and dynamic (10^{3}–4×10^{3}/s) strain rates and evaluated three deformation mechanisms: slip, twinning, and intergranular cracking. They found low-strain-rate deformation caused limited damage at strains of 0.25 and high-strain-rate deformation led to catastrophic failure at strains between 0.05 and 0.10. As the strain rate was increased from 10^{-3} to 10^{3}/s, ductile-to-brittle transition occurred.

Lennon and Ramesh [19] investigated the thermomechanical response of pure polycrystalline tungsten over a wide range of strain rates and temperatures. They tested an equiaxed recrystallized microstructure and a heavily deformed extruded microstructure that was loaded in compression along the extrusion axis. They conducted low strain rate (10^{-3}–10^{0} s^{-1})

and high strain rate (10^3–$10^4 s^{-1}$) compression experiments. They observed substantial plastic deformations of recrystallized W under compression at room temperature and the flow stress was rate-dependent. Intergranular microcracks were developed during the compressive deformations. Under quasi-static loadings, several large axial splitting cracks were found and many small, uniformly distributed microcracks were developed under dynamic loadings. They observed increasing nucleation rate of microcracks with increasing strain rate and large plastic deformations of extruded tungsten under compression, with a flow stress that increased with deformation rate. The strain hardening of the extruded W was lower than that of the recrystallized material, and was insensitive to the strain rate. The strain hardening at high-temperatures at low and high strain rates was found to be insensitive to the temperature and the flow stress showed strong temperature-dependence at low homologous temperatures.

2.1.1 Tungsten Heavy Alloys as KE Penetrators

Tungsten heavy alloys (THAs) are used in long-rod penetrators. Penetration of high-speed, high-aspect-ratio projectiles can usually be divided into two categories: axial and transverse. Axial penetration refers to the usual case, in which the stress at the projectile/target interface is mainly parallel to the projectile axis. Transverse penetration refers to the case in which the stress is mainly transverse to the projectile axis. Transverse penetration most commonly occurs when a projectile strikes a target element with an angle of attack. This case includes the scenario in which the target itself has a velocity that is not parallel to the penetrator velocity. Transverse penetration is very common during the defeat of modern armors. In axial

penetration, the dominant deformation mode in the penetrator is plastic flow. However, in transverse penetration the dominant structural response is penetrator fracture.

THAs are dual-phase composites produced by liquid phase sintering of mixed W as the major constituent and a small amount of transition metals such as Ni, Fe powders as the binder phase. They typically consist of relatively isolated W grains contained in a continuous matrix of a solid-solution alloy, such as WFeNi or WCoNi. Modern penetrator alloys are 90–95 mass% W, with Ni and either Fe or Co in a 7:3 mass% ratio. These alloys are most commonly processed by liquid-phase sintering, producing W grains with average diameters from 20 to 50 μm, largely influenced by sintering time and temperature. They have a high density of 16-18.5 g/cm^3, high strength, moderate ductility and good thermal conductivity. The penetration power increases with increasing density and slenderness ratio of the penetrators. The slenderness ratio is controlled by the strength and ductility of the materials used for penetrators. The penetration performance is usually evaluated by the diameter of the tunnel formed upon penetration through the armor plate. It is often deteriorated because of the increased diameter of the penetration tunnel resulting from the mushrooming effect due to the heavy plastic deformation at the penetrator head. The penetration performance is improved when adiabatic shear bands are easily formed. The adiabatic shear band is formed by the abrupt concentration of heat generated from dynamic deformation, i.e. under the adiabatic condition without any heat transfer. Upon high-speed impact of a WHA penetrator, a number of adiabatic shear bands can be formed, along which cracks propagate. This causes easy fall-off of the edge

of the penetrator head and then the reduction of the diameter of penetration tunnel, thereby improving the penetration performance.

Understanding the dynamic deformation behavior and the mechanism of adiabatic shear banding of the THAs were essential for alloy design, fabrication process, and microstructural modification to improve the dynamic properties and the penetration performance. Kim *et* al. [20] investigated the microstructures of adiabatic shear bands formed by high-speed impact in a tungsten heavy alloy penetrator. They observed heavily elongated tungsten particles and reaction products such as tungsten oxides on the surface region of the debris due to the local temperature rise during high-speed impact. They found some adiabatic shear bands near the surface cracks of the remaining penetrator. Their microstructural observation of the shear bands suggested the minimization of the tungsten–tungsten particle interfaces and the optimization of the fabricating process to improve the penetration performance of the THAs.

Studies on the adiabatic shear band formation upon high-speed impact of WHAs were essential to improve the penetration performance, but there were difficulties in analyzing the process of shear strain of hundreds and thousands percent concentrated along an extremely shallow area in an extremely short span of tens of μs. Accordingly, different testing methods simulating the actual process of high-speed impact and of the evaluation techniques in association with the impact were investigated. Kim *et* al. [21] investigated dynamic and quasi-static torsional deformation behavior of a 93W–4.9Ni–2.1Fe WHA and conducted

torsional tests on WHA specimens fabricated through sintering, heat-treatment, swaging, and aging processes using a torsional Kolsky bar under dynamic loadings.

Their dynamic torsional test results showed that the shear stress increased, while the shear strain decreased, with the maximum shear stress rising in the order of the as-sintered, the as-heat-treated, the as-swaged and the as-aged specimens. The as-swaged and the as-aged specimens showed a higher possibility of the adiabatic shear band formation. Bless *et* al. [22] investigated dynamic fracture of tungsten heavy alloys using 1-D strain fracture and transverse impact. They concluded that meso-scale failure in tungsten alloys was little affected by strain rate but changed with stress state, and that grain cleavage was the main failure mechanism for transverse fracture. They observed grain fracture occurring early in the damage process and substantial matrix failure as the fracture developed. Grain strength was considered as an important property for penetrator alloys.

It was reported that adiabatic shear deformation and mechanical properties of WHAs could also be enhanced by refinement of the microstructures of WHAs. Many researchers have investigated refined microstructures of WHAs through several techniques including alloying refractory elements such as Mo and Re [23] and mechanical alloying (MA) [24].The MA process is an advanced fabrication process that can produce ultra-fine and homogeneous alloy powders. Ho J. Ryu *et* al. **[**25**]** fabricated 93W–5.6Ni–1.4Fe tungsten heavy alloys by mechanically alloying W, Ni and Fe powders in a tumbler ball mill and obtained a

nanocrystalline size of 16 nm and fine lamellar spacings of 0.2 μm in mechanically alloyed powders. They consolidated mechanically alloyed powders into green compacts and solid-state sintered them at 1300°C for 1 h in a hydrogen atmosphere. Their sintered alloys had fine W particles of 3 μm in diameter and a relative density above 99 %. Their sintered WHAs exhibited a high yield strength of about 1100 MPa due to a fine microstructure, but showed reduced elongation and impact energy because of a large area fraction of brittle W/W interfaces and low matrix volume fraction.

Oxide dispersion strengthened (ODS) THAs have been considered as promising candidates for advanced KE penetrator due to their characteristic fracture mode compared to conventional THAs. Lee *et* al. [26] mechanically alloyed 94W–4.56Ni–1.14Fe–0.3Y_2O_3 powders and solid-state sintered them at 1300–1450°C for 1 h in hydrogen atmosphere and liquid phase sintered them at temperatures of 1465–1485°C for 0–60 min. The ODS THAs had a relative density above 97% with contiguous W grains after primary solid-state sintering. The two-stage sintered ODS THAs showed finer microstructure and higher mechanical properties than conventional liquid phase sintered counterparts.

2.1.2 Nano-W as KE Penetrators

Conventional coarse-grained W (CG-W) exhibits poor ductility and high DBTT. The DBTT increases with increasing strain rate, leading to fracture with little or no macroscopic plastic deformation below DBTT. At room temperature, CG-W behaves like a ceramic and

exhibits a strong tension-compression asymmetry and tensile failure with out any ductility. Its ultimate tensile stress is only half of the compression flow stress and show a failure mode typical of most brittle ceramics (intergranular fracture), which is caused by its high susceptibility to soluble interstitial impurities. The impurities segregate along the grain boundaries (GBs) that are the weak links during mechanical straining. Some experimental observations showed that severe plastic deformation (SPD) in the form of equal-channel angular pressing (ECAP) or ECAP followed by low temperature rolling reduced the grain size to ultrafine grain (UFG) level [27-28]. SPD is a technique that starts with a coarse-grained material and the grain size is reduced to UFG or NC regime with increasing plastic deformation. Wei *et* al. [29] refined commercial bulk W to ultrafine structure via SPD and first observed shear localization in the UFG-W under uniaxial dynamic compressive loading. Their SPD processed UFG-W exhibited enhanced strength and ductility and reduced strain hardening and strain rate hardening. Conventional polycrystalline W exhibited only uniform plastic deformation without shear localization under the same test conditions. Wei *et* al. [30] also investigated the quasi-static and dynamic mechanical failure of UFG W under uniaxial compression. They refined the starting material of large grain size to ultrafine microstructure with grains sizes of 500 nm via SPD. Their UFG W during quasi-static compression showed vanishing strain hardening with its flow stress of 2 GPa, twice that of conventional coarse grain W. The quasi-statically loaded samples showed no evidence of cracking in contrast to conventional W exhibiting axial cracking. Under uniaxial dynamic compression, UFG W showed significant flow softening and a peak stress of 3 GPa. The strain rate sensitivity of the

UFG W was reduced to half the value of the conventional W. They observed shear localization and cracking of the UFG W under dynamic uniaxial compression, which was a desirable deformation mode for KE penetrators. Wei *et* al. [31] obtained fully dense nanocrystalline tungsten by high-pressure torsion (HPT) at 500°C and the strengths under quasi-static compression and dynamic compression were 3.0 GPa and 4 GPa, respectively. They found that grain boundaries were mostly of the large-angle type with high energy and well defined. The authors observed edge dislocations within the grains and hypothesized that edge dislocations and depleted impurity concentrations along pre-existing GBs contributed to enhance the ductility of nc-W. The specimens under dynamic compression showed localized shearing followed by cracking and subsequent failure, similar to their UFG counterparts processed by equal-channel angular pressing plus cold rolling. The shear band width in the HPT-processed NC-W was found to be less than 5 μm, which was much smaller than that observed in the UFG counterparts.

UFG or nanocrystalline (NC) structures can be achieved through several processing techniques, including severe plastic deformation (SPD) [32] and powder metallurgy.

2.2 Processing of Nano-Powders

2.2.1 Green Density of Nano-Powders

The agglomeration of nano-powders generally decreases the density of green bodies

pressed from those powders and can be correlated with increasing attraction between particles with decreasing particle size due to van der Waals interaction. Different densities can be obtained depending upon the strength and morphology of the agglomerates. Particles of soft agglomerates attracted by weak van der waals interaction can slide into voids of the green body during compaction. Hard agglomerates have much stronger bonding between particles and have necking between adjacent particles. Large shear forces are needed for neck cleavage before the sliding of these particles can occur. Ferkel *et* al. [33] investigated the effect of nanopowder de-agglomeration on the densities of nanocrystalline ceramic green bodies and their sintering behavior. They cracked some strong agglomerates by short ball-milling and reduced the amount of necks between particles. The green densities of ball milled alumina and yttria-stabilized zirconia were increased by up to 15% compared to corresponding unmodified powders, which was attributed to the sliding of nanoparticles and smaller strong agglomerates into voids during compaction. They also found ball-milled powders exhibited increased sintering activity.

2.2.2 Sintering of Nano-Powders

The driving force during sintering is the decrease in free energy that accompanies the reduction of interfacial area. In sintering, the growth of the contact area between the particles takes place by the transport of materials across the contact interface or around pores under conditions of sintering temperature, time and atmosphere. Interparticle contact area depends on particle size and shape, particle size distribution, and compacting pressure. When particles are

loosely packed, there are few points of contact. The number and total area of contacts is increased with decreasing particle size. Kothari [34] experimentally studied the initial sintering kinetics of W powders with an average particle size of 3 μm in the temperature range of 1100 ^{o}C to 1500 ^{o}C. His results supported the theory that sintering of W powder in the temperature range of 1100 ^{o}C to 1500 ^{o}C was controlled by grain boundary diffusion. He [35] also experimentally investigated the effects of a range of particle sizes on the sintering kinetics of tungsten powder. His results indicated that grain boundary diffusion was the dominant mechanism for material transport during the sintering of W powder of particle sizes <4um and surface diffusion was the mechanism of material transport of W compacts with particle sizes of 14-16 μm. He determined the activation energies of 101 kcal/mole for fine particles (< 4 μm) and 72 kcal/mole for coarse particles (14-16 μm). Dense bulk W with UFG or NC microstructure is very difficult to achieve because it has a very high melting point and is susceptible to interstitial impurities. Jain *et* al. [36] obtained nanocrystalline tungsten powders containing HfO_2 and Y_2O_3 as dopants using a solution synthesis technique. Each oxide significantly reduced the particle and crystallite sizes of the as-synthesized tungsten powders and grain size from 2 um to 0.5 μm.

2.2.3 Colloid Processing

Colloidal processing is widely used for forming ceramics. Colloid processing of ceramics has received increasing attention and been widely investigated because it produces

green bodies with higher densities and more homogeneous microstructures. The colloidal approach prepares stable suspensions with repulsive forces between particles. Laarz *et* al [37] dispersed WC-Co powders in aqueous media with polyethylenimine and found that the mixing of powder, water, and PEI above 0.3 wt.% was sufficient to obtain well-dispersed, low-viscous 20 vol.% WC–Co suspensions without the need for pH adjustment. Their suspensions showed a long-term stability with little changes of steady shear properties over 36 hours. They attributed the mainly electrostatically driven adsorption of the cationic PEI onto the negatively charged WC particles to the stabilization of the WC–Co suspensions. PEI has been used as a dispersant in other systems such as SiC and TiO_2 in aqueous media. Zhang *et* al. [38] used PEI as a dispersant for tape casting of SiC powders in aqueous media and their zeta potential study showed that SiC particle surface was negatively charged without PEI and the adsorptions of PEI increased the zeta potential and isoelectric point. Their adsorption isotherms were described as high-affinity type and SiC slurries of 50 vol.% were stable with thixotropical behavior. Tang *et* al. [39] studied the dispersion of an aqueous suspension of nano-sized TiO_2 particles stabilized with PEI and showed that PEI was an effective surfactant to disperse naon-sized TiO_2 suspensions. They obtained well-dispersed suspensions by modifying the surface charges of the TiO_2 particles and observed a high adsorption affinity of PEI at high pH values and a low adsorption affinity at low pH values.

3. EXPERIMENTAL PROCEDURE

3.1 Characterization of the As-Received Nano-W Powders

Commercially available W nanopowders, supplied by U.S. Army Research Laboratory were manufactured by a wet chemistry method followed by hydrogen reduction. These powders were used in this work and characterized. The as-received W powders were placed on a carbon tape and examined using a scanning electron microscope (SEM) JEOL 6400F under an acceleration voltage of 10 KeV. Ultrasonication has been extensively used to disperse powders since it can be especially effective for submicrometer powders [40]. 20 g of W powders were dispersed in 10 ml water using an ultrasonic cell disruptor with a tip size of 1/16 inch (Misonix XL2000) under a power of 10 watts for 30 minutes to break down some agglomerates. 30 ml of water was then added, and the suspension was ultrasonicated for two min. The suspension was centrifuged at 8000 rpm for 20 min and the supernatant liquid was removed, then 10 ml of water was added and ultrasonicated at 10 watts for 30 minutes. The suspension was again centrifuged at 8000 rpm for 25 minutes, and the supernatant liquid was removed. Finally, 10 ml of water was added, and ultrasonicated at 10 watts for 3 minutes. One drop of the suspension was taken right after ultrasonication for SEM examination.

For transmission electron microscopy (TEM), 0.01 g of the as-received W powders was ultrasonicated in 1 ml of ethyl alcohol using an ultrasonic cell disruptor (Misonix XL2000) under a power of 5 watts for 5 minutes. One drop of the suspension was put on a copper grid right after ultrasonication and examined using a TECNAI F30 TEM under an acceleration voltage of 300 KeV. The as-received W powders were also characterized by X-ray diffraction (XRD) using Rigaku D/Max XRD. A 40 KeV Copper x-ray tube was used with Datascan 4 acquisition software. The scan rate employed was 1.2 degree/min, with 2-theta range of 30 to 90 degrees.

The as-received W powders were characterized using PHI 600 auger electron spectroscopy (AES), with accelerating voltage of 3 KeV, to examine the surface chemistry. W powders were placed on aluminum foil, and loaded into the chamber at high vacuum. X-ray photoelectron spectroscopy (XPS) (Physical Electronics 5400 ESCA) was also employed to examine the surface oxidation state of nano-W powders. The as-received W powders were put on aluminum foil. The specimen was loaded into the chamber that was pumped down to a high vacuum. Mg K_α (1253.6 ev) X-rays were used to irradiate the W powders.

3.2 Dispersion of Nano-W Powders

3.2.1 Measurement of Zeta Potential as a Function of pH

The zeta potential is a measure of the stability of colloidal suspensions. Suspensions at

pH values close to the isoelectric point (IEP) may flocculate rapidly because the repulsion may not be sufficient to overcome the van der Waals attraction. Far away from the IEP, the rate of flocculation should be slower.

The electrokinetic properties of aqueous W suspensions were determined using a PALS Zeta Potential Analyzer (Brookhaven Instruments). Electrokinetic measurements were carried out on dilute W suspensions. 0.01 g of the as-received W powder was ultrasonicated in 10 ml of water (0.1wt. %). The suspension pH was adjusted by adding HCl or NaOH solutions and the suspension was ultrasonicated before each measurement. The electrophoretic measurements were conducted right after the sample preparation to minimize the effect of oxidation and dissolution. The Smoluchowski equation was used to calculate the zeta-potential.

3.2.2 Measurement of Viscosity as a Function of pH

The following procedure was used to measure the viscosity as a function of pH.

1. 100 g of W powders were dispersed in 20 ml water under an ultrasonic power of 20 watts for 15 minutes. 30 ml water was added and mixed with tungsten suspension. They were centrifuged at 8500 rpm for 15 minutes. The supernatant was very blue because tungsten oxide on the surface dissolved in water and removed.
2. Repeated step 1 four times and the supernatant was still blue.
3. Repeated step 1 four times and the supernatant was less blue each time.
4. The pH of the supernatant increased after each wash and reached 3.03 after the 10th wash

and 3.08 after the 11th wash. The W slurry became more and more stable after each wash due to increasing zeta potential and electrostatic repulsion between particles.

5. 6.5 ml water and 0.5 ml 20 wt.% tetramethylammonium hydroxide pentahydrate (TMAH) (Alfa Aesar, MA, USA) water solution were added to the centrifuged tungsten and ultrasonicated. The molecular formula of TMAH is $(CH_3)_4NOH{\cdot}5H_2O$.

A viscometer of model RVDV Pro-II (Brookfield, MA, US) was used to measure the viscosities of a 20 vol.% W suspension at various pH values. The pH value was increased by addition of 20 wt.% aqueous TMAH solution. As a strong organic base, TMAH does not show the side effects caused by other inorganic bases, such as possible contamination of NaOH, or low stability of NH_4OH (evaporation of NH_3). TMAH was also successfully used as a dispersant for aqueous SiC suspensions [41]. A spindle was immersed in the W suspension and rotated at different speeds, namely, 5,10,20,50 and 100 rpm at an adjusted pH value and the viscosities at all rotational speeds were recorded.

3.2.3 Measurement of pH as a Function of Ultrasonic Time and W Concentration

The effect of ultrasonic time and W concentration on the suspension pH was investigated. 0.5, 2 and 5 g of W powders were ultrasonicated in 10ml water under a power of 17 watts and the corresponding solid loadings by volume were 0.26 %, 1.03 % and 2.53 %, respectively. The pH value was measured every 10 minutes.

In order to demonstrate that dispersion became worse after longer ultrasonic time, 10 g of W powders were dispersed in 10 ml water under an ultrasonic power of 5 watts for 10 minutes and corresponding solid loading was 4.94 vol.%. The pH values after ultrasonic time of 5 and 10 minutes were 2.32 and 2.17, respectively. One drop of the suspension was taken 5 and 10 minutes after ultrasonication for SEM examination. The suspension was washed with 40 ml water, centrifuged and the supernatant liquid was removed. The washed tungsten was dispersed in 10 ml water under an ultrasonic power of 5 watts for 5 minutes and the suspension pH was 2.43. One drop of the suspension was taken 5 minutes after ultrasonication for SEM examination.

3.2.4 De-agglomeration by Ultrasonication, Dilution with Water and Centrifugation

The as-received W powders have a blue tungsten oxide layer on the surface. It may be formed by oxidation in air and has a loose structure. It dissolves fast in water and produces H^+ and rapidly decreases the suspension pH. After repeated ultrasonication and washing with water, the blue tungsten oxide can be removed, leading to slower dissolution of W and increase in pH. The following experiments were performed to support the above points. 4 g of the as-received W powders and 4 g of repeatedly water-washed W powders were ultrasonicated in two separate tubes containing 1.9 ml of water under a power of 10 watts. The solids loading was 10 vol.%. The pH values were measured after ultrasonication for 1,10, 20 and 30 minutes.

3.2.4.1 De-agglomeration of 20 g of 10.4 vol.% W Suspension

20 g of W powders were dispersed in 10 ml water under an ultrasonic power of 10 watts for 30 minutes and the corresponding solid loading was 10.4 vol.%. One drop of the suspension was taken from the lower portion right after ultrasonication for SEM examination. 30 ml of water was added to the suspension. It was ultrasonicated for 2 minutes and the pH was 2.4. The suspension was centrifuged at 8000 rpm for 20 minutes and the supernatant liquid was removed. 10 ml of water was added to the centrifuged W and ultrasonicated at 10 watts for 30 minutes. It was washed with 30 ml of water for the 2nd time and the suspension pH was 3.77 without ultrasonication. After ultrasonication at 10 watts for 20 seconds, the pH dropped to 3.4. The suspension was centrifuges at 8200 rpm for 25 minutes and the supernatant liquid was removed. The centrifuged W was ultrasonicated at 10 watts in 10 ml of water for 3 minutes and the pH was 2.49. One drop of the suspension was taken from the lower portion right after ultrasonication for SEM examination.

3.2.4.2 De-agglomeration of Large Particles of 10 g of W

Large and small particles coexist in W powders and larger particles settle down faster than smaller ones. This experiment was focused on increasing suspension pH and reducing the sizes of some soft agglomerates by repeated ultrasonication and washing with water. The experimental procedure is as follows:

1. 10 g of W were dispersed in 10 ml water under an ultrasonic power of 10 watts for 10 minutes and the pH was 1.95. One drop of the suspension was taken from the lower portion

right after ultrasonication for SEM examination.

2. The suspension was washed with 40 ml of water for the 1st time, centrifuged at 8000 rpm for 20 minutes and the supernatant liquid was removed. The centrifuged W was ultrasonicated at 10 watts in 10 ml of water for 6 minutes and the pH was 2.42. The solid loading was 4.94 vol.%. One drop of the washed suspension was taken from the lower portion right after ultrasonication for SEM examination. After 3.5 hours, 5.8 g of W settled down and the upper W suspension was transferred into a glass vial. The settled W powders had larger particle sizes than the upper ones and were ultrasonicated at 10 watts for 10 minutes. It was washed with 40ml water for the 2nd time and centrifuged at 8000 rpm for 20 minutes. The supernatant liquid was removed and tungsten was ultrasonicated at 10 watts for 6 minutes in 10 ml water. The pH values after ultrasonication of 4 and 6 minutes were 2.66 and 2.56, respectively.
3. After 16 hours, 5.6 g of W settled down and the upper W suspension was transferred into a tube. The lower portion of 5.6 g of W was ultrasonicated at 10 watts for 10 minutes and washed with 40 ml of water for the 3rd time. The suspension was centrifuged at 8000 rpm for 20 minutes and the supernatant liquid was removed. The centrifuged W was ultrasonicated in 10 ml of water at 10 watts for 6 minutes. The pH values after ultrasonication of 4 and 6 minutes were 3.13 and 2.99, respectively. It was washed with 40 ml of water for the 4th time and centrifuged at 8000 rpm for 20 minutes. The supernatant liquid was removed and the centrifuged W was ultrasonicated in 10 ml of water at 5 watts for 30 minutes.

3.2.4.3 De-agglomeration of 20 g of W with Water 10 times

Twenty g of the as-received W powders were mixed with 10 ml of water in a centrifuge tube and the solid loading was 9.4 vol.%. The suspension liquid level was marked. The pH of the suspension was measured right after ultrasonication. Then 40 ml water was added to the suspension and centrifuged for 15 minutes. The upper supernatant was removed and water was added to the previously marked position to ensure the solids loading remained the same. After 10 cycles of ultrasonication and washing, the 9.4 vol.% slurry was ultrasonicated for 2 minutes. The pH of the suspension was about 3. A drop of the suspension was cast on a plastic film. After drying, the pellet was examined by SEM on both sides.

3.2.5 Slip Casting of W Slurry

In slip casting, a slurry is poured into a permeable mold commonly made from gypsum. The microporous mold provides a capillary suction pressure, on the order of 0.1 to 0.2 MPa, which draws the liquid (the filtrate) from the slurry into the mold. A consolidated layer of solids, referred to as a cast, form on the walls of the mold. After a sufficient thickness of the cast has formed, the surplus slip is poured out and the mold and the cast are allowed to dry. Normally, the cast shrinks away from the mold during drying and can be easily removed. USG Pottery Plaster was purchased from United States Gypsum Company, and used for molds. 55 parts water was weighed in a glass beaker. 100 parts powder was sprinkled into water slowly and

evenly and mixed thoroughly for 2 minutes. Then suspension was poured into a cylindrical container. When it was partially dried, a steel cylinder 0.5 inch in diameter was inserted into the center of plaster. After the plaster was dried, the cylinder was pulled out. The plaster was dried in air for at least 2 days before it was used for slip casting.

3.2.5.1 Slip Casting of 6 Batches of 20 g of W Slurries

Six batches of 20 g of W powders were ultrasonicated in water and slip cast into pellets. The processing details for batch 1 are as follows:

1. 20 g of W powders were ultrasonicated in 20 ml water using a power of 25 watts for 10 minutes. 30 ml water was added into the slurry. It was centrifuged at 8500 rpm for 15 minutes. The supernatant was blue and removed. Step 1 was repeated once.
2. 0.5 ml water and 0.8 ml 9.1wt.% aqueous TMAH solution were added to the centrifuged tungsten. They were ultrasonicated using 4 watts for 2 minutes, but the viscosity was too high for slip casting. 10 ml water was added and they were ultrasonicated using 20 watts for 15 minutes and washed for the 3rd time followed by centrifugation.
3. 10 ml water was added and the mixture was ultrasonicated using 12 watts for 2 hours and was washed for the 4th time. 10 ml water was added and they were ultrasonicated using 20 watts for 30 minutes and washed for the fifth time. 1 ml of 33 wt.% aqueous TMAH solution was added and ultrasonicated using 4 watts for 2 minutes. The viscosity was too high for slip casting because the pH of the slurry was 9.6, which was too high.
4. They were washed for the 6th and 7th times and the pH of the supernatant was reduced to

4.8. 0.5 ml water was added and they were ultrasonicated using 4 watts for 3 minutes. The viscosity was low and two cylindrical specimens were cast easily. The first one was cast without vacuum.

Batch 2 was processed as follows:

1. 20.986 g of W powders were ultrasonicated in 20 ml water using a power of 25 watts for 10 minutes. 30 ml water was added into the slurry. It was centrifuged at 8500 rpm for 15 minutes. The supernatant was very blue and removed.
2. Repeat step 1.
3. 0.5 ml water and 0.7 ml 11 wt.% aqueous TMAH solution were added to the centrifuged tungsten. They were ultrasonicated using 5 watts for 4 minutes. The slurry could flow. 10 ml water was added and they were ultrasonicated using 18 watts for 15 minutes and washed with 30 ml water for the 3rd time. They were centrifuged at 8500 rpm for 13 minutes and the supernatant liquid was dark blue and had a pH 2.97. 10 ml water was added and ultrasonicated using 10 watts for 80 minutes. They were washed with 30 ml water for the 4th time. They were centrifuged at 8500 rpm for 13 minutes and the color of supernatant liquid was much lighter than that of the previous one and had a pH 3.08.
4. 10 ml water was added and ultrasonicated using 20 watts for 15 minutes. They were washed for the 5th time. The supernatant liquid was slightly blue and had a pH 3.05. 1ml of 33 wt.% TMAH water solution and 1ml of water were added and they were ultrasonicated using 4 watts for 3 minutes. After 1 day, 10 ml water was added and they were ultrasonicated using

5 watts for 30 seconds and the slurry had a pH 5.54.

5. They were washed with 30 ml of water for the 6th time and centrifuged at 8500 rpm for 10 minutes. The supernatant liquid was slightly blue and had a pH 5.18. 1.18 g of water and 0.3 g of 11 wt.% TMAH water solution were gradually added and they were ultrasonicated using 4 watts for 3 minutes. Then they were shaken by hands to aid mixing. The viscosity was gradually reduced with the addition of water and TMAH.

The 3rd batch was processed as follows:

1. 20.68 g of W powders were ultrasonicated in 20 ml water using a power of 25 watts for 10 minutes. 30 ml water was added into the slurry. It was centrifuged at 8500 rpm for 15 minutes. The supernatant was very blue and removed.
2. Step 1 was repeated once. 10 ml water and 0.7 ml of 11wt.% TMAH water solution were added to the centrifuged tungsten. They were ultrasonicated using 18 watts for 15 minutes and had a pH 2.28 and washed with 30 ml water for the 3rd time. They were centrifuged at 8500 rpm for 15 minutes and the supernatant liquid was dark blue. 10 ml water was added and they were ultrasonicated using 10 watts for 60 minutes and washed with 30 ml water for the 4th time. They were centrifuged at 8500 rpm for 10 minutes. 10 ml water was added and they were ultrasonicated using 20 watts for 15 minutes and washed for the fifth time. The supernatant liquid was slightly blue. 1ml of 33 wt.% TMAH water solution and 1 ml of water were added. They were ultrasonicated using 4 watts for 3 minutes. After 3 hours, 10 ml water was added and they were ultrasonicated using 5 watts for 30 seconds and the

slurry had a pH 5.06. They were washed with 30 ml of water for the 6th time and centrifuged at 8500 rpm for 15 minutes. The supernatant liquid was white. 0.9 g of water was added and ultrasonicated using 4 watts for 3 minutes. Then they were shaken by hands to aid mixing.

The 4th batch was processed as follows:

1. 20 g of W powders were ultrasonicated in 20 ml water using a power of 25 watts for 14 minutes. 30 ml water was added into the slurry. It was centrifuged at 8500 rpm for 10 minutes. The supernatant was very blue and removed.
2. Step 1 was repeated once. 10 ml of water and 0.7 g of 11 wt.% TMAH water solution were added to the centrifuged tungsten. They were ultrasonicated using 18 watts for 20 minutes and washed with 30 ml water for the 3rd time. They were centrifuged at 8500 rpm for 15 minutes. 10 ml water was added and they were ultrasonicated using 10 watts for 80 minutes and washed with 30 ml water for the fourth time. They were centrifuged at 8500 rpm for 15 minutes. 10 ml water was added and they were ultrasonicated using 20 watts for 15 minutes and washed for the 5th time. The supernatant liquid was slightly blue. 1ml of 33 wt% TMAH water solution and 10ml of water were added. They were ultrasonicated using 20 watts for 30 minutes and 15 watts for 2.25 hours. The pH of the slurry was 4.76.
3. They were washed with 40 ml of water for the 6th time and centrifuged at 8500 rpm for 15 minutes. The supernatant liquid was very blue and removed. 10 grams of water and 0.3 g of 33 wt.% TMAH water solution were added and ultrasonicated using 15 watts for 7 minutes.

They were washed with 40 ml of water for the 7th time and centrifuged at 8500 rpm for 11 minutes. The supernatant liquid was slightly black and had a pH 6.31. 0.8 g of water was added and ultrasonicated using 4 watts for 3 minutes. The slurry was viscous and had a pH of 3.98. 10 g water and 0.4 g 33wt% TMAH water solution were added and ultrasonicated using 10 watts for 10 minutes. They were washed with 40 ml of water for the 8th time and centrifuged at 8500 rpm for 11 minutes. The supernatant liquid was white and had a pH of 6.72. 0.8ml water was added and sonicated using 4 watts for 3 minutes. The slurry had a pH of 6.32. 20 g of water was added and ultrasonicated using 10 watts for 1 minute. They were washed with 40 ml of water for the 9th time and centrifuged at 8500 rpm for 11 minutes. 0.6 g of water was added and sonicated using 4 watts for 2 minutes. they were shaken by hands to aid mixing.

The 5th batch was processed as follows:

1. 20 g of W powders were ultrasonicated in 20 ml water using a power of 25 watts for 17 minutes. 30 ml of water was added into the slurry. It was centrifuged at 8500 rpm for 14 minutes. The supernatant was very blue and removed. 10 ml water and 1 g of 33 wt% TMAH water solution were added to the centrifuged tungsten. They were ultrasonicated using 18 watts for 165 minutes and washed with 30 ml water for the 2nd time. They were centrifuged at 8500 rpm for 15 minutes. 10 ml of water and 1 g of 33 wt.% TMAH water solution were added to the centrifuged W. They were ultrasonicated using 20 watts for 70 minutes and the slurry pH was 7.01. They were washed with 30 ml water for the 3rd time

and centrifuged at 8500 rpm for 15 minutes. The supernatant was very blue and removed. 15 ml water was added and ultrasonicated using 14 watts for 12 minutes. They were centrifuged at 8500 rpm for 32 minutes. The supernatant was slightly black and had a pH 4.48.

2. 15 ml of water and 1 g of 33 wt.% (TMAH) water solution were added to the centrifuged tungsten. They were ultrasonicated using 15 watts for 54 minutes and the slurry pH was 11.54. They were washed with 30 ml water for the 4th time and centrifuged at 8500 rpm for 20 minutes. The supernatant was slightly yellow and removed. 15 ml water was added and they were ultrasonicated using 16 watts for 17 minutes and washed for the 5th time. Then they were centrifuged at 8500 rpm for 20 minutes and the supernatant liquid had a pH of 6.19. 10ml of water were added. They were ultrasonicated using 15 watts for 9 minutes. They were washed for the 6th time and centrifuged at 8500 rpm for 16 minutes and the supernatant liquid had a pH of 5.11. 10 g of water and 0.15 g of 33 wt.% TMAH water solution were added and ultrasonicated using 10 watts for 10 minutes. They were washed with 40 ml of water for the 7th time and centrifuged at 8500 rpm for 20 minutes. The supernatant liquid had a pH 6.19. 0.3 g of water was added and ultrasonicated using 4 watts for 1 minute. The slurry was viscous and had a pH of 4.2. 0.25 g of 11 wt.% and 0.05 g of 33 wt.% TMAH water solution were added and shaken by hands to aid mixing.

For the 6th batch of W powders, 20.25 g of W powders were ultrasonicated in 20 ml water using a power of 15 watts for 15 minutes. 30 ml of water was added into the slurry. It was

centrifuged at 8500 rpm for 15 minutes. The blue supernatant was removed. 1 g of 33 wt.% TMAH and 10 ml water were added and ultrasonicated using 12 watts for 90 minutes. It was washed with 30 ml water for the 2nd time and centrifuged at 8500 rpm for 20 minutes. The very blue supernatant liquid had a pH of 4.31 and removed. 0.5 g of 33 wt.% TMAH and 10 ml were added and ultrasonicated using 12 watts for 30 minutes. The slurry pH was 6.31. It was washed with 30 ml water for the 3rd time and centrifuged at 8500 rpm for 20 minutes. The supernatant was still very blue and removed. 0.7 ml of water was added and stirred using a magnetic stirrer for 1 hour.

3.2.5.2 Slip Casting of 2 Batches of 50 g of W Slurries

The 1st batch of 50 g of W slurry was processed as follows:

1. 50 g of W powders were ultrasonicated in 15 ml water and 0.5 ml of 33 wt.% TMAH water solution using a power of 30 watts for 1 minute. The slurry was very viscous due to a low pH of 1.66. 2 ml of 33 wt.% TMAH water solution was added and they were ultrasonicated using a power of 20 watts for 16 minutes. The pH was increased to 4.19 and led to a much lower viscosity. The pH was reduced to 3.14 after ultrasonication under a power of 20 watts for 20 minutes.
2. 1 ml of 33 wt.% TMAH water solution was added and they were ultrasonicated for 40 minutes under a power of 20 watts and the pH was 3.45. 1 ml of 33 wt.% TMAH water solution was added and they were ultrasonicated for 2.5 hours under a power of 20 watts and the slurry pH was 4.88. 30 ml of water was added and they were centrifuged at 8500

rpm for 25 minutes. The supernatant was very blue and removed.

3. They were dispersed in 20 ml water using an ultrasonic power of 20 watts for 15 minutes and washed with 30 ml water for the second time. They were centrifuged and the supernatant was still very blue and removed. They were dispersed in 20 ml water using an ultrasonic power of 20 watts for 30 minutes and washed with 30 ml water for the third time. They were centrifuged and the supernatant removed.1 ml of 33 wt.% TMAH water solution was added and they were ultrasonicated for 3 minutes under a power of 5 watts. The slurry was viscous because of the high pH of 7.28.
4. They were dispersed in 20 ml water using an ultrasonic power of 20 watts for 15 minutes and washed with 30 ml water for the fourth time. They were centrifuged and the supernatant removed. 10 ml water and 1 ml of 33 wt.% TMAH water solution was added and they were ultrasonicated for 50 minutes under a power of 12 watts. The slurry pH was 7.15 and was reduced to 7.01 after ultrasonication for 20 minutes under a power of 12 watts. 0.25 ml of 33 wt.% TMAH water solution was added and they were ultrasonicated for 15 minutes under a power of 20 watts and the slurry pH was 6.66.
5. They were dispersed in 20 ml water using an ultrasonic power of 20 watts for 15 minutes and washed with 30 ml water for the 5th time. They were centrifuged and the supernatant removed. Repeated this step three times, namely, the 6th, 7th and 8th washing.
6. 2 ml of water and 0.01 ml of 33 wt.% TMAH water solution was added and they were ultrasonicated for 5 minutes under a power of 5 watts. The solid loading is 25 vol.% and the slurry pH was 5.06. One cylindrical specimen was obtained by slip casting. The slurry pH

was adjusted to 5.16 and another specimen was obtained by slip casting and its dry weight was 2.78 grams.

7. They were dispersed in 20 ml water using an ultrasonic power of 20 watts for 15 minutes and washed with 30 ml water for the 9th time. They were centrifuged and the supernatant removed. Repeated this step once, namely, the 10th washing. The pH was adjusted to 6.36 and another specimen was obtained by slip casting.

The 2nd batch was processed as follows:

1. 50 grams of W powders were ultrasonicated in 20 ml water using a power of 20 watts for 17 minutes. 30 ml water was added into the slurry. It was centrifuged at 8500 rpm for 14 minutes. The supernatant was very blue and removed. 10 ml water and 1 gram of 33 wt.% TMAH water solution were added to the centrifuged tungsten. They were ultrasonicated using 16 watts for 162 minutes and washed with 30 ml water for the 2nd time. They were centrifuged at 8500 rpm for 25 minutes. The supernatant was very blue and removed. 15 ml of water and 1 gram of 33 wt.% TMAH water solution were added to the centrifuged tungsten. They were ultrasonicated using 16 watts for 100 minutes. They were washed with 30 ml water for the 3rd time and centrifuged at 8500 rpm for 16 minutes. The supernatant was still very blue and had a pH of 6.16.
2. 15 ml water and 1 gram of 33 wt.% TMAH water solution were added to the centrifuged W. They were ultrasonicated using 15 watts for 2.5 hours. They were washed with 30 ml water for the 4th time and centrifuged at 8500 rpm for 16 minutes. The supernatant was still very

blue and had a pH of 6.51. 15 ml water was added to the centrifuged tungsten and ultrasonicated using 15 watts for 3 hours. They were washed with 30 ml water for the 5th time and centrifuged at 8500 rpm for 15 minutes. The supernatant was still very blue and had a pH of 5.55.

3. 15 ml water and 0.15 g of 33 wt.% TMAH water solution were added to the centrifuged W and ultrasonicated using 15 watts for 100 minutes. They were washed with 30 ml of water for the 6th time and centrifuged at 8500 rpm for 13 minutes. The supernatant liquid was slightly black and had a pH of 6. 15 ml of water was added to the centrifuged tungsten and sonicated using a power of 13 watts for 1 hour. 0.2 gram of 33wt.% TMAH was added and sonicated using 15watts for 73 minutes. They were washed with 30 ml water for the 7th time and centrifuged at 8500 rpm for 20 minutes. The supernatant was blue and had a pH of 5.79. 0.2 gram of 33% TMAH and 15 ml water were added and sonicated using 15 watts for 4 hours. They were washed with 30 ml water for the 8th time and centrifuged at 8500 rpm for 20 minutes. The upper supernatant liquid was slightly yellow and lower supernatant liquid consisting of very fine tungsten particles was black and had a pH of 5.35.
4. 0.2 gram of 33wt.% TMAH and 15 ml water were added and sonicated using 15 watts for 3.5 hours and the slurry had a pH of 4.34. 0.3 gram of 33 wt.% TMAH was added to the slurry and sonicated for 30 minutes. They were washed with 30 ml water for the 9th time and centrifuged at 8500 rpm for 25 minutes. The supernatant liquid was blue and had a pH of 5.89 and removed. 15 ml of water and 0.15 gram of 33 wt.% TMAH were added to the centrifuged tungsten and sonicated using 15watts for 5 min and the pH of the slurry was 6.52.

It was washed with 30 ml water for the 10th time and centrifuged at 8500 rpm for 20 minutes. The upper supernatant liquid was slightly yellow and lower supernatant liquid consisting of very fine tungsten particles was black and had a pH of 6.26. 1.5 grams of water was added to the centrifuged tungsten and sonicated for 2 minutes using 4 watts. The slurry was shaken by hands to aid mixing. 9 pellets were slip cast.

5. The remaining tungsten was ultrasonicated using 15 watts for 10 minutes and washed for the 11th time. It was centrifuged at 8500 rpm for 17 minutes and the supernatant liquid was slightly blue and had a pH of 3.48. 0.15 gram of 33 wt.% TMAH and 20 grams of water were added and ultrasonicated using 15 watts for 30 minutes. It was washed with 30 ml of water and centrifuged at 8500 rpm for 15 minutes. 10 ml of water was added to the centrifuged tungsten and sonicated using 10 watts for 20 minutes. The pH of the slurry was 2.86 and 0.5 gram of 33 wt.% TMAH was added to increase its pH. It was sonicated using 13 watts for 3 minutes and washed with 30 ml water for the 13th time. It was centrifuged at 8500 rpm for 15 minutes and the supernatant liquid was slightly blue and had a pH of 6.66. 1 gram of water was added to the centrifuged tungsten and sonicated using 4 watts for 1 minute. The slurry was stirred for 20 minutes using a magnetic stirrer and became more homogeneous.

3.2.5.3 Slip Casting of 100 Grams of W Slurry

1. 100 grams of W powders were dispersed in 20 ml water under an ultrasonic power of 20 watts for 15 minutes. 30 ml water was added and mixed with W suspension. They were

centrifuged at 8500 rpm for 15 minutes. The supernatant was very blue because tungsten oxide on the surface dissolved in water and removed.

2. Repeated step 1 four times and the supernatant was still blue. Repeated step 1 four times and the supernatant was less blue each time. The pH of the supernatant increased after each wash and reached 3.03 after the 10th wash and 3.08 after the 11th wash. The tungsten slurry became more and more stable after each wash due to increasing zeta potential and electrostatic repulsion between particles.
3. 6.5 ml of water and 0.5 ml of 20 wt.% TMAH water solution were added to the centrifuged W and sonicated. The lower portion of the washed tungsten (~40 g) was washed 3 times and the supernatant liquid changed from blue to white and had a pH of 3.55. 10 g of water and 0.3 g of 33 wt.% TMAH water solution were added and ultrasonicated under a power of 10 watts for 5 minutes. The pH of the slurry was increased to 4.7. They were centrifuged at 6000 rpm for 15 minutes and the supernatant liquid was blue again. 2.05 grams water, 0.7 g of 11 wt.% TMAH and 0.3 g of 33 wt.% TMAH water solution were added and they were shaken by hands to aid mixing. The pH of the slurry was 5.11 and dropped to 4.4 after 16 hours.
4. They were washed for the 17th time and the supernatant was slightly blue. They were washed for the 18th time and the supernatant was slightly black with a pH of 4.57. They were dispersed in 10 ml of water using a power of 8 watts for 10 minutes and washed with 40 ml water for the 19th time. They were centrifuged at 6000 rpm for 13 minutes and the supernatant was slightly blue with a pH of 3.11. They were dispersed in 10 ml water using a

power of 6 watts for 10 minutes and washed with 40 ml water for the 20th time. They were centrifuged at 6000 rpm for 15 minutes and the supernatant was white with a pH of 3.16

5. 1 g of water and 0.25 g of 33 wt.% TMAH were added and then 0.55 g of 11 wt.% TMAH water solution was added to increase the pH. 2 specimens were slip cast at a pH of 4.9. 2 specimens were slip cast at a pH of 4.98. 2 specimens were slip cast at a pH of 5.07. One specimen made at the pH of 4.98 had the highest density.

3.2.5.4 Slip Casting of Size-Separated Fine W Slurry

1. 50 g of W powders were dispersed in 20 ml of water under an ultrasonic power of 15 watts for 10 minutes. It was washed with 30 ml water and centrifuged at 8500 rpm for 5 minutes. The supernatant liquid was black consisting of very small W particles and collected. 20 ml of water was added and ultrasonicated using 15 watts for 10 minutes, washed again with 30 ml of water, centrifuged at 8500 rpm for 5 minutes. 20 ml of water and 0.25 g of 33 wt.% TMAH were added to the solid precipitate and ultrasonicated using 15 watts for 30 minutes. It was washed with water for the 3rd time and centrifuged at 8500 rpm for 4 minutes. The supernatant liquid was black containing fine particles (~ 1 g) and collected.
2. 15 ml of water and 0.25 g of 33 % aqueous TMAH solution were added and ultrasonicated using 15 watts for 18 minutes and centrifuged at 8500 rpm for 5 minutes. The supernatant liquid was removed. 15 ml of water was added and ultrasonicated for 20 minutes using 15 watts and washed with 40 ml water for the 4th time. It was centrifuged at 8500 rpm for 30 minutes. All collected small particles were combined in one tube and ultrasonicated using 15

watts for 20 minutes. It was washed with water for the 5th time and centrifuged at 8500 rpm for 30 minutes. The supernatant liquid was black with a pH of 3.9 and removed. The centrifuged W was dispersed in 15 ml water under an ultrasonic power of 15 watts for 40 minutes and centrifuged at 8500 rpm for 32 minutes. The supernatant liquid was slightly black with a pH of 4.14.

3. 15 ml of water and 0.25 g of 33 wt.% TMAH were added, and ultrasonicated using 15 watts for 160 minutes. It was washed with 40 ml of water for the 6th time and centrifuged at 8500 rpm for 28 minutes. The supernatant liquid was slightly blue and removed. 15 ml of water was added and sonicated using 15 watts for 40 ml. It was washed with 40 ml water for the 7^{th} time and centrifuged at 8500 rpm for 26 minutes. 0.5 g of 33 wt.% TMAH and 15 ml of water were added and sonicated using 13 watts for 220 minutes. It was washed with 40 ml water for the 8th time and centrifuged at 8500 rpm for 30 minutes. The supernatant was blue and removed. 15 ml water was added, sonicated using 13 watts for 20 minutes and washed with 40 ml water for the 9th time. It was centrifuged at 8500 rpm for 28 minutes. 20 ml of water and 0.25 g of 33 wt.% TMAH were added and sonicated using 13 watts for 3 hours. It was washed with 30 ml water for the 10th time.
4. It was centrifuged at 8500 rpm for 30 minutes. The supernatant liquid was slightly black with a pH of 4.91 and removed. 15 ml water and 0.25 g of 33 wt.% TMAH were added and sonicated using 13 watts for 27 minutes. It was washed with 40 ml water for the 11th time and centrifuged at 8500 rpm for 30 minutes. 15 ml of water and 0.15 g of 33 %wt. TMAH were added and sonicated using 13 watts for 4 hours and washed with 40 ml water for the

12th time. It was centrifuged at 8500 rpm for 20 minutes. The supernatant liquid was black and removed. It was sonicated in 20 ml water using 13 watts for 20 minutes and washed with 30 ml water for the 13th time. It was centrifuged at 8500 rpm for 28 minutes. The supernatant was slightly black with a pH of 4.94. 0.2 g of 33 wt.% TMAH and 15 ml water were added and sonicated using 13 watts for 10 minutes. It was washed with 30 ml water for the 14th time and centrifuged at 8500 rpm for 30 minutes. The supernatant had a pH of 5.56 and removed. 0.8 gram of water and 0.15 g of 11 wt.% TMAH were added to the centrifuged W and stirred using a magnetic stirrer for 24 minutes.

3.2.6 Dispersion of W in Aqueous PEI Solutions

The effects of Poly (ethyleneimine) (PEI) concentration and ultrasonic time on the dispersion of W were investigated. 2 grams of W nanopowders were dispersed in 5 ml of 0.7 %, 0.8 %, 0.9 %, 1 % and 2 % PEI (Mw 10000, Polysciences, Inc. PA, USA) water solutions. The added weight of PEI was on a dry weight of W basis (dwb). It was a liquid polymer and soluble in water. It was a highly branched polyamine with high charge density. Polymers contain primary, secondary, and tertiary amine groups in approximately 25/50/25 ratio. Its chemical formula is $(\text{-NHCH}_2\text{CH}_2\text{-})_x[\text{-N(CH}_2\text{CH}_2\text{NH}_2)\text{CH}_2\text{CH}_2\text{-}]_y$.

Two sedimentation testes were performed. In the 1st test, 2 grams of W powders were ultrasonicated in 5 ml of aqueous PEI solutions under a power of 10 watts for 90 minutes. The PEI weight concentrations studied were 1 %, 1.5 %, 2 %, 2.5 % and 3 %. Suspensions were

contained in glass vials with same size, which were immersed in a water bath during ultrasonication. Rapid settling was observed right after ultrasonication for W suspensions with 1.5 %, 2 %, 2.5 % and 3 % PEI. All suspensions were allowed to sit undisturbed for 24 hours until all settling was completed and a picture was taken. In the 2nd sedimentation test, 2 grams of W powder were ultrasonicated in 5 ml of aqueous PEI solutions under a power of 10 watts for 60 minutes. PEI weight concentrations used were 2.8 %, 3 %, 3.2 %, 3.5 %, 3.9 %, 4.2 %, 4.7 % and 5 %. Suspensions were contained in glass vials with same size, which were immersed in a water bath during ultrasonication. All suspensions were allowed to sit undisturbed for 24 hours until all settling was completed and a picture was taken.

To study the effect of ultrasonic time on the pH and dispersion of the W suspension, 4 g of W powders were dispersed in 5 ml of 1 % PEI water solution under an ultrasonic power of 4 watts for 22 hours. The pH values were measured during ultrasonication and a drop of the suspension was taken after 10 and 22 hours for SEM examination.

4 g of W powders were dispersed in 5 ml of 1 % PEI water solution under an ultrasonic power of 6 watts. The measured pH values after 5, 8 and 10 hours were 5.94, 5.88 and 5.86, respectively. After rest for 36 hours, the suspension was ultrasonicated using 10 watts for 2 hours and the pH was 7.07. A drop of the suspension was put in a Teflon film for SEM examination.

Two experiments were performed as listed below. 2 g of W powders were dispersed in 6 ml of 5 % PEI water solution under an ultrasonic power of 29 watts for 10 hours. The suspension was centrifuged and the supernatant liquid was withdrawn. 1 ml of water was added

and ultrasonicated. It was centrifuged and the supernatant liquid was removed. 1ml water was added and ultrasonicated and pH value was 7.6. One drop of the suspension was placed on a teflon film, dried and examined via SEM.

2 g of W powders were dispersed in 6 ml of 5 % PEI water solution under an ultrasonic power of 20 watts for 1.5 hours. The suspension was centrifuged and the supernatant liquid was removed. 1 ml water was added and ultrasonicated. It was centrifuged and the supernatant liquid was withdrawn. 1 ml water was added and ultrasonicated. One drop of the suspension was placed on a teflon film and examined via SEM.

3.2.7 Dispersion of W in Aqueous PAH Solutions

W powders were dispersed in aqueous Poly (allylamine hydrochloride) (PAH) (M_w 15,000) (Sigma-Aldrich Inc., MO, USA) solutions. The molecular formula of PAH is C_3H_8ClN and its structure is shown below:

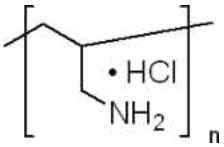

There are following processing variables for dispersing W nanopowders:

- PAH concentration and volume
- Volume percent of W in the suspension
- Ultrasonic power and time

- The number of washing the W suspension with water

In this experiment, 0.5 gram of W nanopowders were dispersed in 10 ml of PAH aqueous solutions with various concentrations to find the optimum PAH concentration. The W suspensions were washed with water once and twice to find the effect of washing on dispersion. 0.5 gram of W nanopowders were dispersed in 10 ml of PAH aqueous solutions under an ultrasonic power of 15 watts for 20 minutes. PAH aqueous solutions with PAH concentration of 0.01, 0.02, 0.03, 0.04 and 0.05 M were used. A drop of the suspension was placed on a silicon substrate and examined via SEM. 15 ml of water was added to the suspension and was centrifuged at 8000 rpm for 20 minutes. The supernatant liquid was removed. 10 ml of water was added and they were ultrasonicated under a power of 15 watts for 10 min and washed with 15 ml of water for the 2^{nd} time. A drop of the suspension was taken for SEM examination. The suspension was centrifuged and the supernatant liquid was removed. 10 ml of water was added and ultrasonicated under a power of 15 watts for 10 min. A drop of the suspension was taken for SEM examination.

3.2.8 Dispersion of W in Oleic Acid and Ethanol

Oleic acid, technical grade (Sigma Aldrich Inc. MO, USA) and ethanol, reagent (Sigma Aldrich Inc. MO, USA) were used for dispersing W nanopowders. The formula of the oleic acid is $CH_3(CH_2)_7CH=CH(CH_2)_7COOH$. 2 grams of W nanopowders were ultrasonicated in 10 ml of

ethanol and oleic acid. The amounts of oleic acid added were 0.005, 0.01, 0.02 and 0.1 gram. Oleic acid and ethanol were first mixed and ultrasonicated for 2 minutes under a power of 4 watts. 2 grams of W powders were added to the solution and ultrasonicated under a power of 10 watts for 30 minutes. Every 10 minutes after sonication, a drop of the suspension was placed onto a silicon substrate for SEM examination.

0.01 gram oleic acid was first mixed with 15 ml ethanol and ultrasonicated. 2 grams of W nanopowders were ultrasonicated in the solution under a power of 15 watts for 30 minutes to study the effect of ultrasonic power on the dispersion of W nanopowders.

0.02 gram of oleic acid was mixed with 20 ml ethanol and ultrasonicated. 4 grams of W powders were added to the solution and ultrasonicated under a power of 18 watts for 30 minutes. The oleic concentration was 0.5 wt.%. Every 10 minutes after sonication, a drop of the suspension was placed onto a silicon substrate for SEM examination. 3 hours after ultrasonication, some W nanopowders settled to the bottom. 0.013 gram of oleic acid was added to the suspension and ultrasonicated under a power of 18 watts for 30 minutes. The oleic concentration was increased to 0.8 %.

0.1 gram of oleic acid was mixed with 10 ml ethanol and ultrasonicated for 1 minute. 2 grams of W nanopowders were added to the solution and ultrasonicated under a power of 10 watts for 25 minutes.

3.2.9 Dispersion of W in Fish Oil and Ethanol

Fish Oil from Menhaden (FO) is one of the most common deflocculants/dispersants and contains more than 20 different types of fatty acids. It is a steric hindrance deflocculant. 0.01 g of Fish Oil from Menhaden (Sigma Aldrich Inc. MO, USA) was mixed with 10 ml of ethanol and then 2 grams of W powders were added into the solution. They were ultrasonicated under a power of 13 watts for 30 minutes.

0.015 g of FO was first thoroughly mixed with 10 ml ethanol and then 2 grams of W nanopowders were added into the mixture. They were ultrasonicated under a power of 10 watts for 30 minutes. A drop of the suspension was taken right after ultrasonication for SEM examination.

0.035 g of FO was mixed with 10 ml of ethanol and then 2 grams of W nanopowders were added into the mixture. They were ultrasonicated under a power of 10 watts for 30 minutes. A drop of the suspension was taken right after ultrasonication for SEM examination.

0.54 g of FO was mixed with 10 ml of ethanol and then 2 grams of W powders were added into the solution. They were ultrasonicated under a power of 10 watts for 30 minutes.

3.3 Sintered W

3.3.1 Sample Preparation

2 grams of the as-received W powders were uniaxially pressed in a die under various loadings into pellets with 0.5 inch in diameter. 3, 5, 7 and 8 metric tons were applied to compress the specimens and the corresponding pressures were 232, 386, 540 and 618 MPa, respectively. Sintering was performed in a hot isostatic press (HIP) furnace (American Hot Isostatic Press Inc., OH, US) under atmospheric pressure.

The 1st slip cast was processed using the following procedure:

1. 10 grams of W powders were dispersed in 10 ml of water under an ultrasonic power of 16 watts for 30 minutes. 45 ml of water was added and centrifuged. The supernatant liquid was removed and 10 ml water was added.
2. The suspension was ultrasonicated under a power of 16 watts for 30 minutes and 45 ml of water was added. The suspension was centrifuged and the supernatant liquid was removed. 10 ml of water was added.
3. Step 2 was repeated once. W was dispersed in 10 ml of water under a power of 10 watts for 5 minutes and 45 ml of water was added. The suspension was centrifuged and the supernatant was removed.
4. Centrifuged W was dispersed in 5 ml of water under a power of 5 watts for 12 minutes. The W slurry was slip cast into pellets in Plaster molds at a 10 vol.% solid loading. After drying, the casts were cold-isostatic pressed (CIP) under a pressure of 350 MPa.

The 2nd slip cast was processed using the following procedure:

1. 10 grams of W powders were dispersed in 10 ml of water under an ultrasonic power of 16 watts for 30 minutes and 45 ml of water was added to the suspension. The suspension was centrifuged and the supernatant liquid was removed. 10 ml of water was added.
2. The suspension was ultrasonicated at 16 watts for 30 minutes. 45 ml of water were added and centrifuged. The supernatant liquid was removed and 10 ml water was added.
3. Step 2 was repeated once. W was dispersed in 15 ml water under a power of 16 watts for 84 minutes. 40 ml water was added to the suspension and it was centrifuged and the supernatant was removed. W was dispersed in 10 ml of water under a power of 10 watts for 3 minutes. 45 ml of water was added and centrifuged. The supernatant liquid was removed and 2 ml water was added. The suspension was ultrasonicated using 5 watts for 12 minutes. The W slurry was slip cast in Plaster molds into pellets at a 20 vol.% solids loading. The casts were cold-isostatic pressed (CIP) under a pressure of 350 MPa.

The densities of sintered samples were measured in distilled water following the Archimedes method. Sintered W specimens were mounted in epoxy and a cross section of each specimen was obtained by using a diamond saw. These cross-sections were ground using an auto-polisher. SiC papers with grit sizes of 60, 120, 240, 400 and 600 were progressively used. They were polished with diamond papers with grit sizes of 3 μm, 1 μm and 0.25 μm using an auto-polisher.

Murakami's reagent (10 g KOH, 10 g $K_3Fe(CN)_6$, 100 g Water) was used for etching polished W specimens to reveal the grain boundaries. 0.5 g of KOH and 5 g of water were first mixed and stirred. 0.5 g of $K_3Fe(CN)_6$ was added into the mixture and stirred. A cotton swab was soaked in the etchant and several quick swipes were made on the specimen until it became cloudy. The specimen was rinsed with running water and cleaned in an alcohol bath in a sonicator. The etched specimens were dried in vacuum before SEM examination.

4. RESULTS

4.1 Characterization of As-received Nano-W Powders

Figure 1(a) shows a scanning electron micrograph obtained with secondary electrons of the as-received tungsten powders. Irregularly shaped agglomerates greater than 1 μm in size were observed. A higher magnification SEM micrograph of the as-received powders, shown in Figure 1(b), reveals nanoscale particles within the agglomerates. Figure 1(c) shows the bulk measurement by energy dispersive spectroscopy (EDS) that confirms the bulk composition of pure tungsten. Ultrasonication, aforementioned, broke up many soft agglomerates and reduced the particle size to 100-300 nm as shown in Figure 1(d).

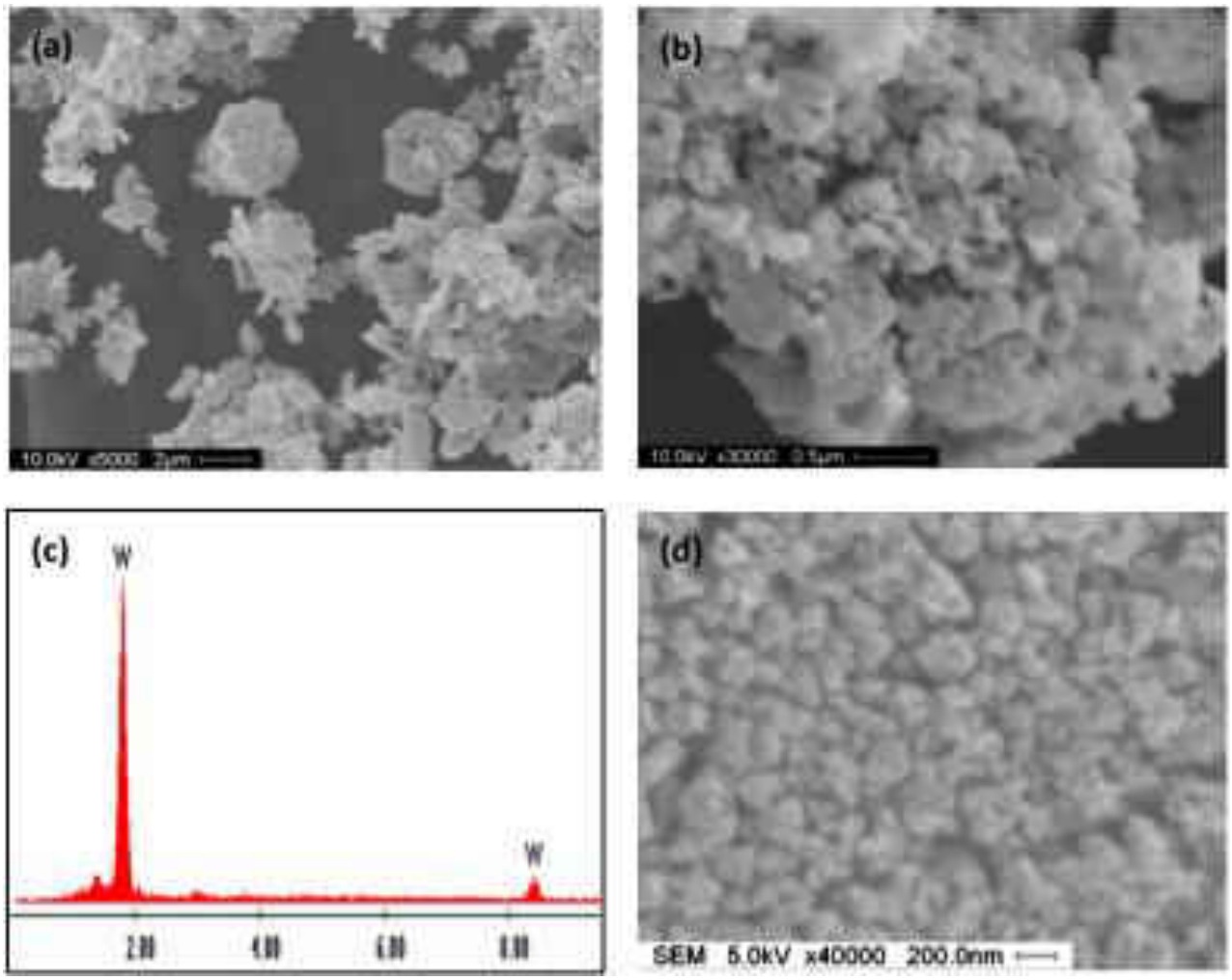

Figure 1: Secondary electron micrographs of the as-received W powder at (a) low magnification and (b) high magnification. (c) Measurement by EDS confirming that the powder is pure W. (d) Secondary electron micrograph after ultrasonication shows the break-down of soft agglomerates.

Figure 2 (a) shows a Bright Field (BF) image of a W particle with an approximate size of 120 nm. An Electron Diffraction pattern from this particle shown in Figure 2 (b) confirms its Body-Centered Cubic (BCC) structure. No other elemental constituents were observed from chemical analysis via EDS. TEM BF photomicrographs of W particles with a size of 100 nm are displayed in Figure 3. EDS identifies W in the particles. The copper peaks come from the copper grids.

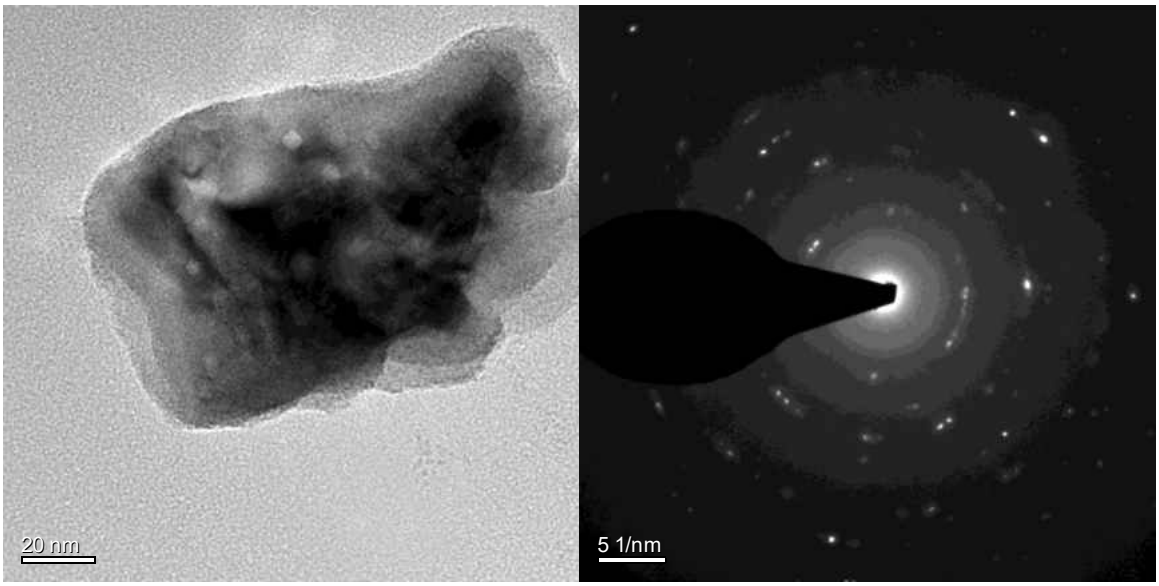

(a) (b)

Figure 2: (a) A TEM BF image and (b) electron diffraction pattern of a W particle.

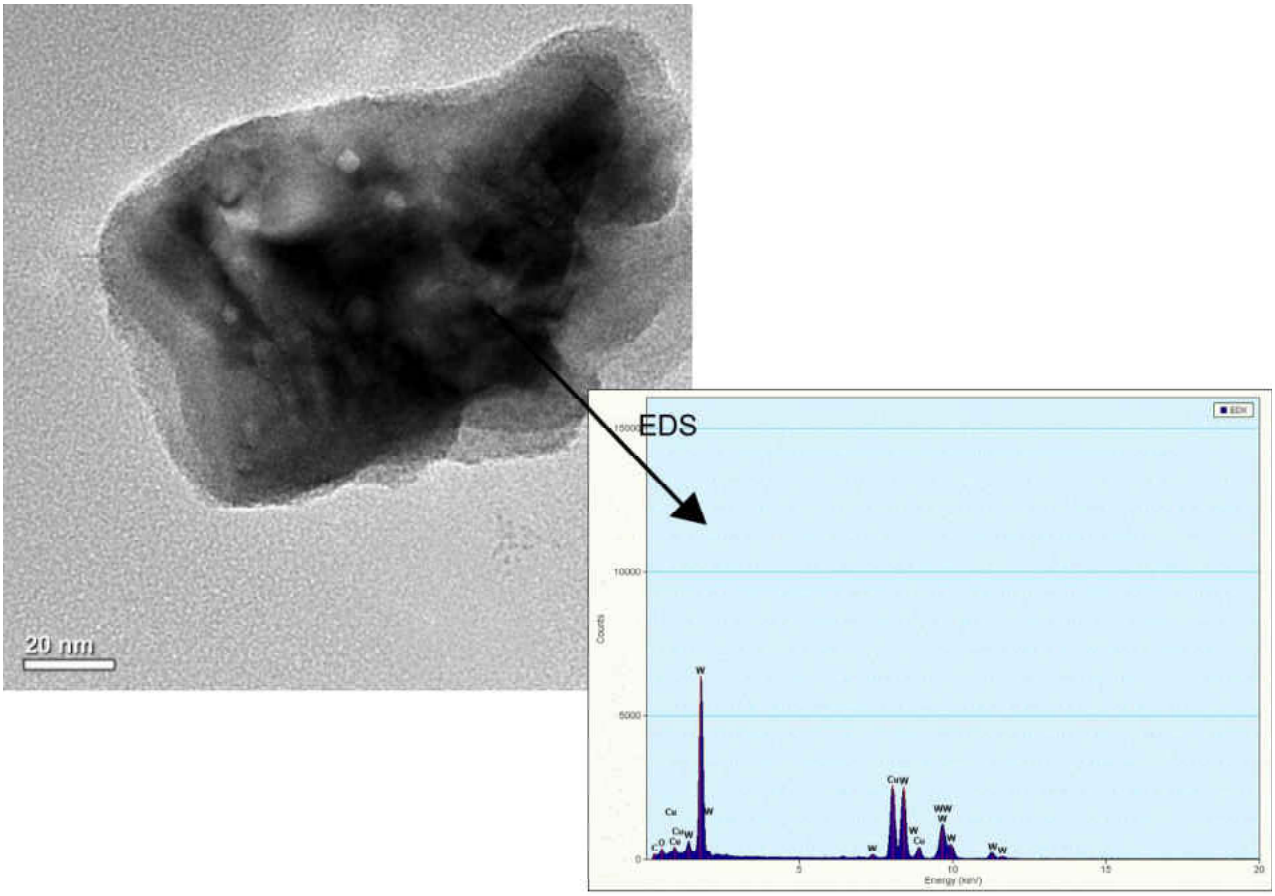

Figure 3: TEM BF photomicrographs and EDS of W particles.

The XRD pattern of the as-received W powder is shown in Figure 4. The measured XRD pattern matches well to the published PDF # 00-004-0806 for pure BCC W. The three major peaks from left to right correspond to the (110), (200), and (211) planes of BCC W.

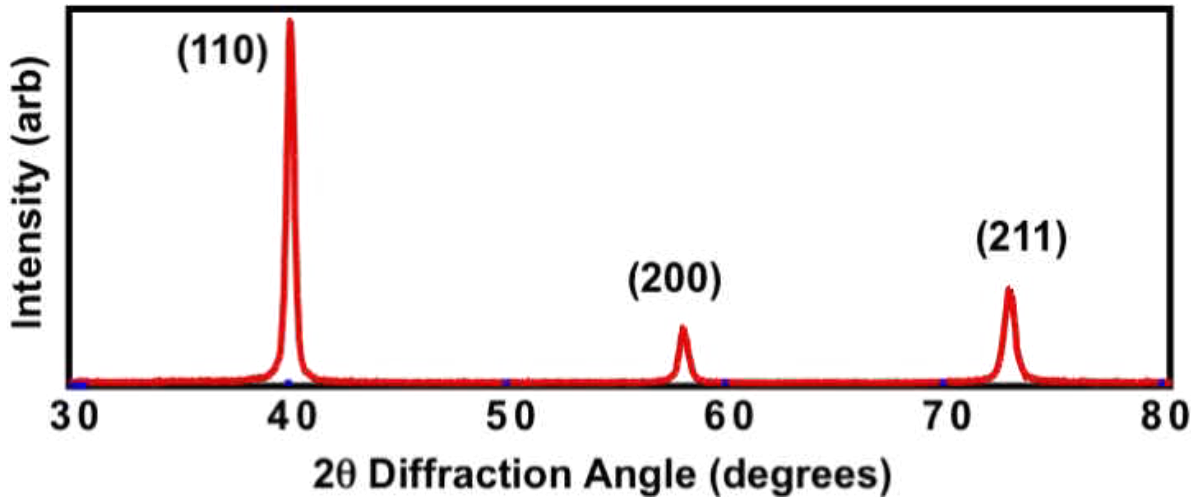

Figure 4: X-ray diffraction diagram of the as-received W powders (Cu $K\alpha_1$ radiation $\lambda = 1.5406$ Å).

Based on the average crystallite size analysis by Jade-7 analysis, the size of the nano W grain was approximated as 21 nm shown in Table 1. Independent analysis of XRD pattern by Scherrer equation also gives a grain size of approximately 20 nm.

Table 1: X-ray diffraction data of the as-received W powders

2-Theta	d (nm)	h k l	Intensity	FWHM	Crystallite size (nm) (software)	Grain size (nm) (Scherrer equation)
40.099	0.2245	110	100	0.376	24	22.5
58.117	0.159	200	17.6	0.441	22	20.6
73.063	0.129	211	35.2	0.528	19	18.7
86.904	0.112	220	10.9	0.569	20	19.2

The Scherrer equation predicts crystallite thickness if crystals are smaller than 1000 Å. If a Gaussian function is used to describe the peak, a prefactor of 0.9 occurs so the Scherrer equation is given in Equation 1

$$t = 0.9\lambda/(B\cos\theta_B) \qquad \text{Equation 1}$$

where λ is the wavelength of x-ray, t is the crystal size, B is the full-width at half maximum (FWHM) in radian, and θ_B is the Bragg angle in degree.

The results of BET gas adsorption measurement are shown in Figure 5 and the specific surface area was determined to be 10.43 m^2/g.

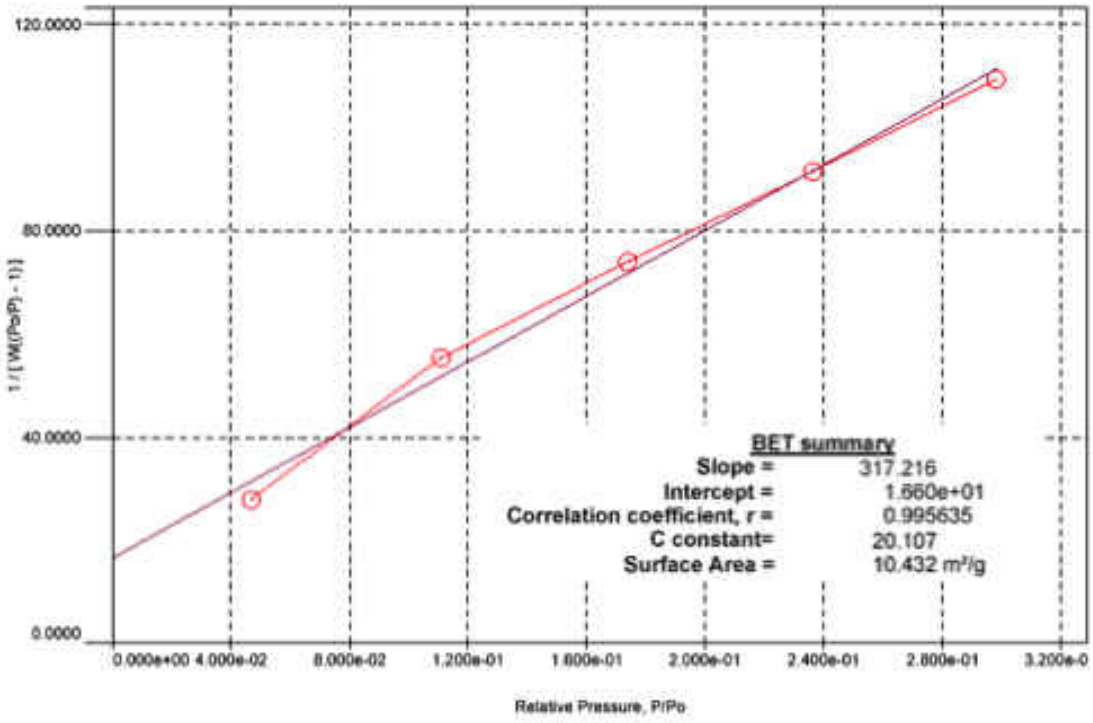

Figure 5: BET measurement of the as-received W nano-powders. From Dr. Weifeng Fei.

Assuming that the powders are not agglomerated and the particles are spherical and dense, the particle size can be estimated [42] from the equation 2:

$$d = \frac{6}{s\rho} \qquad \text{Equation 2}$$

where s is the specific area in m^2/g, and ρ is the density of the solid. Substituting s = 10.4 m^2/g and ρ = 19.25 g/cm^3 into equation (2) gives the average particle size of 30 nm. Since some agglomerates exist, and not all particles are spherical, particle sizes should be larger than 30 nm. Results of laser dynamic scattering of W nanopowders in Figure 6 estimated the particle sizes at approximately 40 nm.

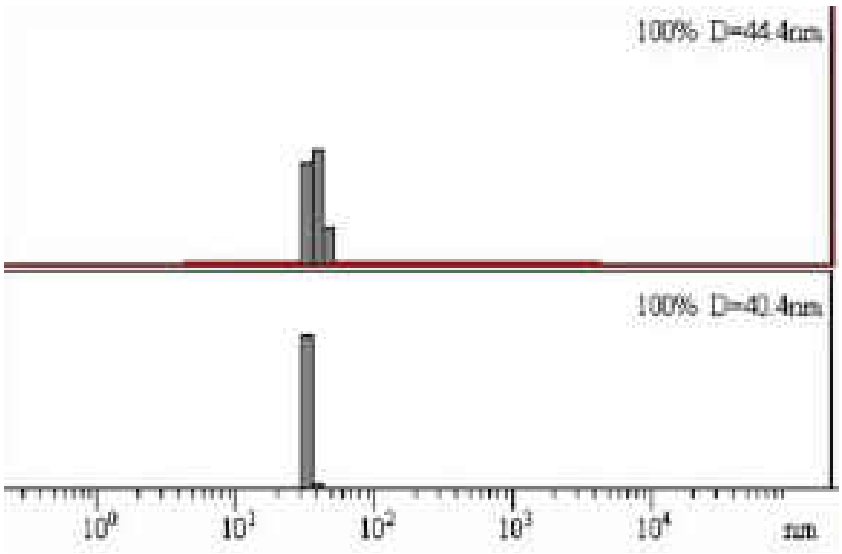

Figure 6: Laser dynamic scattering of W nanopowders. From Dr. Weifeng Fei.

Physical Electronics 600 AES (Auger Electron Spectroscopy) was employed to characterize the W nanopowders. The variations of differentiated number of electrons, dN(E) as a

function of kinetic energy is shown in Figure 7. Analysis software, AugerScan-3 and AugerMap, were employed for interpretation of the data. Three elements, W, O and C, are identified near the surface of W nanopowders. Approximate quantification yields 58.0 atomic % tungsten, 35.6 atomic % oxygen, and 6.3 atomic % carbon.

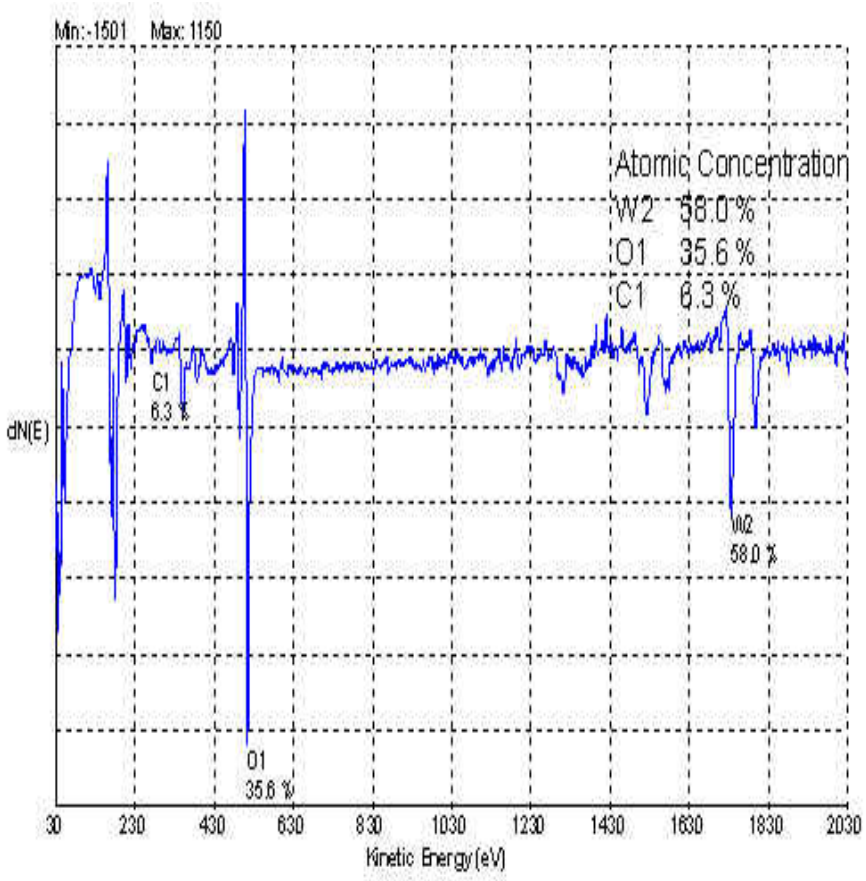

Figure 7: Variations of dN(E) with kinetic energy from AES for the as-received W powders.

Physical Electronics 5400 ESCA (X-ray Photoelectron Spectroscopy) was used to determine the chemical information and possible compounds present in the W nanopowders. Surface analysis by XPS is accomplished by irradiating the sample with monoenergetic soft

x-rays and analyzing the energy of the detected electrons. These photons have limited penetrating power in a solid on the order of 1-10 nm. They interact with atoms in the surface region, causing electrons to be emitted by the photoelectric effects. The emitted electrons have measured kinetic energies given by Equation 3:

$$KE = h\nu - BE - \Phi_s \qquad \text{Equation 3}$$

where $h\nu$ is the energy of the photons, BE is the binding energy of the atomic orbital from which the electron originates, and Φ_s is the spectrometer work function. Because each element has a unique set of binding energy, XPS can be used to identify and determine the concentration of the elements in the surface. Variations in the elemental binding energies (the chemical shifts) arise from difference in the chemical potential and polarizability of compounds. These chemical shifts can be used to identify the chemical state of the materials being analyzed. While ionization occurs to a depth of a few micrometers only those electrons that originate within tens of angstroms below the solid surface can leave the surface without energy loss. These electrons leaving the surface without energy loss produce the peaks in the spectra and are the most useful. The electrons that undergo inelastic loss processes before emerging form the background. A survey was taken from 0 eV to 1100 eV to determine what elements are in the tungsten powders. 5 sweeps was performed and the time/step is 50 ms. Binding energy is 0.5 eV/step. The variations of the number of electrons N(E) created with binding energy is presented in Figure 8. The survey identifies the spectral lines of C1s, O1s and W4f.

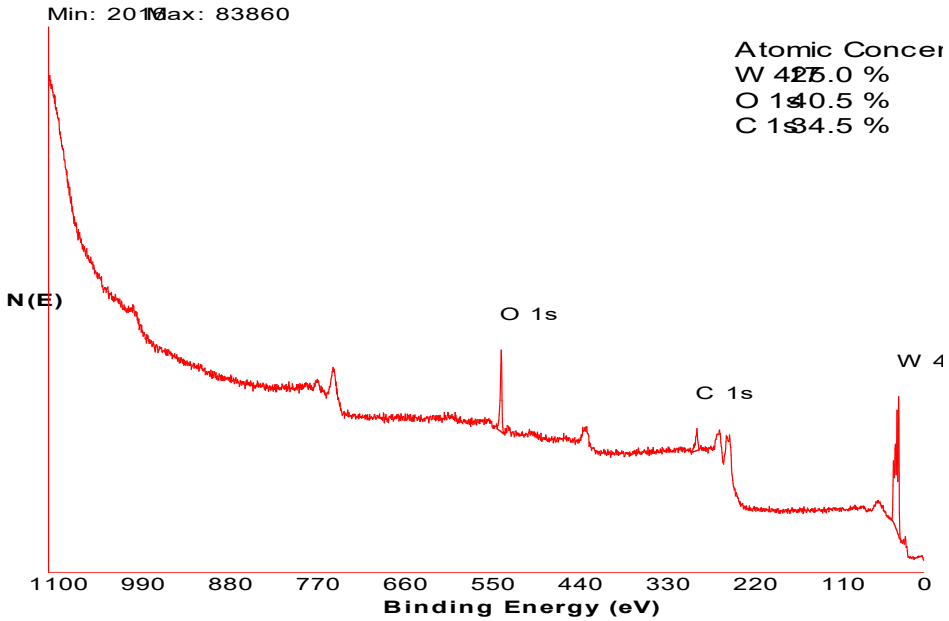

Figure 8: An XPS survey of the as-received W powders identifying spectral lines of C1s, O1s and W4f.

A multiplex was then performed to provide a further analysis with high resolution. Ten sweeps were conducted for each element. The experimental settings included a time/step of 50 ms, pass energy of 35.75 ev and bind energy of 0.05 ev/step. The data were averaged from ten sweeps. The unknown measured spectral lines were identified by using the NIST XPS Database (http://srdata.nist.gov/xps/spectrum.htm). Binding energy was chosen for identifying unknown spectral lines. The binding energies at 284.5 and 530.9 eV correspond to C1s and O1s, respectively, as shown in Figure 9.

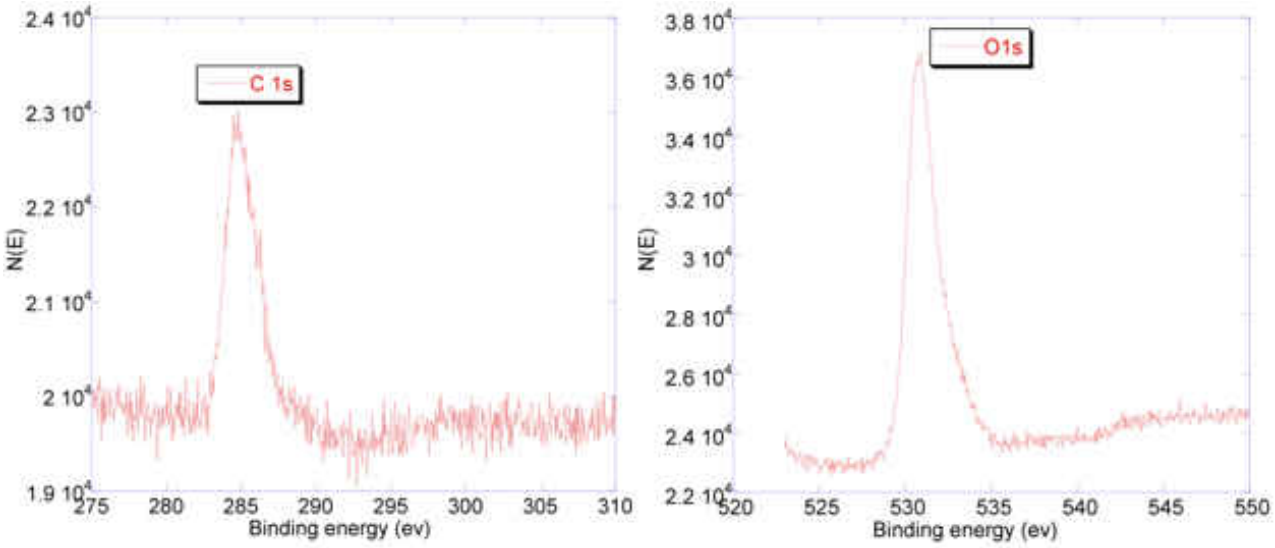

Figure 9: A high resolution XPS spectrum of the as-received W powders identifying C1s and O1s.

In Figure 10, a high-resolution XPS spectrum of W identified BE at 31.06 eV ($W4f_{7/2}$) for pure W, 33.1 eV ($W4f_{7/2}$) for WO_2, 35.6 eV ($W4f_{7/2}$) from WO_3, and 37.7 eV ($W4f_{5/2}$) for WOx/W. The metal surface is essentially covered by oxides, mainly WO_3, and the presence of metallic tungsten signal indicates that the oxide layer is either very thin and/or partial in terms of coverage.

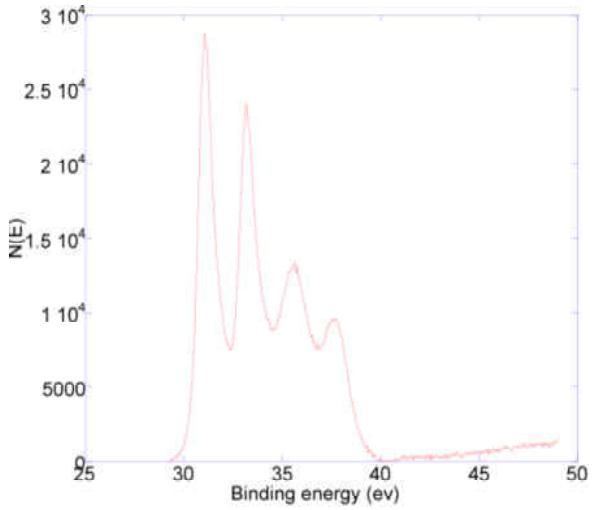

Figure 10: A high resolution XPS spectrum of the as-received W powders identifying $W4f_{7/2}$ and $W4f_{5/2}$

The oxidation of W depends on temperature and the oxygen partial pressure at elevated temperatures. W typically combines with oxygen to form the yellow W trioxide, WO_3, which is the most thermodynamically stable oxide at low temperatures and atmospheric pressures. ESCA investigations have showed that the oxidation of W by oxygen or air starts at room temperature and WO_3 always forms in dry or humid air or in oxygen [43]. Warren et al. [44] have found WO_3 is formed in a dry atmosphere OF oxygen at temperatures from 20 to 500ºC. Other W oxides include WO_2 and W_2O_3. W can also form W carbides such as WC and W_2C.

By subtracting the baselines from XPS, a quantitative analysis was performed to obtain the relative W concentration distributed in different phase constitutes on the surface as listed in Table 2. On average, approximately 50 atom % W existed as metallic W, 37 atom % of W existed as WO_3, and 11 atom % of W existed as WC and less than 2 atom % of W existed as

WO_2.

Table 2: Relative W concentration distributed in different phase constitutes on the surface

Phase constitutes	Area	Area %	Position	Intensity	Relative W concentration distributed in different phase constitutes
W	18611	25.90	31.06	18718	50.20%
	17482	24.30	33.23	15387	
WO_3	16476	22.90	35.6	8657	37.10%
	10238	14.20	37.78	6242	
WC	4349	6.00	31.92	4751	10.90%
	3512	4.90	34.1	3684	
WO_2	643	0.90	34.58	753	1.70%
	610	0.80	36.76	699	

The atomic concentrations of W powder surfaces from AES and XPS are listed in Table 3. The results via these two techniques are roughly comparable.

Table 3: Atomic concentrations of the as-received W powder surface from AES and XPS

Element	Atom % from AES	Atom % from XPS
W	58	40.2
O	35.6	32.3
C	6.3	27.5

In summary, microstructural and spectroscopic characteristics of nanocrystalline W powders were documented. Irregular morphology and agglomerates with sizes greater than 1 μm were observed, while the de-agglomerated particle size ranged from 30 to 100 nm. EDS from SEM and TEM identified the bulk composition as W. Electron and X-ray diffraction analysis confirmed the equilibrium BCC crystal structure of W. The presence of WO_3 and WC with traces of WO_2 was documented using AES and XPS. An understanding of these

characteristics will help improve the secondary powder processing including colloidal dispersion and mechanical milling, which will enhance the green density and methods to introduce grain growth inhibitors for producing fully-dense nanograined W parts.

4.2 Dispersion of Nano-W Powders

Water reacts with W and acts as an oxidizing agent. WO_3, WO_2 and oxide hydrates are formed [45]:

$$W + 2H_2O = WO_3(s) + 2H_2 \quad \text{Equation 4}$$

$$W + 3H_2O = WO_3(s) + 3H_2 \quad \text{Equation 5}$$

$$WO_3 + xH_2O = WO_3.xH_2O \ (x = 1\text{-}2) \quad \text{Equation 6}$$

Total anodic oxidation reaction of W in acidic and weakly-alkaline solutions can be expressed as [46]:

$$W + 3H_2O = WO_3(s) + 6H^+ + 6e^- \quad \text{Equation 7}$$

This oxidation reaction is followed by slow dissolution of the oxide. The point of zero charge (pzc) was found to be pH 2.6 [47]. When pH is close to the pzc of surface W oxide, dissolution of the oxide is water-assisted:

$$WO_3(s) + H_2O = WO_3.H_2O(s) = H_2WO_4(aq) \quad \text{Equation 8}$$

Above the pzc, OH-assisted dissolution is the main mechanism in acidic solution:

$$WO_3(s) + OH^- = WO_4^{2-}(aq) + H^+$$

4.2.1 Zeta Potential as a Function of pH

Figure 11 shows the zeta potential of WO_3 as a function of W suspension pH. The measured IEP of WO_3 was very low, close to a pH 0.4, and agreed well with the reported pH 0.5 [48]. Most zeta potentials were negative over the investigated pH range. Most oxide surfaces are hydrated and there are MOH groups on the surface for an oxide of a metal M. Amphoteric dissociation of surface MOH groups can result in pH dependence of surface charge. The surface hydroxyl groups of W oxide dissociate at low pH, leading to a negative charge over a wide pH range. The zeta potential was more negative with increasing pH and most negative at a pH close to 5, but decreased with further increase in pH. Andersson *et* al. [49] have observed increasingly negative zeta potentials of WO_3 surfaces with increasing pH. A more negative zeta potential corresponds to a larger repulsive electrostatic forces between particle surfaces, and consequently a more stable colloid suspension. Generally, the absolute values of zeta potentials on the particle surfaces should be greater than 40 mV to maintain a relatively stable suspension. From the measured zeta potential data, a zeta potential of -40 mV corresponds to the pH values of 4 and 5.3. Therefore, pH range from 4 to 5.3 results in a relatively stable W suspension.

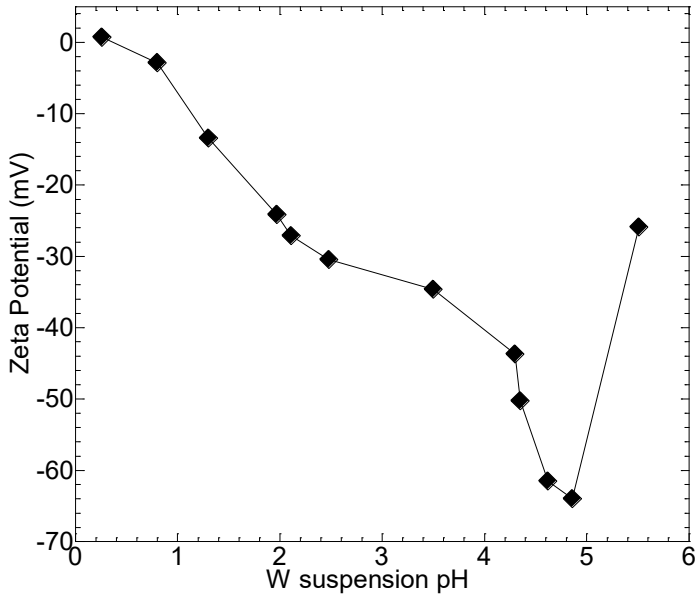

Figure 11: Zeta potential as a function of W suspension pH

4.2.2 Viscosity as a Function of pH

The shear viscosity vs. pH of 20 vol.% W suspension at various rpms is shown in Table 4 and Figure 12. At each rpm, viscosity decreases significantly with increasing pH and reaches a minimum at a pH close to 5, and increases slightly with further increase in pH. The zeta potential and viscosity results are consistent, and both identify the optimum pH 5. Based on the study of hydrolysis of W (VI) via ultracentrifugation and other techniques, Aveston et al. [50] have found that the main solute species of sodium paratungstate solution at pH 5 are $W_{12}O_{41}^{10-}$ and $HW_6O_{21}^{5-}$. At pH 5, the largest electrostatic repulsive forces among particles lead to a most stable colloid and optimum de-agglomeration, which correspond to the lowest suspension viscosity. With the lowest viscosity, the highest solids loading and the highest green density and efficiency can be achieved.

Table 4: Variation of viscosity as a function of 20 vol.% W slurry pH at various rpms

pH	5 rpm (Pa.s)	10 rpm (Pa.s)	20 rpm (Pa.s)	50 rpm (Pa.s)	100 rpm(Pa.s)
3.25	34.8	34.3	28.7	15.9	9.4
3.97	23.2	13.7	8.3	4.68	2.69
4.4	19.4	11.2	6.15	3	1.87
4.79	9.1	5	2.8	1.34	0.8
5	8.4	4.7	2.6	1.26	0.73
5.16	10	5.5	3.1	1.48	0.87
5.31	11	6.1	3.4	1.6	0.92

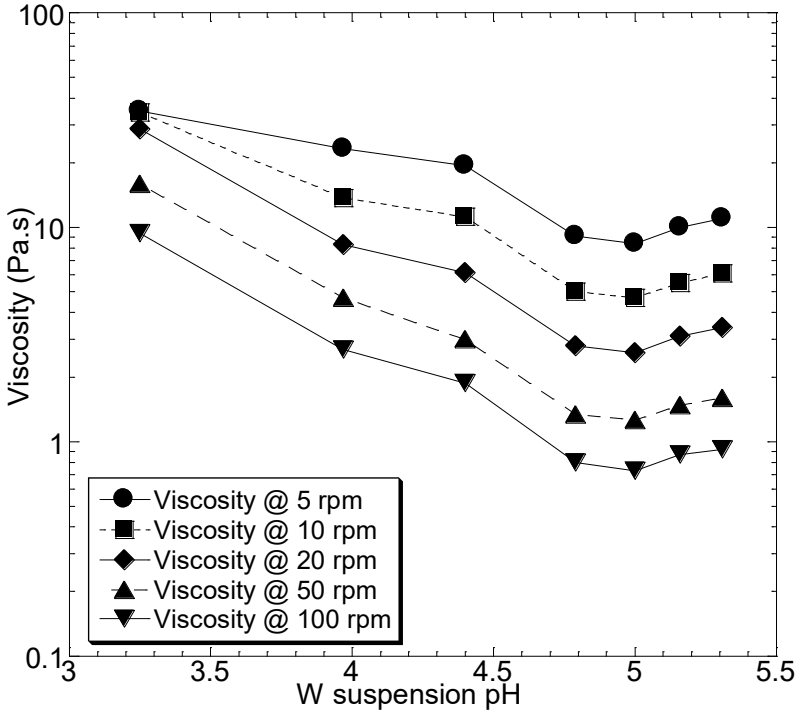

Figure 12: Shear viscosity vs. pH of 20 vol.% W slurry at various rpms.

It is also worth noting that the suspension displays a shear thinning behavior at all pH values because the shear viscosity decreases with increasing spindle rotating speed or shear rate as shown in Figure 13. This rheological behavior is typical of a flocculated suspension. With increasing shear rate, flocs or aggregates are broken down to smaller sizes; this releases liquid

immobilized in the flocs, thus facilitating flow. However, the degree of shear thinning is substantially reduced and the flow curves are nearly Newtonian for a colloidally stable suspension. If only electrostatic stabilization (short range repulsion) is involved in colloidal processing, non-Newtonian behavior will inevitably occur at a high solids loading since the particle spacing becomes shorter. However, some instability to flocculation reduces filtration resistance and increases the casting rate. The decreased stability results in a partially agglomerated slip, which gives larger filtration channels.

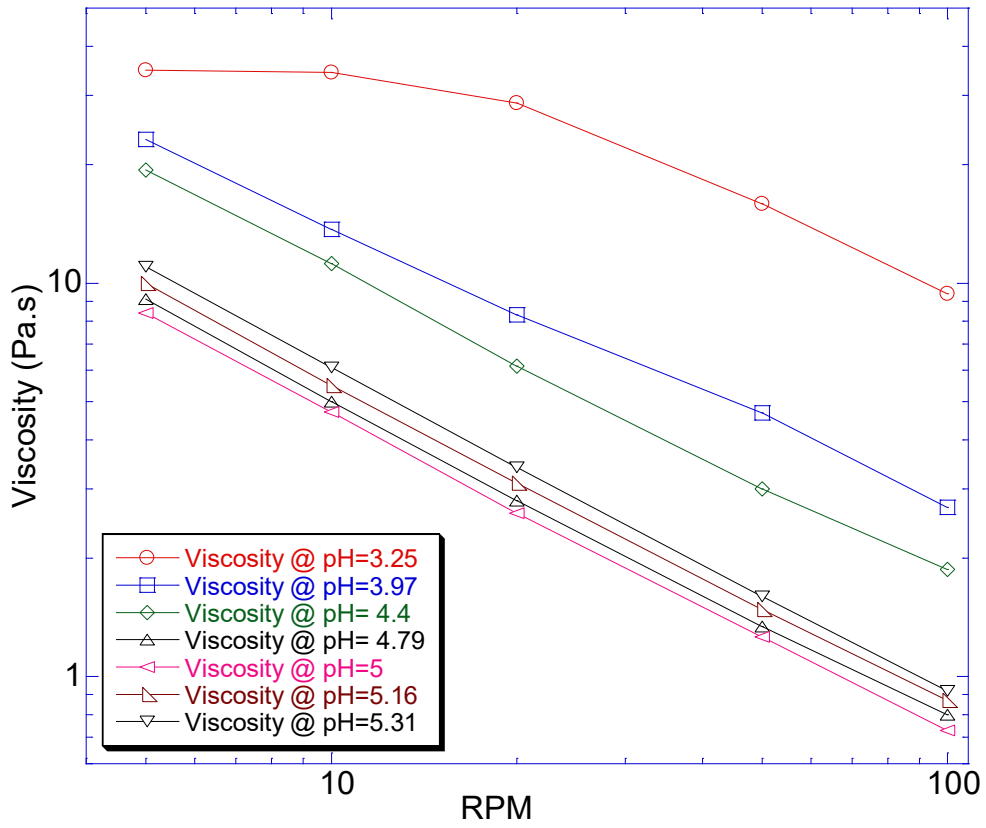

Figure 13: Shear viscosity vs. RPM of 20 vol.% W slurry at the same pH values.

The viscosity at zero rpm was determined by linearly extrapolating the points at 5 rpm

and 10 rpm to zero rpm and obtaining the intercept. The extrapolated viscosities at various pH values are listed in Table 5.

Table 5: Extrapolated viscosities at zero rpm at various pH values

pH	Extrapolated viscosity at 0 rpm (Pa.s)
3.25	35.3
3.97	32.7
4.4	27.6
4.79	13.2
5	12.1
5.16	14.5
5.31	15.9

The correlation between zeta potential and extrapolated viscosity at 0 rpm is shown in Figure 14. Viscosity decreases with increasingly negative zeta potential.

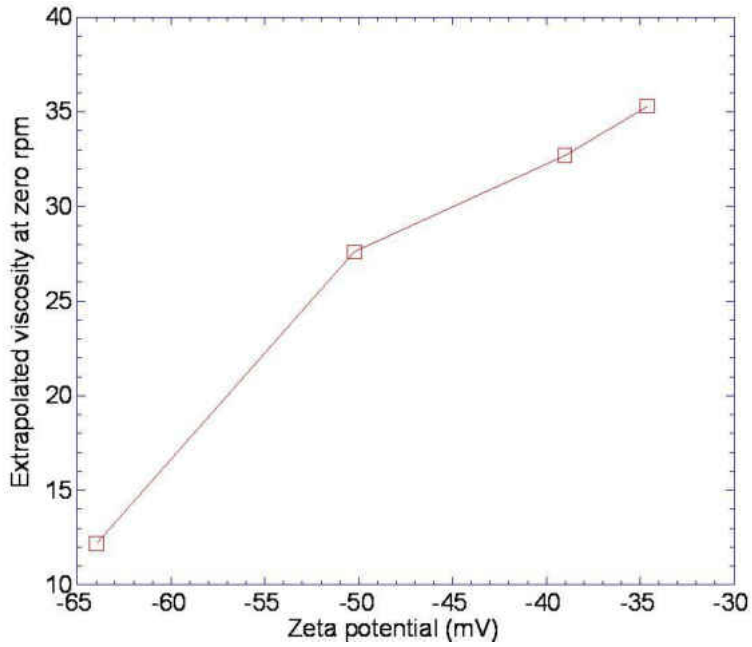

Figure 14: Correlation between zeta potential and extrapolated viscosity at 0 rpm.

4.2.3 pH as a function of Ultrasonic Time and W Concentration

The pH value of a W suspension is a function of (1) ultrasonic time, (2) W concentration, (3) ultrasonic power, (4) repeated ultrasonication and washing with water, and (5) additives such as NaOH. The pH values as a function of ultrasonic time at various solid loadings are shown in Table 6 and Figure 15. The pH values tend to decrease with longer ultrasonic time at the same solid loading.

Table 6: Variation of W suspension pH with ultrasonic time at various solids loadings.

Ultrasonic time (minute)	pH (0.26%)	pH (1.03%)	pH (1.03%)	pH (2.53%)
10	3.21	2.68	2.64	2.32
20	2.86	2.53	2.62	2.17
30	2.81	2.49	2.25	2.22
40	2.61	2.41	2.31	2.23
50	2.52	2.4	2.29	2.08
60	2.49	2.35	2.23	2.09

Figure 16 shows secondary scanning electron micrographs of 10 g of 4.94 vol.% W suspensions after ultrasonication under a power of 5 watts for 5 and 10 minutes. Ultrasonication for 5 minutes led to particle sizes of 200-400 nm, and 10 minutes resulted in much worse dispersion with large agglomerates of greater than 1um. The decrease of the suspension pH from 2.32 at 5 minutes to 2.17 at 10 minutes led to less negative zeta-potentials on the particle surfaces and smaller electrostatic repulsion between particles.

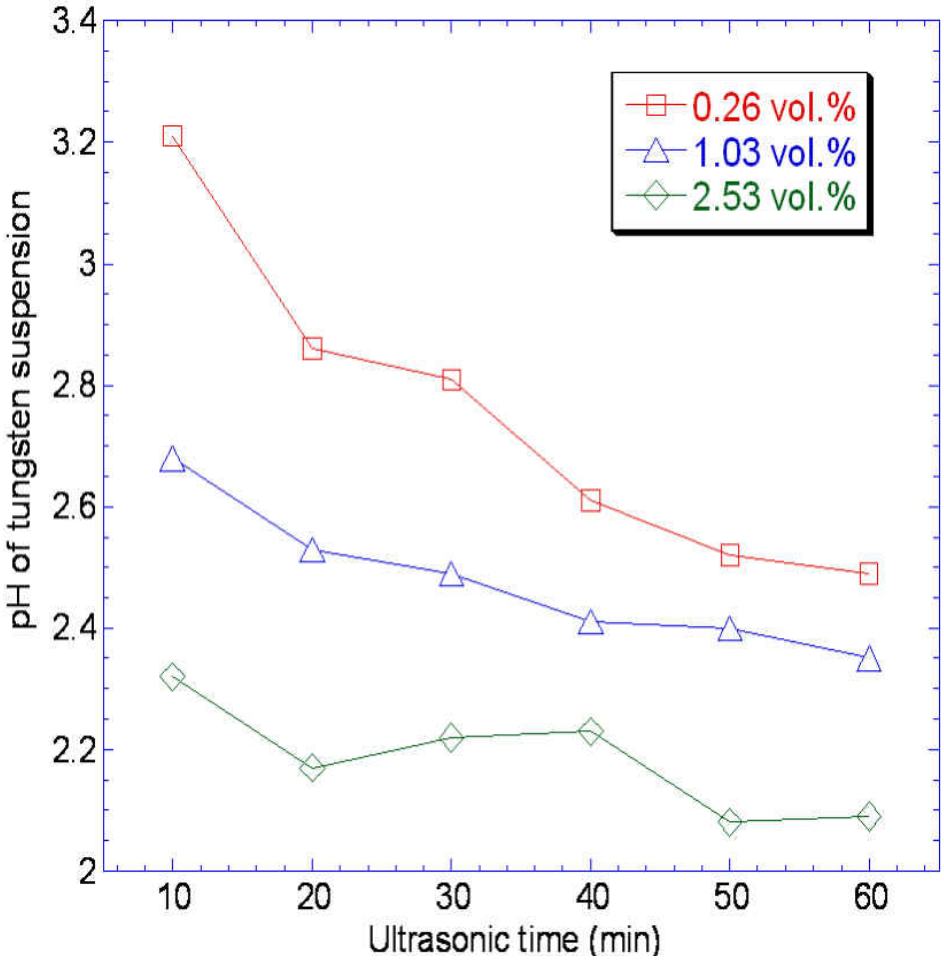

Figure 15: Variation of W suspension pH with ultrasonic time at various solid loadings

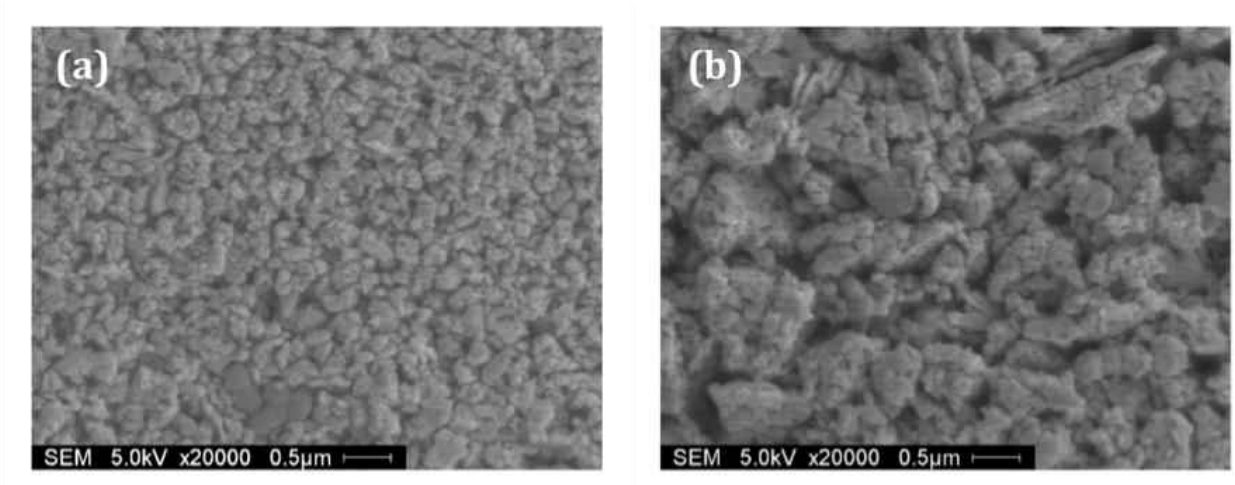

Figure 16: Secondary electron micrographs of 4.94 vol. % W suspensions after ultrasonication under a power of 5 watts for (a) 5 minutes, and (b) 10 minutes.

At the same ultrasonic time, the suspension pH decreased with increasing solid concentration as shown in Figure 17.

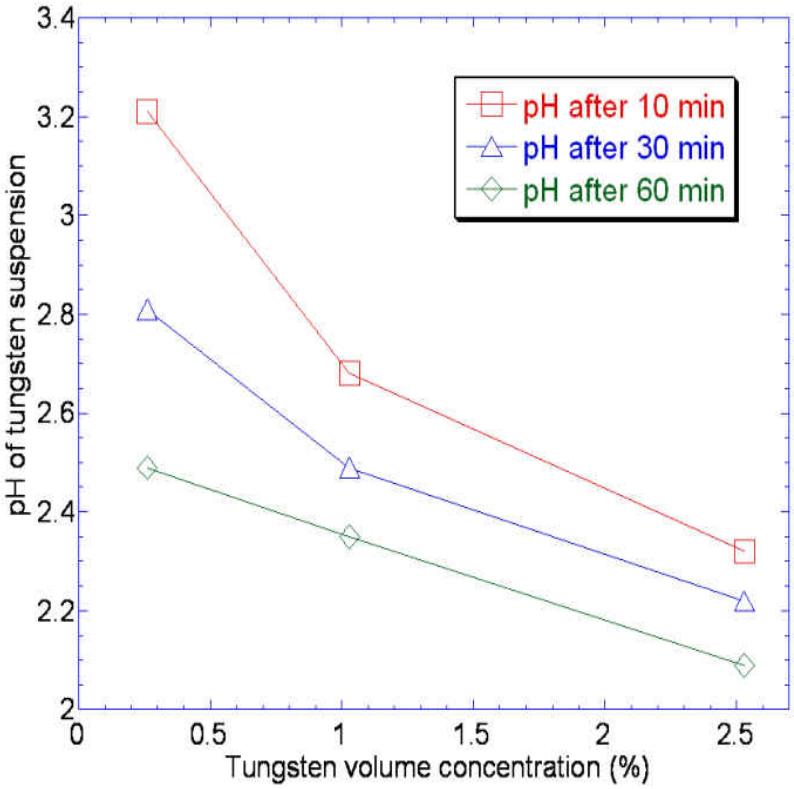

Figure 17: Variation of W suspension pH with W volume concentration at the same ultrasonic time.

The pH values of aqueous W suspensions with different concentrations increased with sitting time after ultrasonication as shown in Table 7.

Table 7: pH of aqueous W suspensions of various concentrations after ultrasonication

Sitting time (hour)	pH (0.26%)	pH (1.03%)	pH (2.53%)
0	2.49	2.23	2.09
13	-	2.43	-
18	2.7	2.49	2.56

To increase the pH of the suspension, drops of 1 M NaOH solution were added to the 10 ml of 0.26% of W suspension until the pH was increased to 6.08. The modified W suspension was ultrasonicated under a power of 17 watts for 1 hour and the pH values of the suspension were measured every 10 minutes. As shown in Table 8, the pH of NaOH-modified 0.26% W suspension continuously decreased with ultrasonic time and reduced by 1.1 after 1 hour and most W settled down to the bottom 12 hours after ulrasonication.

Table 8: pH of NaOH-modified 0.26% W suspension as a function of ultrasonic time.

Ultrasonic time (min)	pH (As-dispersed 0.26% W suspension)	pH (NaOH-modified 0.26% W suspension)
0	-	6.08
10	2.64	5.49
20	2.62	5.35
30	2.25	5.28
40	2.31	5.14
50	2.29	5.01
60	2.23	4.98
12 hour after ultrasonication	2.43	5.04

Another additive, tetramethylammonium hydroxide pentahydrate (TMAH, Alfa Aesar) was added to W suspensions to increase their pH values, and was much better than NaOH. TMAH was used as dispersant for SiC aqueous suspension [51]. It has the molecular formula $C_4H_{13}NO{\cdot}5(H_2O)$ and F.W. 181.23.

4.2.4 De-agglomeration by Ultrasonication, dilution with water and Centrifuge

4.2.4.1 De-agglomeration of 20 grams of 10.4 vol.% W Suspension

Agglomerates always present in the as-received submicron powders must be minimized to enhance densification and avoid defects such as crack-like voids. The agglomeration of nano-powders decreases the density of green bodies pressed from those powders. The irregularly-shaped agglomerates, high surface area and large friction between particles lead to low green densities during dry pressing. The green densities of the uniaxially dry-pressed as-received W powders under various compaction pressures are listed in Table 9. As expected, the green densities are low and only reach a 42 % relative density under a high compaction pressure of 618 MPa. One reason for the low green densities is the irregularly - shaped agglomerates in the as-received W powders. Only slightly higher density can be expected under higher pressure, which is often impractical as the pressing die has to be specially designed.

Table 9: Green densities of the uniaxially dry pressed as-received W powders

Compaction Pressure	232 MPa	386 MPa	618 MPa
Relative density	~36%	~38%	~42%

Polycrystalline W is generally brittle and hard at room temperature, which hinders plastic deformation and particle movement during dry pressing. The large irregular-shaped agglomerates cause large pores during dry compaction. The large pores in the green compact are difficult to remove upon subsequent sintering. The faster sintering agglomerates shrink first and leave even larger pores. The removal of these large pores requires higher temperatures and

longer sintering times, which causes undesirable grain growth. De-agglomeration via aqueous colloidal processing is necessary to increase the green density and make the green compact microstructure more uniform. In aqueous colloidal processing, pH is an important parameter to control to achieve electrostatic repulsion between particles. The zeta potential is a measurement of the stability of colloid suspensions. Suspensions at pH values close to the isoelectric point (IEP) may flocculate rapidly because the repulsion may not be sufficient to overcome the van der Waals attraction. Far away from the IEP, the rate of flocculation is lower.

The as-received W powders have a thin layer of blue W oxide ($WO_{2.9}$) on the surface. It may form by the oxidation in air and has a loose structure. It dissolves fast in water and produces H^+ ions and rapidly decreases the suspension pH. This is the reason why the color of the supernatant liquid after centrifugation is blue. After repeated ultrasonication, washing with water, centrifugation and removal of the supernatant liquid, the blue W oxide can be gradually removed, as witnessed by a clear colorless supernatant liquid after centrifugation. After that, W powders react with water to form a relatively denser WO_3 layer, which dissolves in a slower fashion. Barta and Gorni [52] have experimentally shown that the amount and chemical characteristics of the surface oxide layer influence the properties of the W suspensions and its presence is necessary for deflocculation. The pH vs. ultrasonic time for 10 vol.% suspensions made from the as-received and repeatedly water-washed W powders is shown in Figure 18. The repeatedly water-washed W suspension has much higher pH values than the one made from the as-received W powders after the same ultrasonic time and exhibits slightly less decrease in pH within the initial 10 min. For the as-received powders, ultrasonication for 30 min significantly

reduces the pH to 1.7, which corresponds to a very low zeta potential. The ultrasonic tip stops working due to the decrease in repulsive forces between particles and increase in suspension viscosity. After repeated ultrasonication, washing with water, centrifugation and removal of the supernatant liquid, the suspension pH was increased significantly.

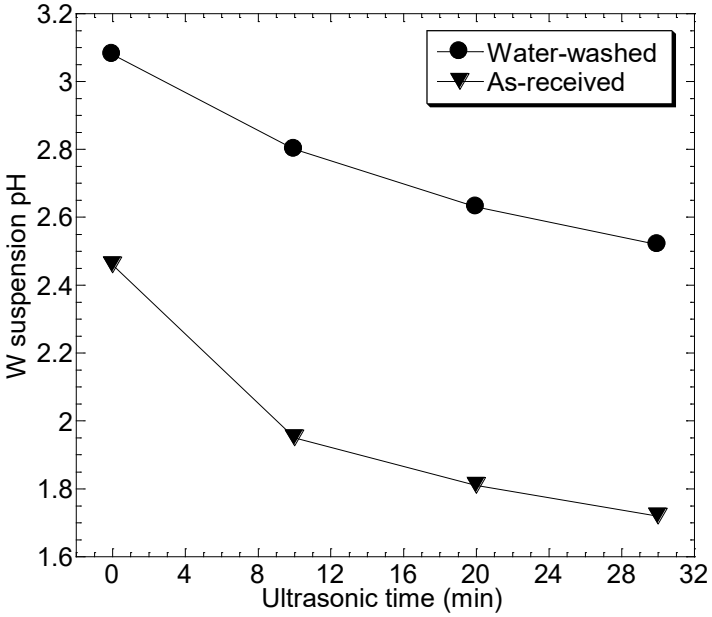

Figure 18: The pH vs. ultrasonic time for 10 vol.% suspensions made from the as-received and repeatedly water-washed W powders under a power of 10 watts.

As shown in Figure 19, agglomerates with sizes of 1 μm are observed after ultrasonication under a power of 10 watts for 30 minutes. Ultrasonication and washing with water twice followed by ultrasonication under at 10 watts for 3 minutes broke down some soft agglomerates to sizes less than 500 nm.

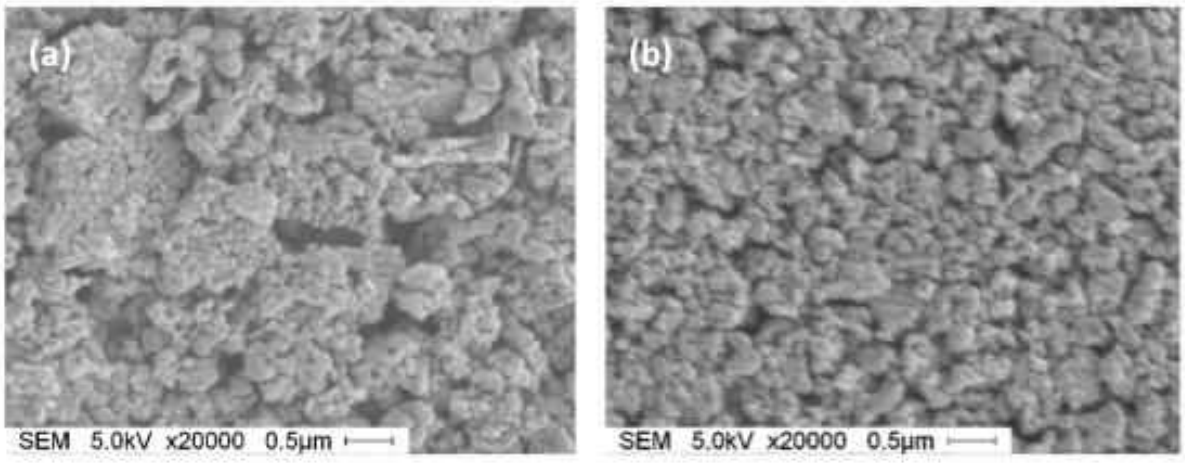

Figure 19: Secondary electron micrographs of 10.4 vol. % W suspensions after ultrasonication under a power of 10 watts for (a) 30 min and (b) 10 watts for 3 min after washing with water twice.

4.2.4.2 De-agglomeration of large particles of 10 grams of W

The W suspension pH increased with increasing number of washing cycle with water after ultrasonication at 10 watts for approximately the same time as shown in Figure 20.

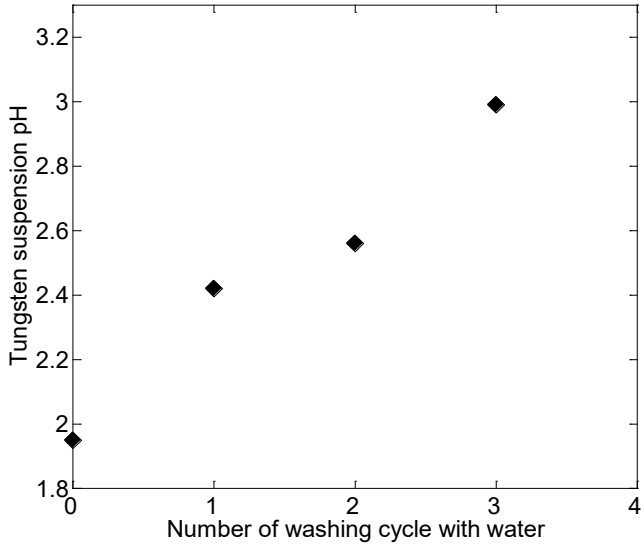

Figure 20: W suspension pH vs. number of washing cycles with water

Figure 21 illustrates secondary scanning micrographs of 4.94 vol. % W suspensions

after 1st washing with water and ultrasonication for 6 minutes and the suspension pH was 2.42.

Dispersion is good and particle sizes are less than 0.5 μm.

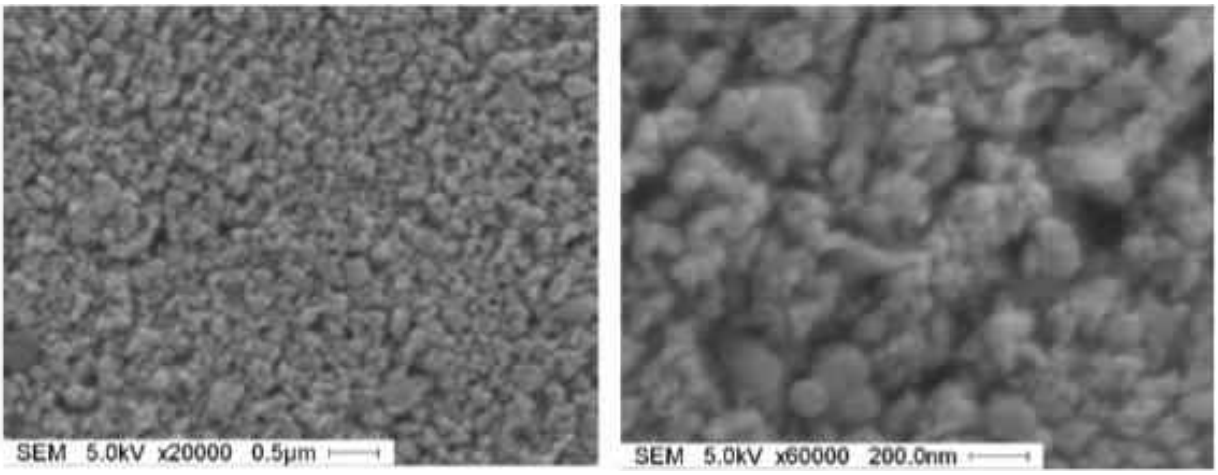

Figure 21 Secondary electron micrographs of 10 g of 4.94 vol.% W suspensions after 1st washing with water and ultrasonication at 10 watts for 6 minutes.

Figure 22 shows secondary electron micrographs of 5.8 g of 2.93 vol. % settled large W suspensions after 2nd washing with water and ultrasonication at 10 watts for 4 and 6 minutes. The W had larger average particle sizes than those without separation shown in Figure 21.

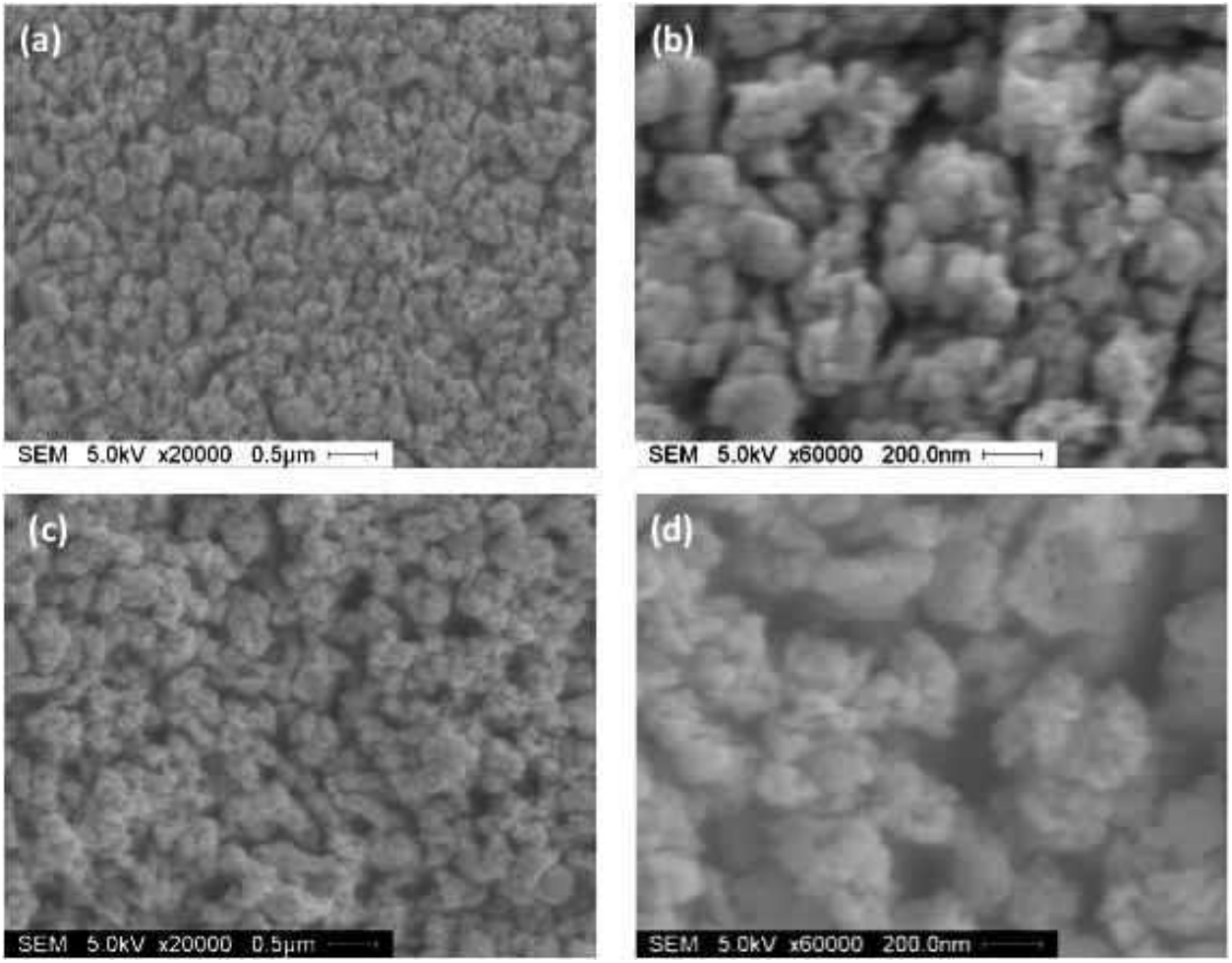

Figure 22 : Secondary electron micrographs of 5.8 g of 2.93 vol.% large settled W suspensions after 2nd washing with water and ultrasonication at 10 watts for (a, b) 4 minutes and (c, d) 6 minutes.

Figure 23 shows secondary electron micrographs of 5.6 g of 2.83 vol. % large settled W suspensions after 3rd washing with water and ultrasonication at 10 watts for 4 minutes. Most particles had sizes less than 500 nm. The pH of the sampled suspension was increased to 3.13.

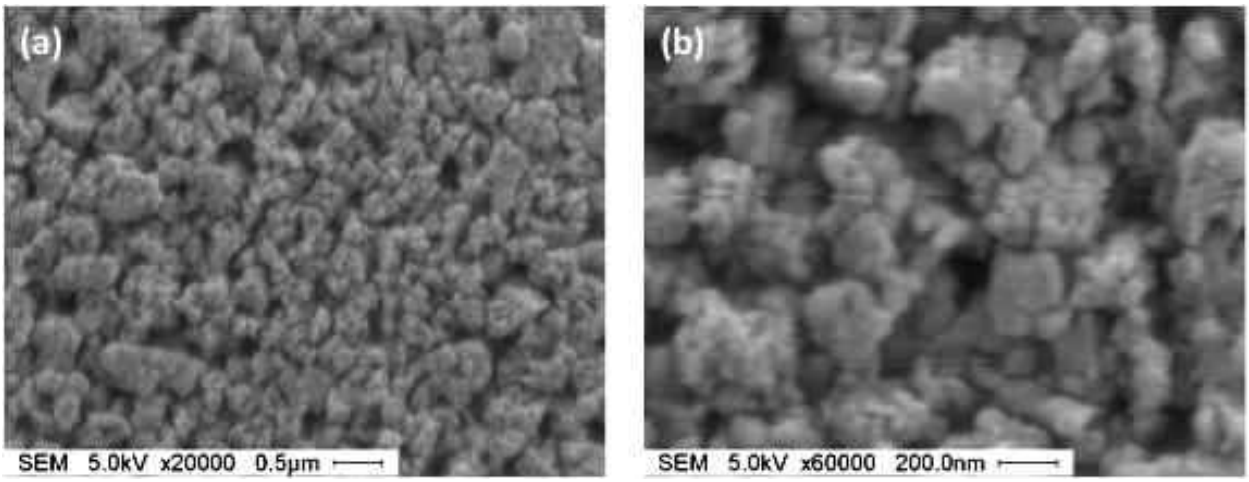

Figure 23 : Secondary electron micrographs of 5.6 g of 2.83 vol.% large settled W suspensions after 3rd washing with water and ultrasonication at 10 watts for 4 minutes.

Figure 24 shows secondary electron photomicrographs of 5.6 g of 2.83 vol. % large settled W suspensions after 4th washing with water and ultrasonication at 5 watts for 10 , 15 and 30 minutes. After 10 minutes, the sizes of some fine particles are approximately 200 nm or less. But 15 and 30 minutes made dispersion worse and led to agglomerates greater than 1 µm in size due to decrease in the W suspension pH with longer ultrasonication time.

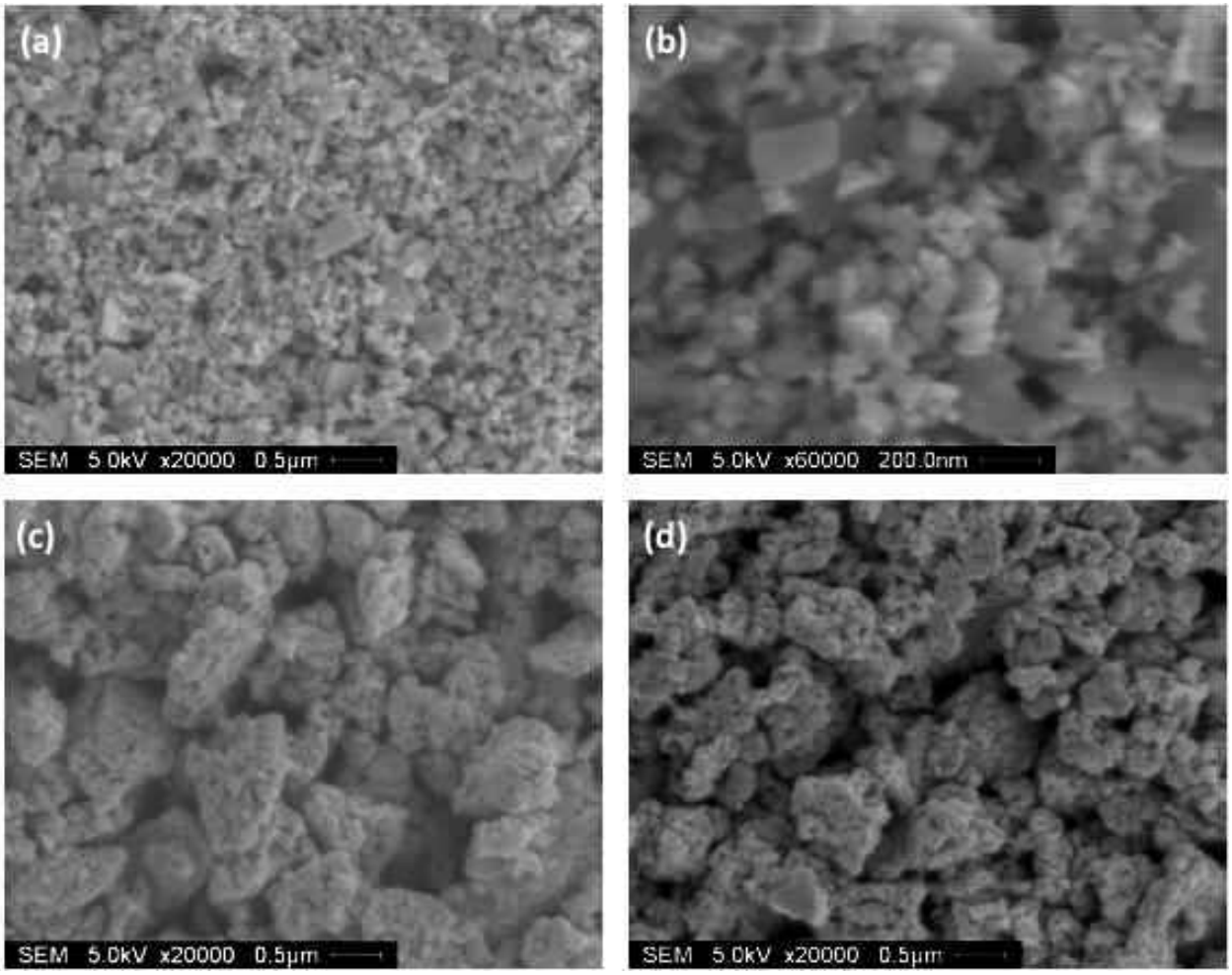

Figure 24 : Secondary electron micrographs of 5.6 g of 2.83 vol.% large settled W suspensions after 4th washing with water and ultrasonication at 5 watts for (a, b) 10 minutes, (c) 15 minutes and (d) 30 minutes.

In summary, ultrasonication and washing of only large particles with water 3 times significantly raised the suspension pH from 1.95 to 2.99 and broke up some soft agglomerates. The de-agglomeration was expected to improve with increasing cycles of ultrasonication and washing with water. Therefore, de-agglomeration involving 10 cycles was performed.

4.2.4.3 De-agglomeration of 20 g of W 10 times

The effect of pH on the de-agglomeration behavior of repeatedly washed W powders is shown in Figures 25 and 26. For a dilute suspension with a 10 vol.% solids loading, particle segregation occurred because smaller particles settled at lower speeds than the coarse ones under gravity force. Figure 25 shows the top surface of the pellet that consists of well packed, de-agglomerated mono-dispersed nanoparticles with sizes ranging from 30 to 70 nm.

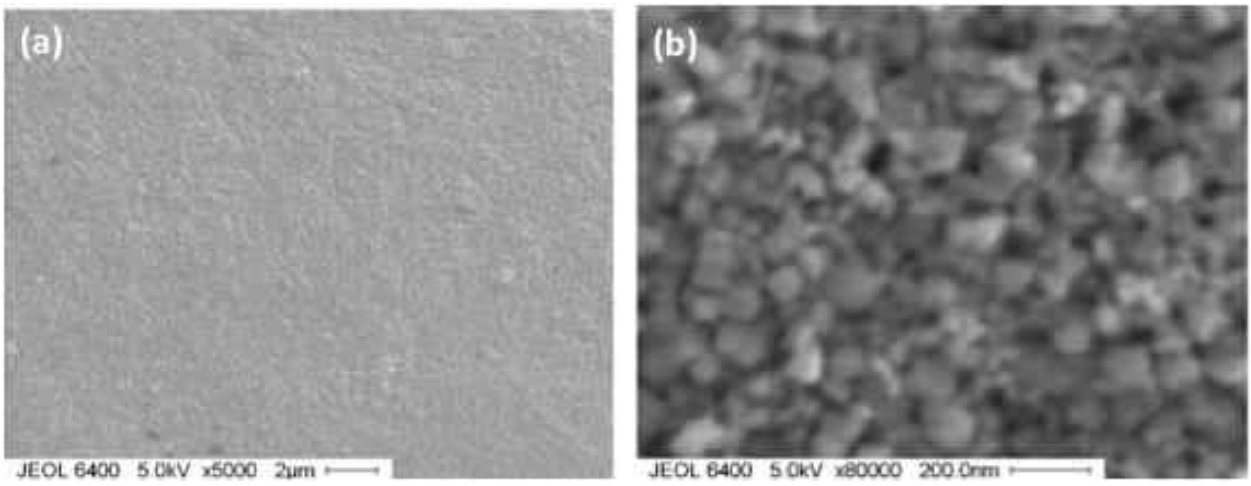

Figure 25 : Top surface of the 9.4 vol.% W slurry after 10 cycles of ultrasonication and washing : (a) low magnification and (b) high magnification.

The bottom side is presented in Figure 26, and it represents the worst condition of the suspension. Some agglomerates are still present and they may be hard-agglomerates, which will never be broken up. The agglomerate size is considerably smaller than that of the as-received nanopowders shown in Figure 1. Better de-agglomeration can be achieved by increasing the suspension pH. Therefore, de-agglomeration using water is feasible. Several methods have been proposed to prevent particle segregation [53]: (1) increasing the solids loading, the consolidate

rate, and the suspension viscosity (2) controlling the particle size, size distribution, and particle interaction forces (3) improving the colloidal stability of the slurry.

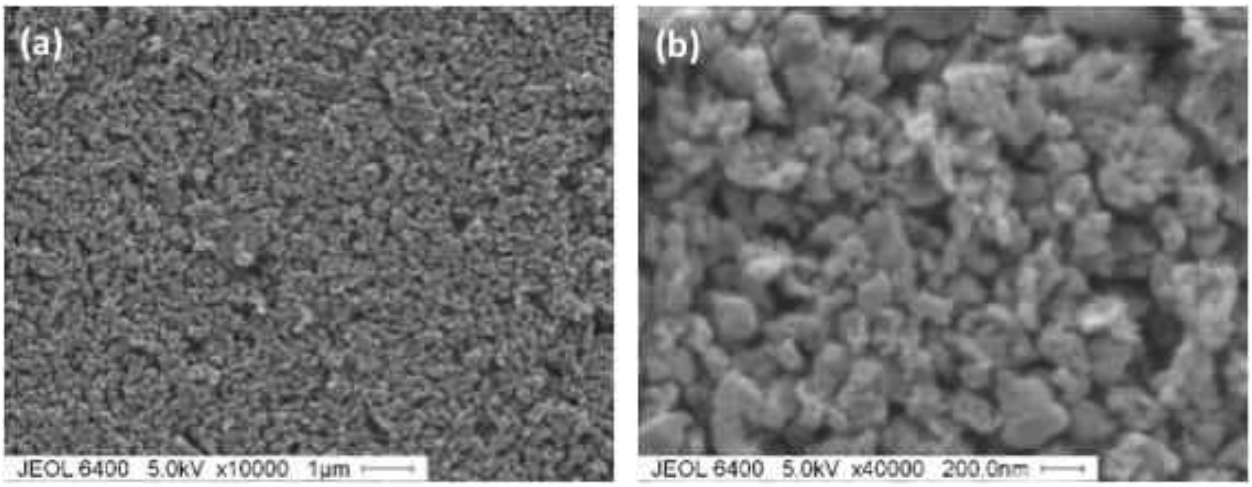

Figure 26: Bottom surface of the 9.4 vol.% W slurry after 10 cycles of ultrasonication and washing: (a) low magnification and (b) high magnification.

4.2.5 Casts of W Slurries

4.2.5.1 Casts of 6 Batches of 20 grams of W Slurries

The cast of the 1st batch weighed 2.525 g, and had a green density of 42 %. It was sintered at 1000 ºC for 5 hours and at 1400 ºC for 2 hours in argon atmosphere. It had a sintered density of 16.79 g/cm^3 or 87.22 % theoretical density.

The pH of the 2nd batch slurry was adjusted to 5.19 and the solids loading was 26.2 vol.%. Three cylindrical specimens were cast. The 1st one was cast one time and had a lower center and higher edge and a dry weight of 2.25 g. The 2nd and 3rd ones were cast three times and the centered was filled each time to produce a roughly flat surface and weighed 3.66 and 5.192 g, respectively. The density of the 3rd one was 6.255 g/cm^3 (32.5% theoretical density).

The pH of the 3rd slurry was 5.53 and the solids loading was 23.64 vol.%. 2 specimens were slip cast. The 1st one weighed 1.965 grams. Its density is 6.91 g/cm^3 (35.9% theoretical density). The 3rd specimen was slip cast at a pH 3.87. It weighed 1.694 grams with a density of 5.96 g/cm3 (30.95% theoretical density). Another cast was obtained at a pH 5.78. It weighed 2.242 grams with a density of 6.3 g/cm^3 (32.73% theoretical density). The cast density as a function of pH is presented in Figure 27. It shows that the density first increases and then decreases with increasing pH.

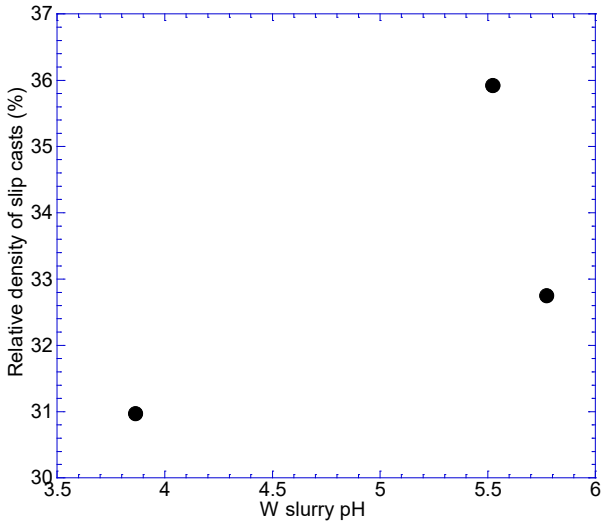

Figure 27: The slip cast density as a function of W slurry pH.

The pH of the 4th W slurry was 5.04 and the solids loading was 25.4 vol.%. 4 pellets were slip cast. The results are listed below:

- Cast 1: weight: 3.137 grams density: 7.356 g/cm^3 (38.2% theoretical)
- Cast 2: weight: 2.982 grams density: 7.053 g/cm^3 (36.6 % theoretical)
- Cast 3: weight: 3.895 grams density: 6.99 g/cm^3 (36.3 % theoretical)

- Cast 4: weight: 2.7 grams density: 6.98 g/cm^3 (36.2 % theoretical)

The pH of the 5th batch of W slurry was 4.9 and the solids loading was 25.4 vol.%. 2 pellets were slip cast. The results are as follows:

- Cast 1: weight: 2.493 grams density: 7.906 g/cm^3 (41.07 % theoretical)
- Cast 2: weight: 3.263 grams density: 7.44 g/cm^3 (38.64 % theoretical)

The solids loading of the 6th batch of W was 25 vol.% and 3 pellets were cast at different pH values.

- Cast 1 at a pH 4.74 weight: 1.814 grams density: 6.366 g/cm^3 (33.07% theoretical)
- Cast 2 at a pH 4.9 weight: 2.222 grams density: 6.131 g/cm^3 (31.85% theoretical)
- Cast 3 at a pH 5.4 weight: 2.868 grams density: 6.014g/cm^3 (31.24% theoretical)

One reason for the low green densities the 6th batch is that the W nanopowders were only washed with water 3 times and the blue tungsten oxide was still present in the slurry before magnetic stirring, leading to rapid decrease in slurry pH and absolute value of zeta potential. Table 10 summarizes the relative densities of all slip casts from 6 batches of 20-gram W slurries.

Table 10: Relative densities of slip casts from 6 batches of 20-gram W slurries

Cast	Batch 1	Batch 2	Batch 3	Batch 4	Batch 5	Batch 6
1	42	32.5	35.9	38.2	41.07	33.07
2	-	-	30.95	36.6	38.64	31.85
3	-	-	32.73	36.3	-	31.24
4	-	-	-	36.2	-	-
Average density	42	32.5	33.19	36.83	39.86	32.05
Standard Deviation	0	0	2.51	0.93	1.72	0.93
Ultrasonic time(hour)	4	2.17	1.83	5.4	5.9	2.25

4.2.5.2 Casts of 2 Batches of 50 grams of W Slurries

The cast of the 1st batch was sintered at 1000°C for 5 hours and at 1400°C for 2 hours. It had a sintered density of 16.448 g/cm^3 or 85.44 % theoretical density. The solids loading of the 2nd batch slurry was 30 vol.%. 3 pellets were slip cast at a pH 5.21. The results are listed below:

- Cast 1: weight: 2.275 grams density: 7.607 g/cm^3 (39.52 % theoretical)
- Cast 2: weight: 2.08 grams density: 7.418 g/cm^3 (38.54 % theoretical)
- Cast 3: weight: 2.048 grams density: 7.888 g/cm^3 (40.98 % theoretical)

Additional pellets were slip cast at a pH 3.97. The results are shown below:

- Cast 4: weight: 2.951 grams density: 7.765 g/cm^3 (40.34 % theoretical)
- Cast 5: weight: 2.9 grams density: 7.568 g/cm^3 (39.32 % theoretical)
- Cast 6: weight: 2.039 grams density: 7.24 g/cm^3 (37.62 % theoretical)
- Cast 7: weight: 2.211 grams density: 7.1 g/cm^3 (36.9 % theoretical)
- Cast 8: weight: 2.129 grams density: 7.619 g/cm^3 (39.58 % theoretical)
- Cast 9: weight: 2.161 grams density: 7.508 g/cm^3 (39 % theoretical)

From the remaining W slurry, 4 pellets were slip cast at a solids loading of 24.45 vol.% and a pH 6.51. The results are listed below:

- Cast 1: weight: 2.19 grams density: 7.766 g/cm^3 (40.34 % theoretical)
- Cast 2: weight: 2.973 grams density: 7.793 g/cm^3 (40.48 % theoretical)
- Cast 3: weight: 2.635 grams density: 7.926 g/cm^3 (41.17 % theoretical)
- Cast 4: weight: 2.519 grams density: 7.724 g/cm^3 (40.13 % theoretical)

0.1 gram water was added to the slurry and the slurry was stirred for 10 minutes. The viscosity was appreciably reduced. The solids loading of the slurry was decreased to 23.53 vol.%. 2 pellets were slip cast.

- Cast 5: weight: 2.915 grams density: 7.974 g/cm3 (41.42 % theoretical)
- Cast 6: weight: 3.24 grams density: 7.872 g/cm3 (40.89 % theoretical)

0.1 gram water was added and the solids loading of the slurry was reduced to 22.1 vol.%. 2 pellets were slip cast at a pH 4.83.

- Cast 7: weight: 2.97 grams density: 7.95 g/cm3 (41.3 % theoretical)
- Cast 8: weight: 2.614 grams density:8.094 g/cm3 (42.05 % theoretical)

Figure 28 shows the cross-sectional SEM micrographs of a cast with a relative density of 41.17 %. Most soft agglomerates were broken up to smaller ones. Compared to the as-received powders, the cast exhibited more uniform particle sizes. Particles were reasonably densely packed, but some cavities between particles were visible. Cold isostatic pressing can

make those cavities smaller and further increase the green density.

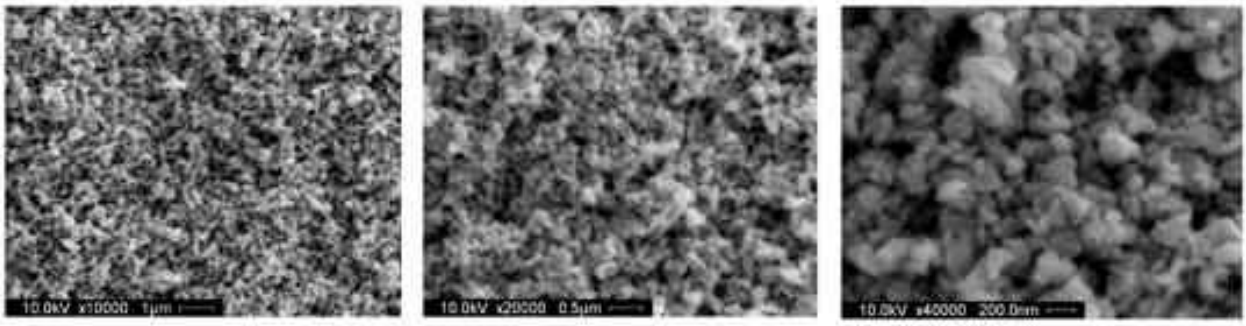

Figure 28: Secondary electron micrographs of the cross-section of a cast with a density of 41.17 %.

4.2.5.3 Casts of Size-separated Fine W Slurry

Slip casting of the size-separated fine W slurry is more challenging because the pH drops faster due to higher reactivity of fine W particles with water. Therefore, the slurry pH was carefully monitored during stirring. The 1st pellet was slip cast at a solids loading of 27.8 vol.% and a slurry pH of 4.72. It had a lower center and much higher edge because the viscosity was relatively high and the slurry had difficulty flowing. 0.1 g of 11 wt.% TMAH solution and 0.15 gram water were added to the slurry and it was stirred for 7 minutes. The solids loading was reduced to 26.7 vol.% and the 2nd pellet was slip cast at a pH 4.83. It still had a lower center and much higher edge because the slurry viscosity was still high. 0.33 gram water and 0.1 gram of 33 wt.% TMAH solution were added and the solid loading was 24.3 vol.%. The 3rd pellet was slip cast at a pH 6.06 and had a lower center and high edge. The densities of the 1st batch of casts were not measured, but expected to be low. One reason is that the fine particles were very small and had high specific surface areas, therefore more reactive and had a higher dissolution rate of surface oxides than coarser ones. 24 minutes of stirring was too long generating a high

concentration of H^+ and thus decreasing the pH value of the slurry.

The remaining slurry was washed with water for the 15th time. 0.25 g of 33 wt.% TMAH solution and 20 ml of water were added and the suspension was ultrasonicated using 13 watts for 30 minutes. The suspension was washed with 30 ml of water for the 16th time and centrifuged at 8500 rpm for 30 minutes. The supernatant liquid had a pH 6.01 and removed. 0.77 g of water was added to the centrifuged W and was stirred by a magnetic stirrer for 8 minutes. The solids loading was 27.8 vol.% and the slurry viscosity was relatively low and could easily flow. The 4th pellet was slip cast twice at a pH 4.9. It took 15 minutes for the first layer to dry and another 15 minutes for the second layer to dry. Its weight was 3.842 grams and had a density of 7.949 g/cm^3 (41.293 % theoretical density). The 5th pellet was slip cast twice at a pH 4.7. It weighed 3.623 grams and had a density of 7.739 g/cm^3 (40.2 % theoretical density). The 6th pellet was slip cast at a pH 4.4 and had a lower center and high edge because the viscosity was increased.

The 2nd slurry was stirred for only 8 minutes and had much lower viscosity than the 1st one. This is the main reason why the 2nd batch of casts had higher densities than the 1st batch of casts. The remaining slurry was ultrasonicated in 15 ml water under a power of 14 watts for 20 minutes. It was washed with 30 ml of water for the 17th time and centrifuged at 8500 rpm for 30 minutes. 20 ml of water and 0.5 g of 33 wt.% TMAH solution were added to the centrifuged W and the mixture was ultrasonicated under a power of 14 watts for 15 minutes. It was washed with 30 ml water for the 18th time and centrifuged at 8500 rpm for 28 minutes. The slightly

yellow supernatant liquid with a pH of 6.12 was removed. 0.4 gram water was added to the centrifuged W and the mixture was stirred using a magnetic stirrer for 5 minutes. The solids loading was 28.7 vol.% and the viscosity was relatively low. The 7th pellet was slip cast. It took 15 minute for the slurry to dewater. Its weight was 3.98 grams.

Slip casting of size-separated fine W slurry was different from slip casting of W slurry without size-separation. The size-separated fine W slurry had a much lower casting rate than the slurry without size separation. It took about 15 minutes for the fine W slurry to dewater in a plaster mold while it took about 3 minutes for the slurry without size-separation to dewater at the same solids loading. A dense cast formed from the well-dispersed fine W slip had a low permeability and so the casting rate was low. These observations can be explained by slip casting mechanisms. Several investigators adopted the model of Adcock and McDowall [54], which neglects the resistance of mold to liquid flow and treats the slip casting process in terms of liquid flow through the porous consolidated layer. Application of Darcy's law gives a parabolic relation for the increase in the cast thickness, L_c, with time t:

$$L_c^{\,2} = \frac{2K_cPt}{\eta_L(V_c/V_s - 1)} \qquad \text{Equation 9}$$

where K_c is the permeability of the cast, p is the pressure difference across the cast (assumed to be constant and equal to the suction pressure of the mold), η_L is the liquid viscosity, V_c is the

volume fraction of the solids in the cast, and V_s is the volume fraction of solids in the slurry. For a cast consisting of spherical monodisperse particles with a diameter D, the permeability of the cast, K_c can be expressed as:

$$K_c = \frac{D^2(1-V_c)^2}{180V_c^2} \qquad \text{Equation 10}$$

The size-separated fine W cast had a much smaller average particle diameter and so exhibited a lower permeability and casting rate than the cast without size-separation. The dense cast from a well-dispersed slip had a low permeability therefore the casting rate was low. Such low casting rates are not economical and feasible for industrial operations so the slip is partially deflocculated. Aksay and Schilling [55] have investigated the filtration resistance for various consolidated layers having different sizes of monosized particles and different packing densities. They demonstrates that to increase the filtration rate, the particle size should be increased and/or the packing densities should be decreased. They also show that particle sizes close to 100 nm gives a very high filtration resistance even at a low packing density of the layer. 100 nm is the lower limit of ideal powders and is a critical particle size below which problems with various forming techniques accumulate. The problems include powder agglomeration and decreased solid loading in the slips.

Slip casting of size-separated fine W slurry is also different from slip casting of W slurry

without separation, because the axial shrinkage of the slip cast from the separated fine W slurry is slightly larger than that from the W slurry without size-separation. The degree of shrinkage depends on the particle size distribution. A higher proportion of fine particles results in a larger shrinkage.

In addition, the size-separated fine W slurry requires shorter magnetic stirring time (~8 minutes) than the W slurry without size-separation (~24 minutes) before slip casting. The reason is that the size-separated fine W slurry has a higher reactivity and dissolution rate in water due to a higher surface area therefore exhibits faster drop in suspension pH than the the W slurry without size separation.

A picture of the 4th fine W cast is presented in Figure 29 (a). It had a diameter of 0.49 inch and weighed 3.842 g. Its density was 7.95 g/cm^3 or 41.29 % theoretical density. It was a cast with a high density we obtained. Figure 29 (b) shows a secondary electron micrograph of the top surface of the slip cast.

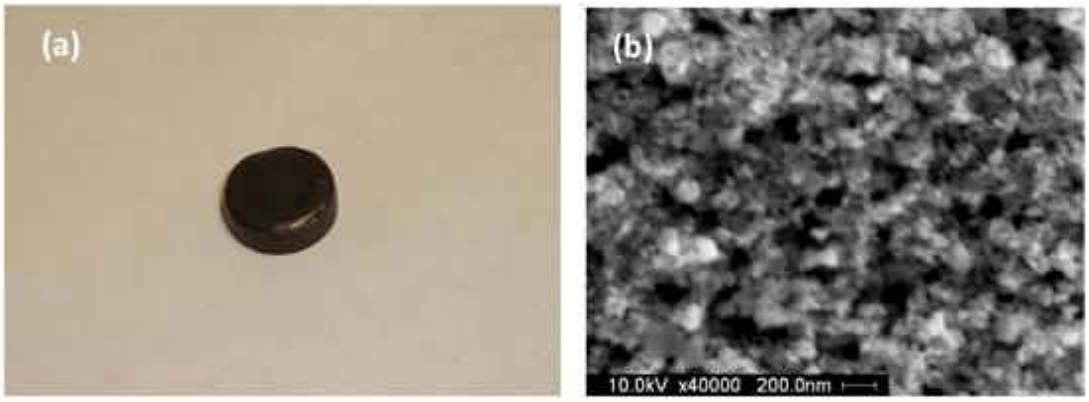

Figure 29: (a) The 4th cast of size-separated fine W slurry (b) A secondary electron micrograph of the top surface of the cast.

Figure 30 shows secondary electron micrographs of the cross-section of one fine cast with a 40.2 % relative density. No large agglomerates with sizes larger than 300 nm are observed and typical particle sizes are approximately 100 nm. Particles are closely packed and no large pores are found.

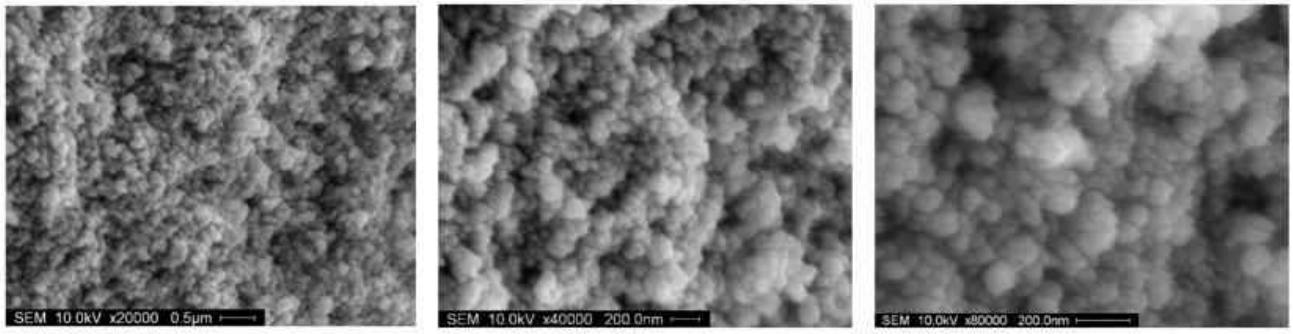

Figure 30: secondary electron micrographs of the cross-section of the 5th cast of size-separated fine W powders.

Size-separated fine casts had much smaller particle sizes than those without size separation as shown in Figure 31.

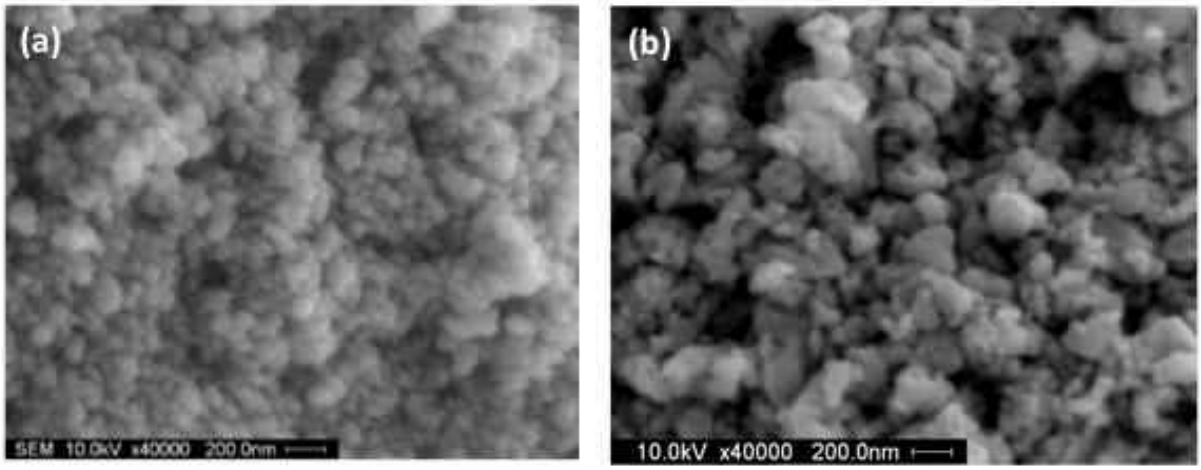

Figure 31: SEM micrographs of the cross-section of (a) the 5th cast of size-separated W and (b) a cast without size separation.

In summary, repeated ultrasonication and washing removed initial surface oxides of the as-received W powders and inhibited the reactivity of W nanoparticles to water and broke down some agglomerates, leading to more stable suspensions. The pH of W slurry played an important role and was adjusted close to 5 to obtain the lowest viscosity and highest solids loadings. The W oxides produced during repeated washing may hinder sintering process. Hydrogen reduction before sintering can reduce some W oxides and facilitate densification.

4.2.6 W in Aqueous PEI Solutions

PEI is a cationic polyelectrolyte that acts as a weak base due to the pH-dependent protonation of its amine groups in water. At a pH 2, 70 % of the amine groups carry a positive charge, while the charged fraction decreases with increasing pH. PEI is weakly charged when pH is increased above 8-9. PEI is expected to adsorb to a negatively charged surface. WO_3 is

acidic and is negatively charged above its isoelectric point. Previous study showed that PEI adsorbed on WO_3 over a wide pH and induced an electrosteric repulsion leading to a charge reversal from negative to positive [56].

4.2.6.1 Effect of PEI concentration on the dispersion of W powders

Figure 32 shows the SEM micrographs of 2 g of W powders dispersed in 5 ml of 0.7 %, 0.8 % and 0.9 % PEI water solutions. Figure 33 shows the SEM micrographs of 2 g of W powders dispersed in 5 ml of 1 % and 2 % PEI water solutions. 0.9 % and 1 % PEI resulted in better dispersion and smaller particle sizes than other concentrations.

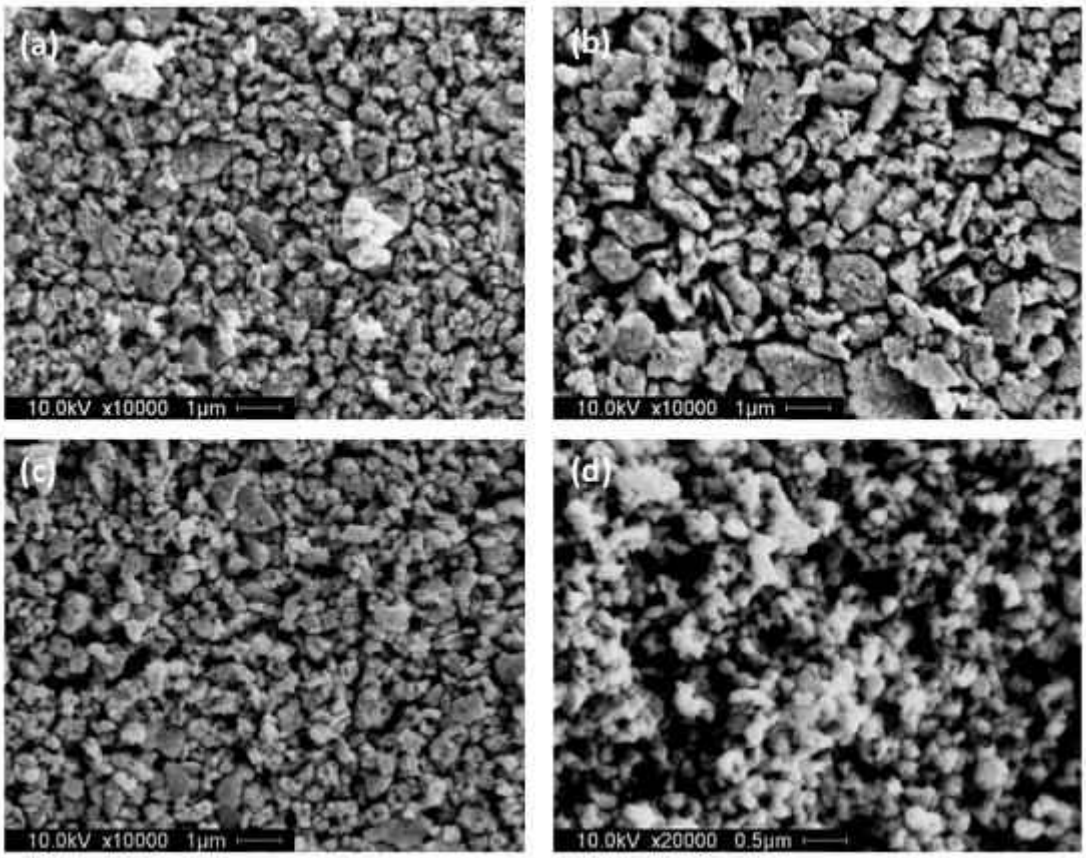

Figure 32: Secondary electron micrographs of the bottom sides of 2 g of W in 5 ml of (a) 0.7 % , (b) 0.8 % and (c, d) 0.9 % aqueous PEI solutions.

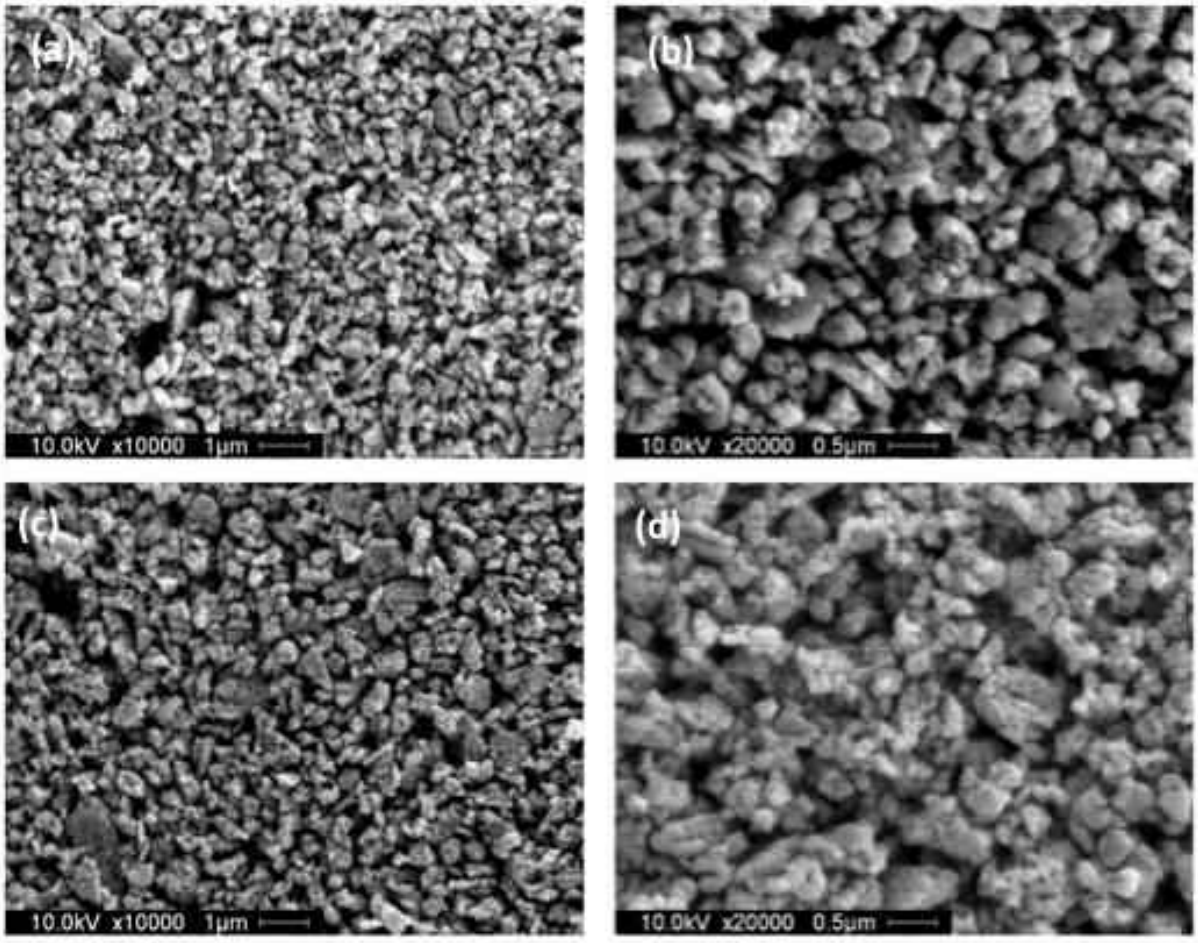

Figure 33: Secondary electron micrographs of the bottom sides of 2 g of W in 5 ml of (a, b) 1 %, and (c, d) 2 % aqueous PEI solutions.

Figure 34 illustrates the sedimentation of 2 grams of W powders after ultrasonication under a power of 10 watts for 90 minutes in 5 ml of aqueous PEI solutions. The suspension with 1% PEI exhibited black supernatant liquid and the lowest packed-bed height. The other suspensions had clear supernatant liquid and the packed-bed height decreased with increasing PEI concentration from 1.5 % to 3 %.

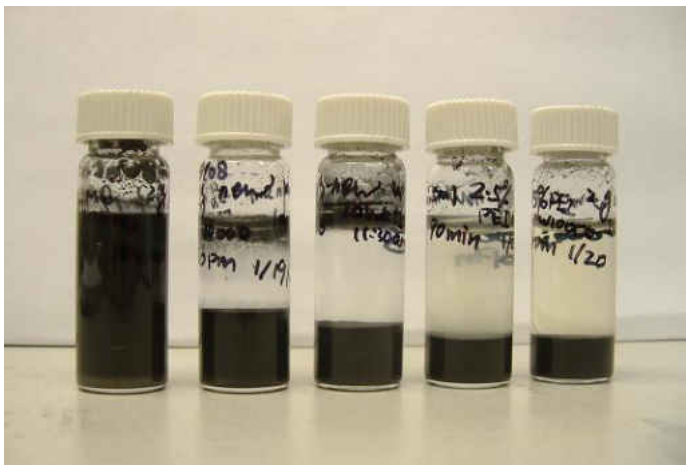

Figure 34: Sedimentation of 2 grams of W powder after ultrasonication under a power of 10 watts for 90 minutes in 5 ml of PEI water solution. PEI concentration from left to right is 1 %, 1.5 %, 2 %, 2.5 % and 3 %.

Figure 35 shows the sedimentation of 2 grams of W powder after ultrasonication under a power of 10 watts for 60 minutes in 5 ml of PEI water solution. The packed-bed height decreases with increasing PEI concentration from 2.8 % to 4.7 %. 4.7 % shows the smallest packed-bed height.

Figure 35: Sedimentation of 2 grams of W powder after ultrasonication under a power of 10 watts for 60 minutes in 5ml of PEI water solution. The PEI concentration from left to right is 2.8 %, 3 %, 3.2 %, 3.5 %, 3.9 %, 4.2 %, 4.7 % and 5 %.

Based on the packed-bed height and supernatant liquid color, the optimum PEI concentration was 1 %. Higher PEI concentrations and excessive organic were not necessary and detrimental to W. PEI concentrations lower than 1% were not enough to cover the surfaces of all W particles. The SEM micrographs in Figure 33 also showed 1% PEI led to the best dispersion, therefore the effect of ultrasonic time on the dispersion of W powders in 1% PEI water solution was investigated.

4.2.6.2 Effect of ultrasonic time on the dispersion of W powders

The pH values of 4 grams of 4 vol.% W in 5ml of 1% PEI under a power of 4 watts decreased with longer ultrasonic time as shown in Figure 36.

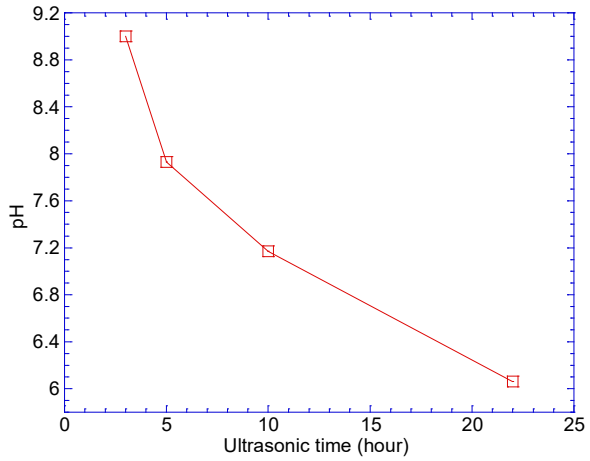

Figure 36: Variation of pH with ultrasonic time for 4 vol.% W in 1 %PEI water solution

Figure 37 shows the SEM micrographs of the bottom sides of the 4 grams of 4 vol.% W suspensions in 1 % PEI after ultrasonication for 10 and 22 hours under a power of 4 watts. Longer ultrasonication resulted in slightly better dispersion and smaller particles.

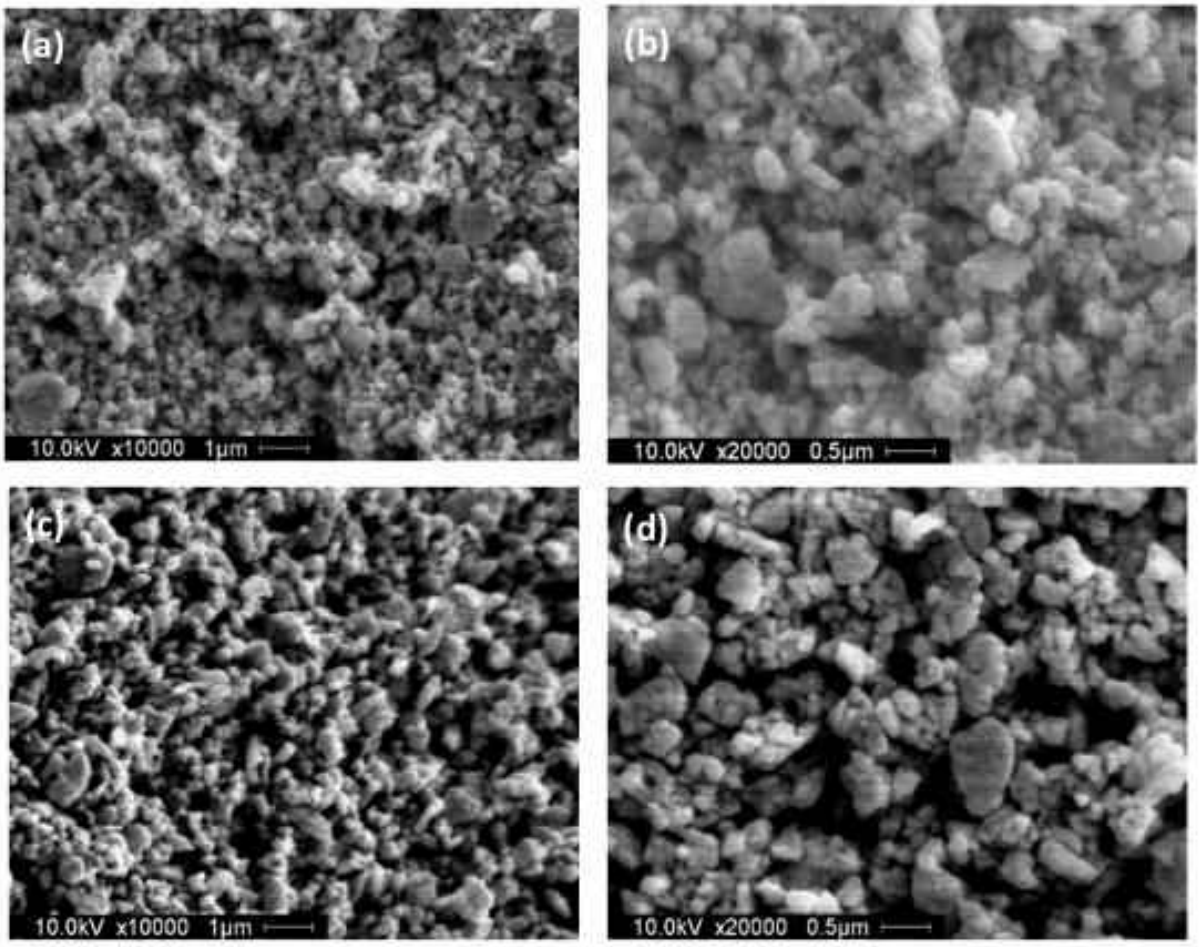

Figure 37: SEM micrographs of the bottom sides of the 4 g of 4 vol.% W suspensions in 1 % PEI after ultrasonication for (a, b) 10 hours, and (c, d) 22 hours using 4 watts.

Figure 38 shows the SEM micrographs of the bottom sides of 4 vol.% W suspensions with 1 % PEI after ultrasonication under a power of 6 watts for 5, 8 and 10 hours. Ultrasonication for 10 hours led to the best dispersion and typical sizes of agglomerates/ particles were less than 1 µm. The measured pH values after 5, 8 and 10 hours were 5.94, 5.88 and 5.86, respectively and were reasonably stable.

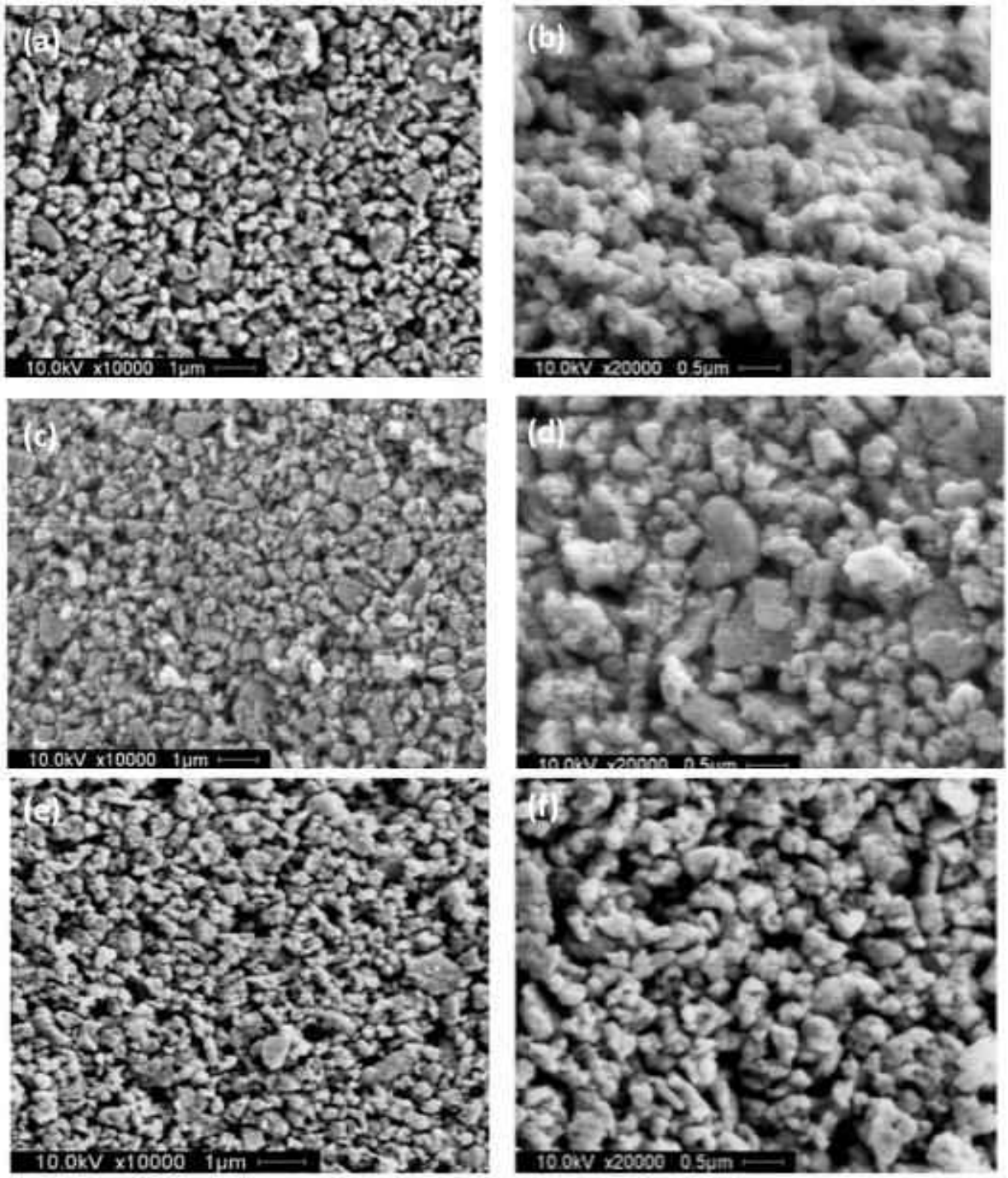

Figure 38: SEM micrographs of 4 grams of 4 vol.% W in 1 % PEI water solution after ultrasonication for (a, b) 5 hrs, (c, d) 8 hrs, and (e, f) 10 hrs using 6 watts.

Figure 39 shows the SEM micrographs of the bottom sides of 2 grams of W ultrasonicated in 6 ml of 5 % PEI under a power of 20 watts for 10 hours followed by washing

with water twice.

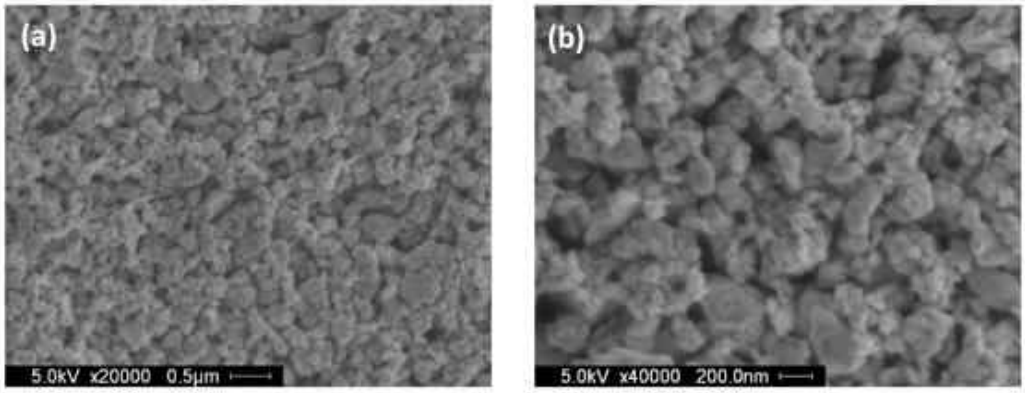

Figure 39: SEM micrographs of 2 grams of W ultrasonicated in 6 ml of 5 % PEI under a power of 20 watts for 10 hours followed by washing with water twice.

Figure 40 shows the SEM micrographs of the bottom sides of 2 grams of W ultrasonicated in 6 ml of 5 % PEI under a power of 20 watts for 1.5 hours followed by washing with water twice. Ultrasonication under a power of 20 watts for 10 hours and 1.5 hours resulted in similar dispersion. After washing with water twice, most excess PEI in the suspensions were removed.

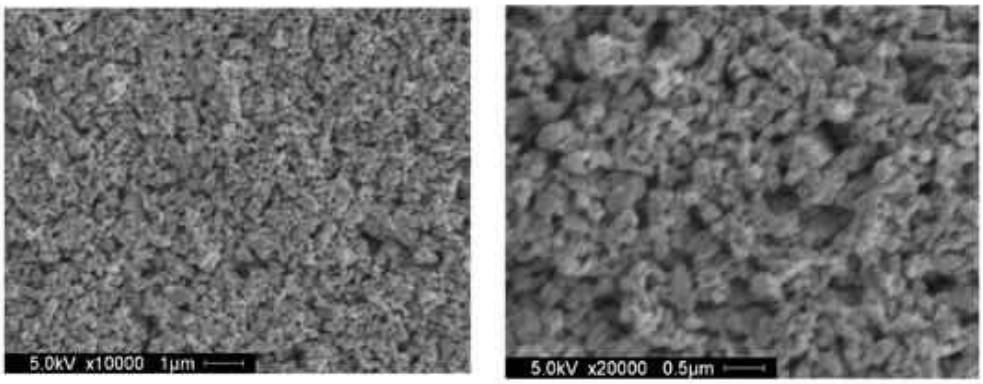

Figure 40: SEM micrographs of 2 grams of W ultrasonicated in 6 ml of 5 % PEI under a power of 20 watts for 1.5 hours followed by washing with water twice.

2 grams of W powers were ultrasonicated in 5 ml of 0.8 % PEI water solution under a power of 3 watts for 130 minutes. A picture was taken 40 hours after ultrasonication as shown

in Figure 41 and the upper liquid was still black. Another 2 grams of W powders were ultrasonicated in 5 ml of 0.8 % PEI water solution under a power of 6 watts for 130 minutes and another picture was taken 14 hours after ultrasonication shown in Figure 41. All W settled down and the upper portion of the liquid was clear indicating bad dispersion. At the same W and PEI concentrations, and ultrasonic time, 3 watts resulted in better dispersion than 6 watts. One reason for this is that it is more favorable for PEI to be adsorbed onto the W particle surfaces under a lower ultrasonic power.

Figure 41: 2 grams of W powers ultrasonicated in 5 ml of 0.8 % PEI water solution for 130 minutes under a power of (left) 3 watts, and (right) 6 watts.

4.2.7 W in Aqueous PAH Solutions

Figure 42 shows the SEM micrographs of 0.5 g of W nanopowders dispersed in 10 ml of 0.01 M PAH water solution. Polymer bridging was observed for unwashed W powders and W particles were stuck together. Washing once or twice with water removed some excessive PAH and significantly reduced the sizes of agglomerates to 400 nm. Washing 3 times with water resulted in worse dispersion because there was no enough PAH to cover the total W surface.

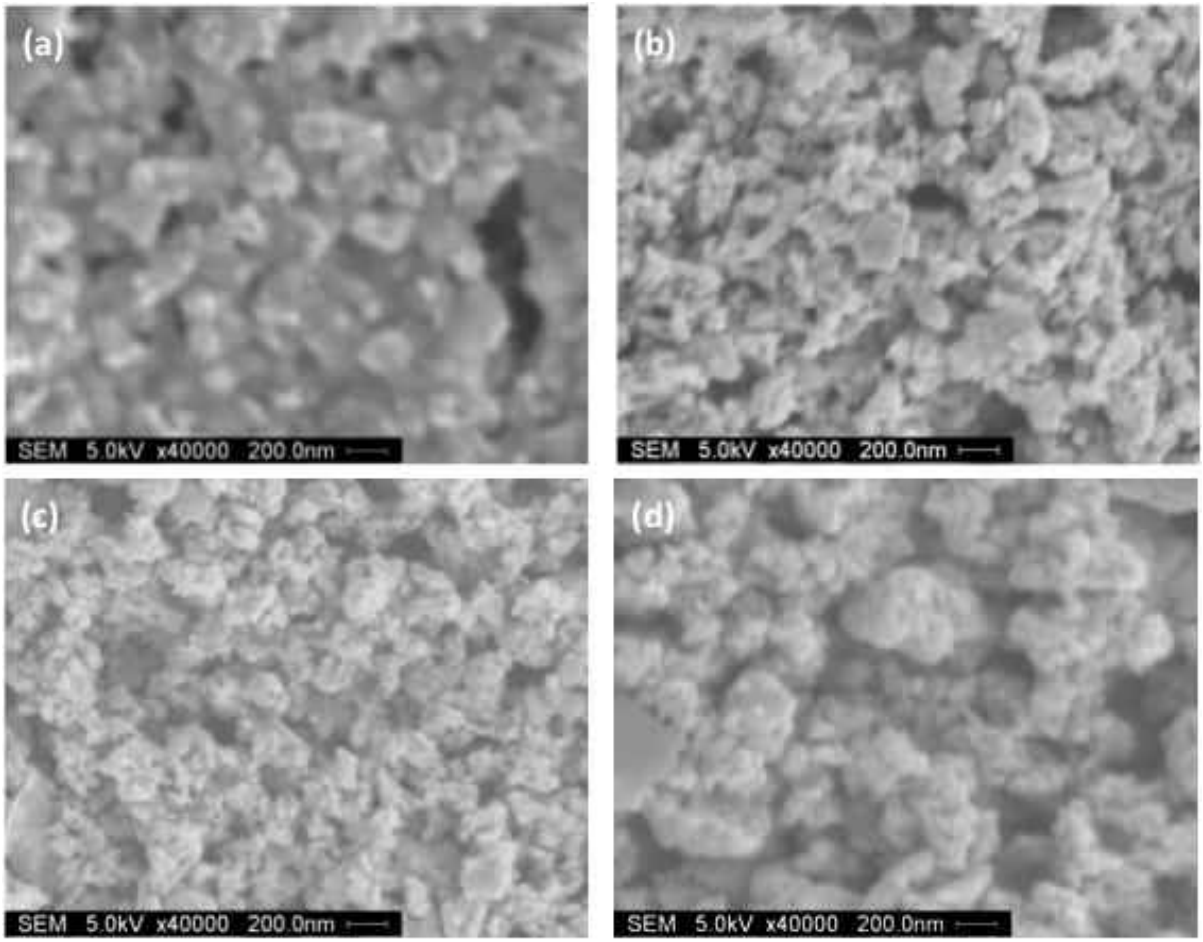

Figure 42: SEM micrographs of 0.5 g of W powder in 10 ml of 0.01 M PAH. (a) unwashed, (b) washed once with water, (c) washed twice with water and (d) washed with water 3 times.

Figure 43 shows the SEM micrographs of 0.5 g of W in 10 ml of 0.02 M PAH water solution. Dispersion improved with increasing cycle of washing with water. Washing with water 3 times significantly reduced the sizes of agglomerates.

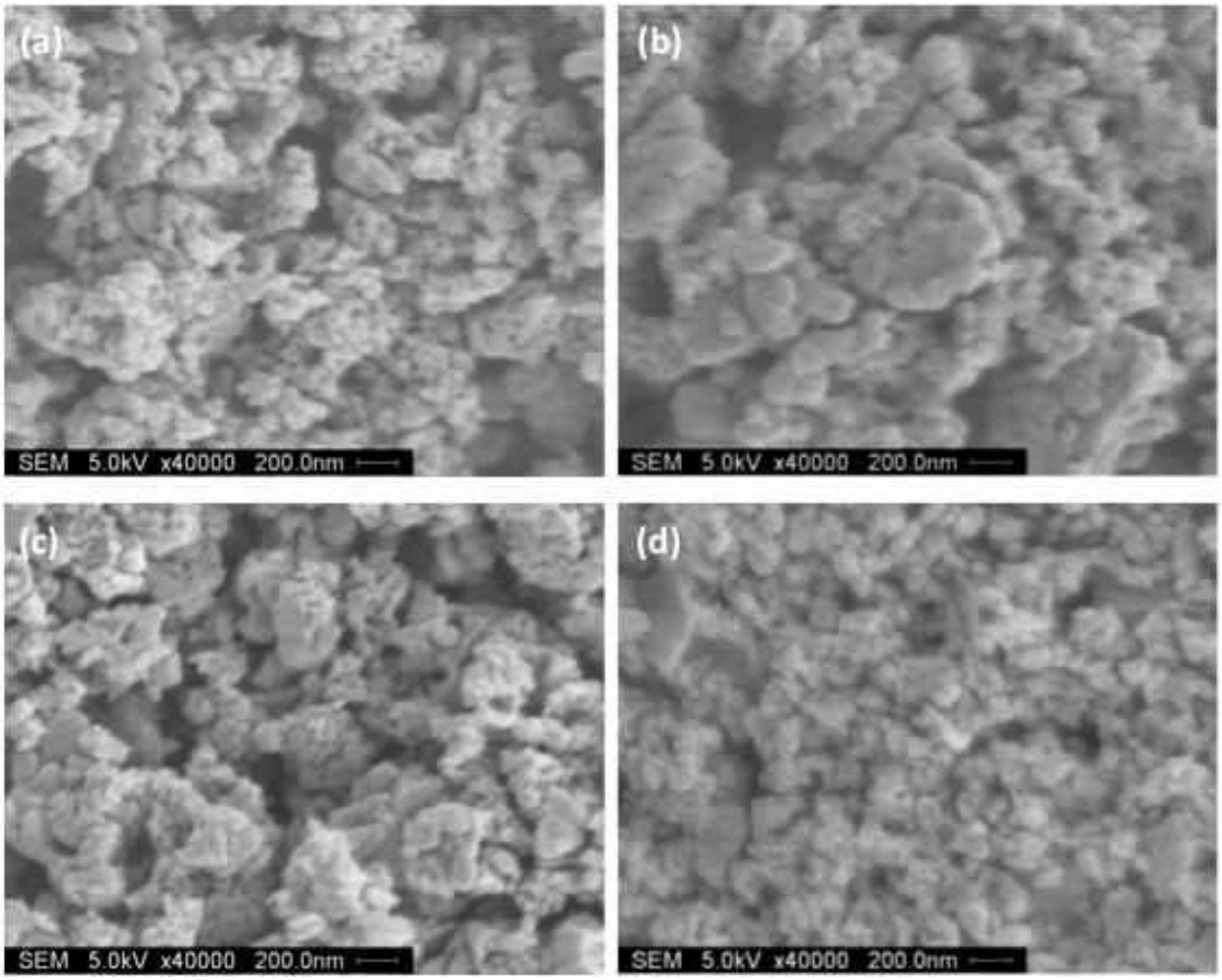

Figure 43: SEM micrographs of 0.5 g of W powder in 10 ml of 0.02 M PAH. (a) unwashed, (b) washed with water once, (c) washed with water twice, and (d) washed with water 3 times

Figure 44 shows the SEM micrographs of 0.5 g of W nanopowders in 10 ml of 0.03 M PAH water solution. Significant agglomeration was observed in unwashed and washed-once W particles. Washing twice obviously improved the dispersion and typical agglomerate sizes ranged from 200 to 500 nm.

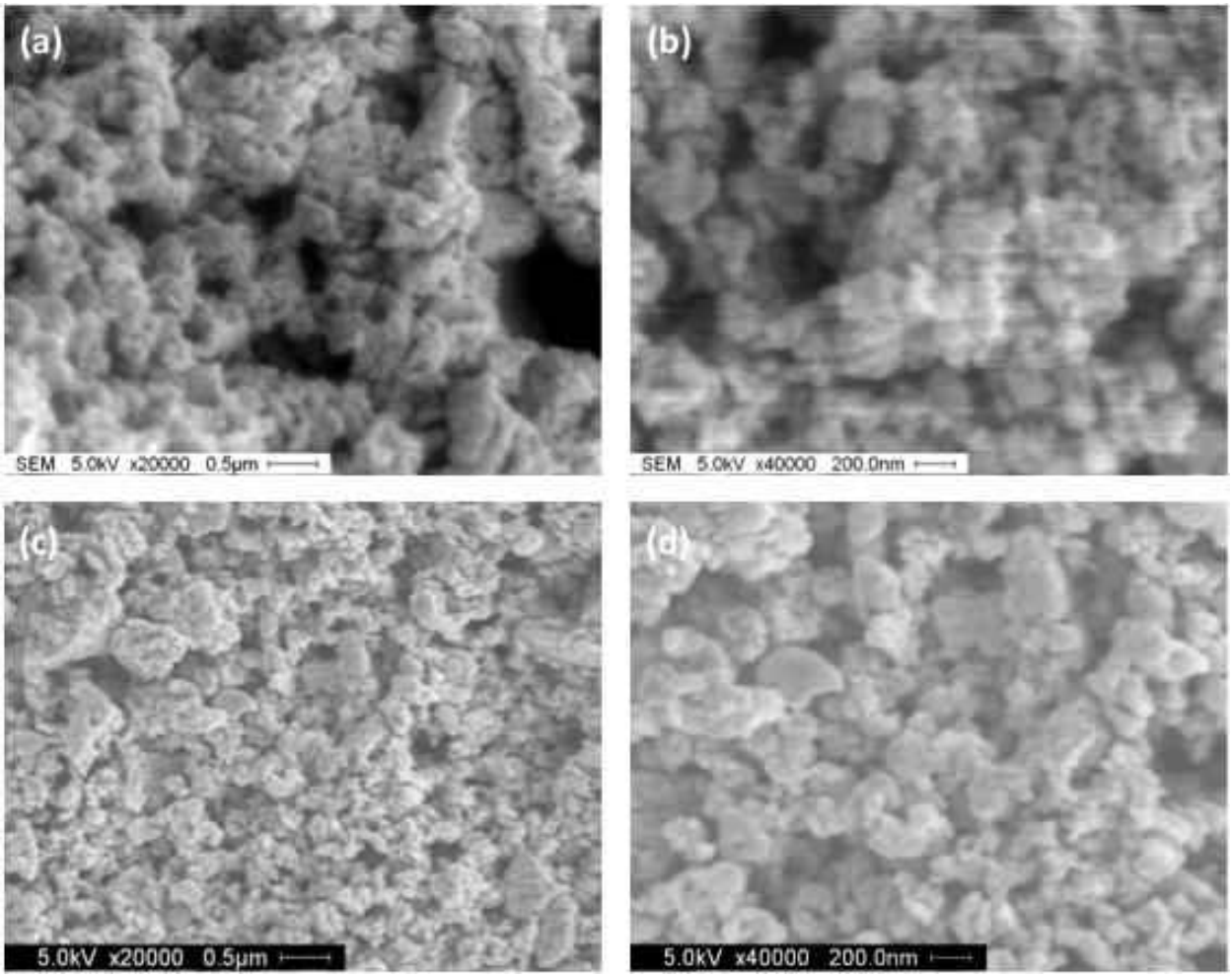

Figure 44: SEM micrographs of 0.5 g of W powder in 10 ml of 0.03 M PAH. (a) unwashed, (b) washed once with water, and (c, d) washed twice with water.

Figure 45 shows the SEM micrographs of 0.5 g of W nanopowders in 10 ml of 0.04 M PAH water solution. Typical sizes of agglomerates for unwashed powders were 1-2 μm and slightly reduced to 1 μm after washing once. Washing twice greatly reduced the sizes of agglomerates to 200-500 nm.

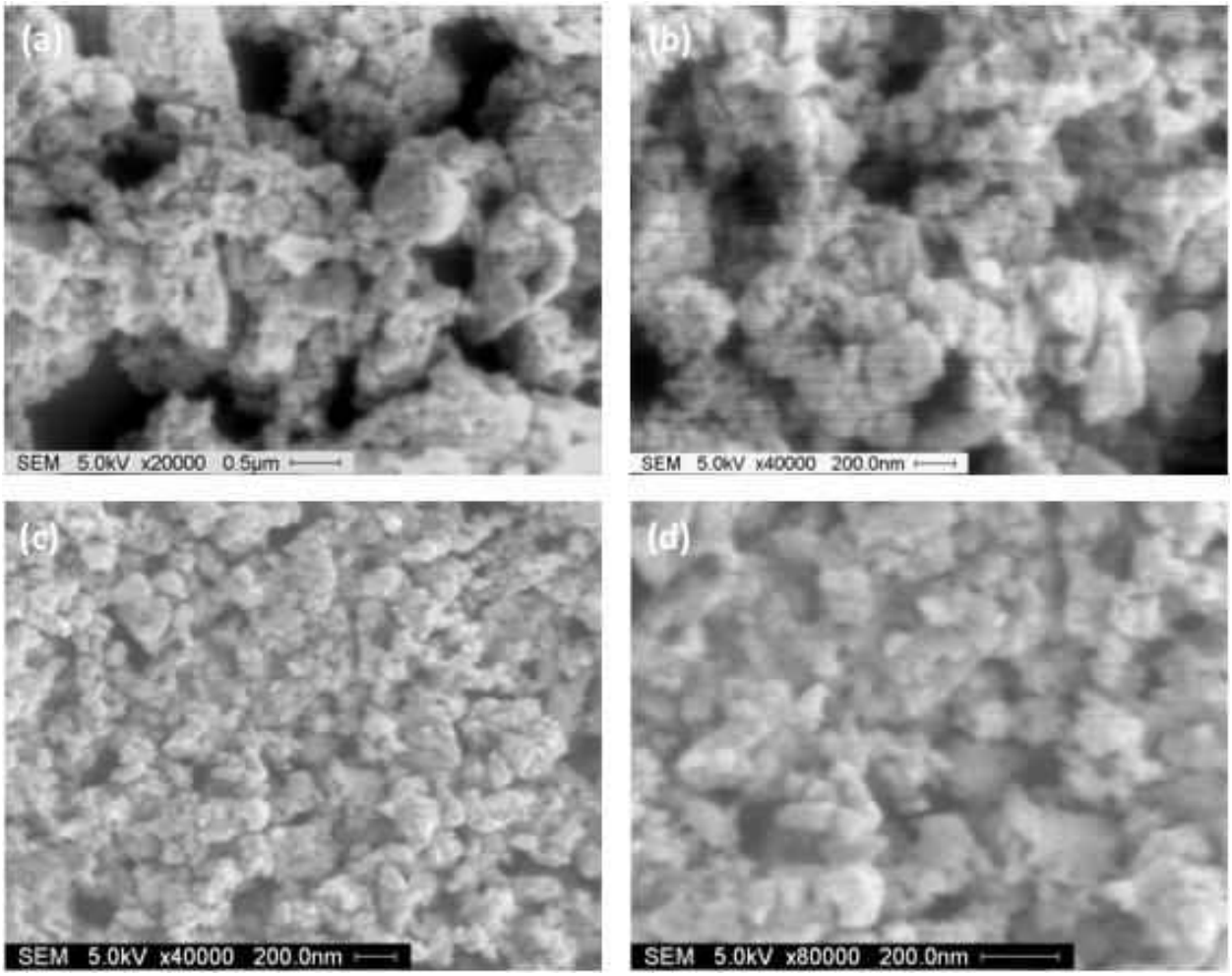

Figure 45: SEM micrographs of 0.5 g of W powder in 10 ml of 0.04 M PAH. (a) unwashed, (b) washed with water once, (c, d) washed with water twice.

Figure 46 illustrates the SEM micrographs of 0.5 g of W nanopowders in 10 ml of 0.05 M PAH water solution. Agglomerates with sizes of 1-2 μm were observed for the unwashed W powders and W powders washed with water twice. The reason is that 0.05 M PAH was too high leading to bridging of PAH.

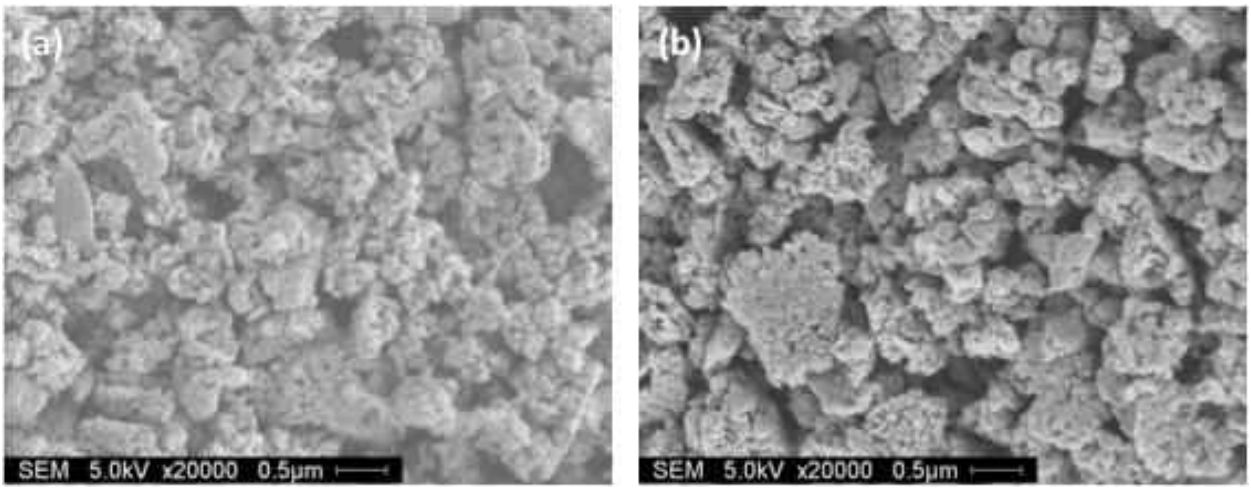

Figure 46: SEM micrographs of 0.5 g of W powder in 10 ml of 0.05 M PAH. (a) unwashed, and (b) washed twice with water.

The typical agglomerate sizes of 0.5 g of W powders in 10 ml of 0.01-0.05 M PAH water solutions based on SEM observations are listed in Table 11. Washing with water twice for W powders in 0.03 M and 0.04 M PAH water solutions significantly improved the dispersion and the sizes of agglomerates ranged from 200-500 nm.

Table 11: Agglomerate sizes of 0.5 g of W powders in 10 ml of 0.01-0.05 M PAH

Variable	10 ml (unwashed)	10ml (washed once)	10ml (washed twice)
0.01M PAH	Bridging of PAH	~400 nm	200-400 nm
0.02M PAH	600 nm-1μm	600 nm-1μm	400-600 nm
0.03M PAH	~1μm	~1 μm	200-500 nm
0.04M PAH	1-2 μm	~1 μm	200-500 nm
0.05M PAH	~1-2 μm	~1-2 μm	~1 μm

4.2.8 W in Oleic Acid and Ethanol

Oleic acid is a deflocculant/dispersant. The effects of oleic acid concentration and ultrasonic time on the dispersion of W nanopowders in ethanol were investigated. 0.005, 0.01, 0.02 and 0.1 gram of oleic acid were mixed with 2 grams of W nanopowders and the corresponding oleic acid weight concentrations relative to W were 0.25 %, 0.5 %, 1 % and 5 %, respectively. The desired amount of oleic acid was mixed in 10 ml of ethanol and then 2 grams of W powders were ultrasonicated in the solution. One benefit of using ethanol and oleic acid was absence of water in the solution therefore no dissolution of W occurred. Figure 47 shows the SEM micrographs of 2 grams of W dispersed in 0.25 % oleic acid and 10 ml of ethanol under an ultrasonic power of 10 watts. Agglomerates with sizes of 1 μm were observed after 10, 20 and 30 minutes.

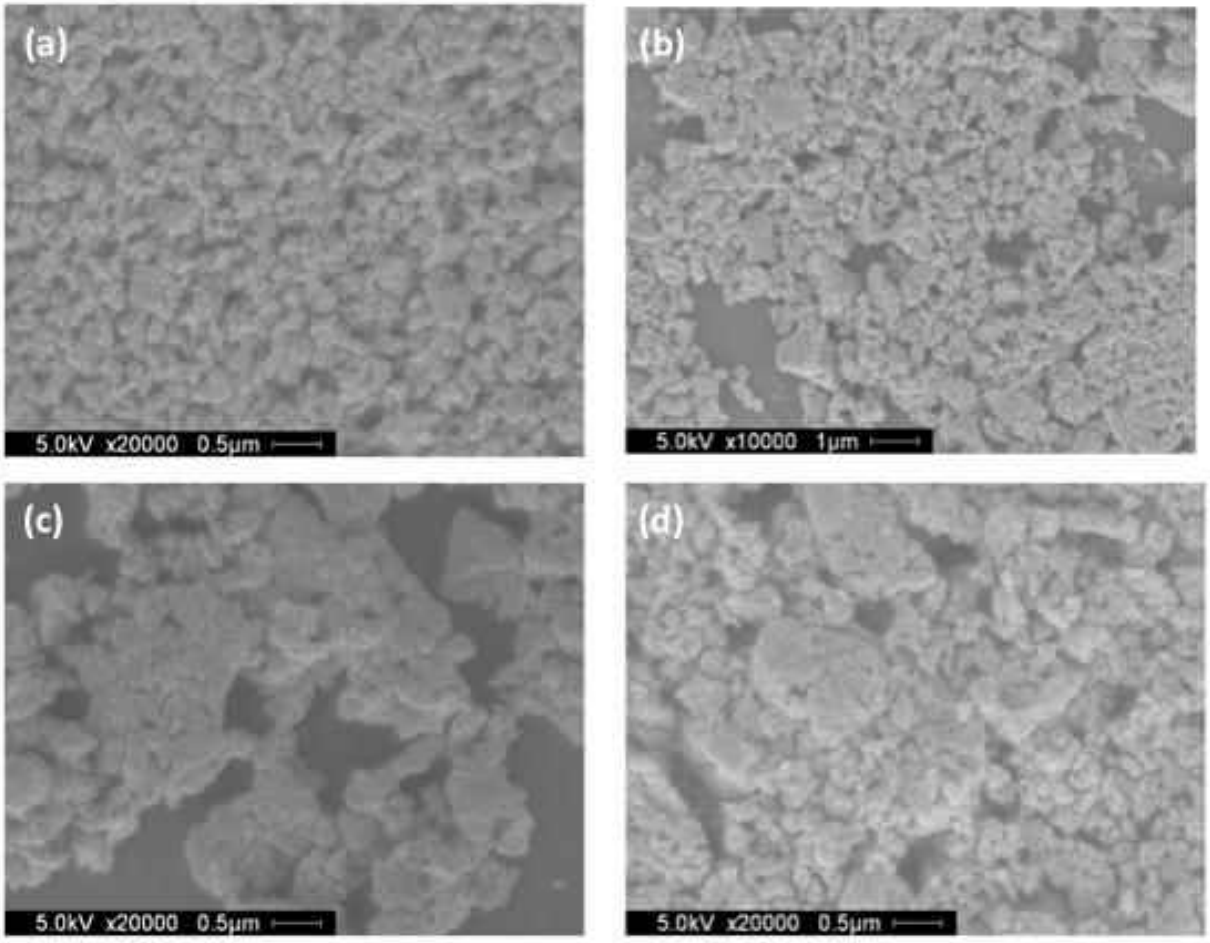

Figure 47: SEM micrographs of 2 g of W dispersed in 0.25 % oleic acid and 10 ml of ethanol under an ultrasonic power of 10 watts for (a) 10 min, (b, c) 20 min, and (d) 30 min.

Figure 48 presents the SEM micrographs of 2 grams of W powders dispersed in 0.5 % oleic acid and 10 ml of ethanol under an ultrasonic power of 10 watts. Large agglomerates (1-2 µm) were observed after ultrasonication for 10 minutes and were broken up to much smaller particles after ultrasonication for 20 minutes. Ultrasonication for 25 minutes resulted in smaller particle sizes ranging from 50 to 150 nm in one layer of W particles. After ultrasonication for 30 minutes, typical particle sizes ranged from 100 nm to 300 nm. Dispersion became worse after ultrasonication for 35 minutes.

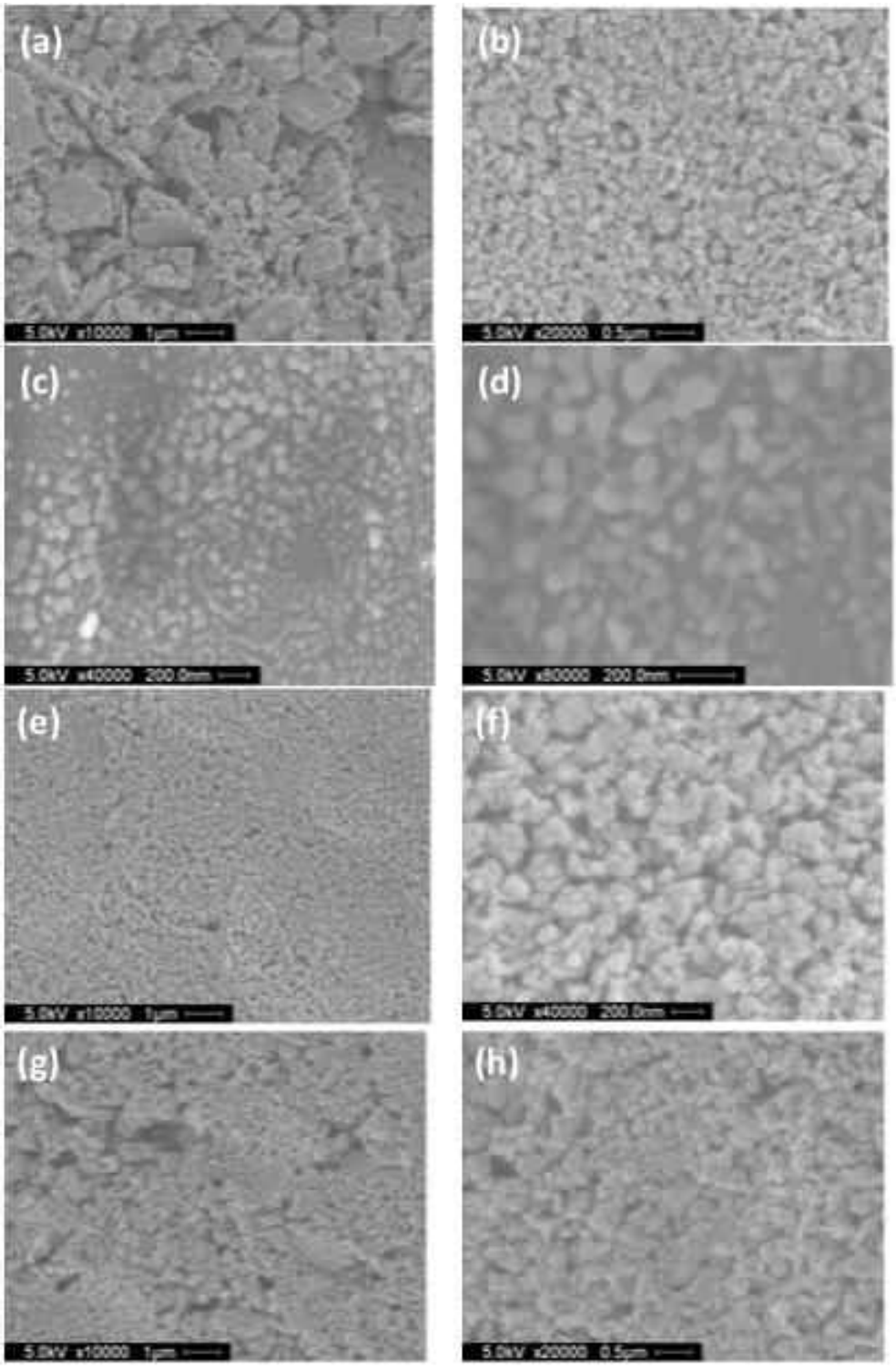

Figure 48: SEM micrographs of 2 g of W dispersed in 0.5 % oleic acid and 10 ml of ethanol under an ultrasonic power of 10 watts for (a) 10 min, (b) 20 min, (c, d) 25 min, (e, f) 30 min, and (g, h) 35 min

To study the effect of ultrasonic power on the dispersion, 2 grams of W powers were dispersed in 0.5 % oleic acid under an ultrasonic power of 15 watts and the SEM micrographs are presented in Figure 49. Ultrasonication for 10 minutes led to the smaller particle sizes and dispersion became worse after 20 and 30 minutes, which was in contrast to the results shown in Figure 48. One reason is that it took shorter time to obtain the best dispersion under a higher ultrasonic power. One common observation in both cases was the worse dispersion after some time because water may be absorbed into ethanol.

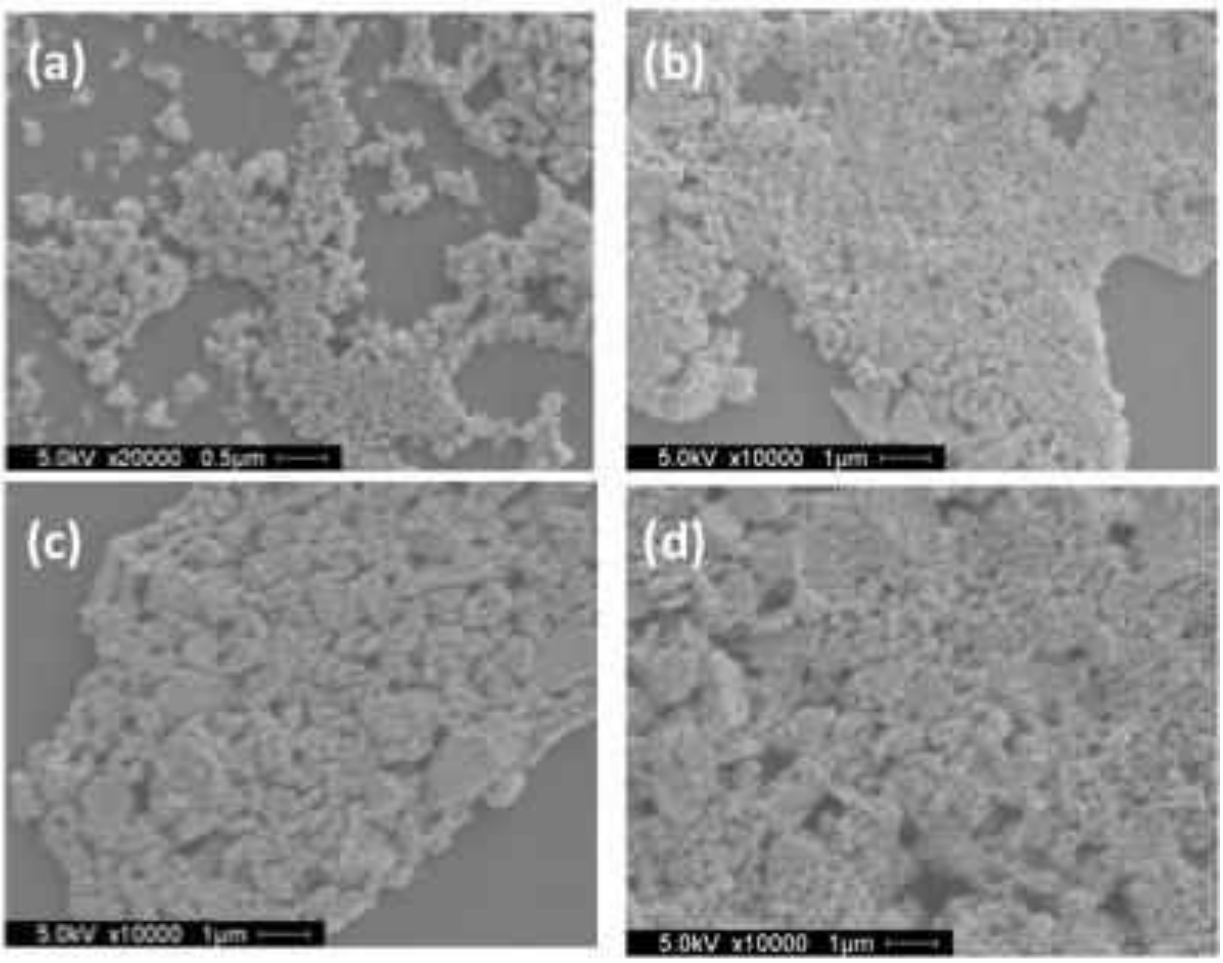

Figure 49: SEM micrographs of 2 g of W dispersed in 0.5 % oleic acid and 15 ml of ethanol under an ultrasonic power of 15 watts for (a, b) 10 min, (c) 20 min, and (d) 30 min.

Figure 50 shows the SEM micrographs of 4 grams of W nanopowders dispersed in 0.5 % and 0.8 % oleic acid and 20 ml of ethanol under an ultrasonic power of 18 watts. 0.8 % oleic acid led to better dispersion than 0.5 % oleic acid. The typical particle sizes ranged from 100 to 200 nm after ultrasonication for 10 minutes in 0.8 % oleic acid suspension.

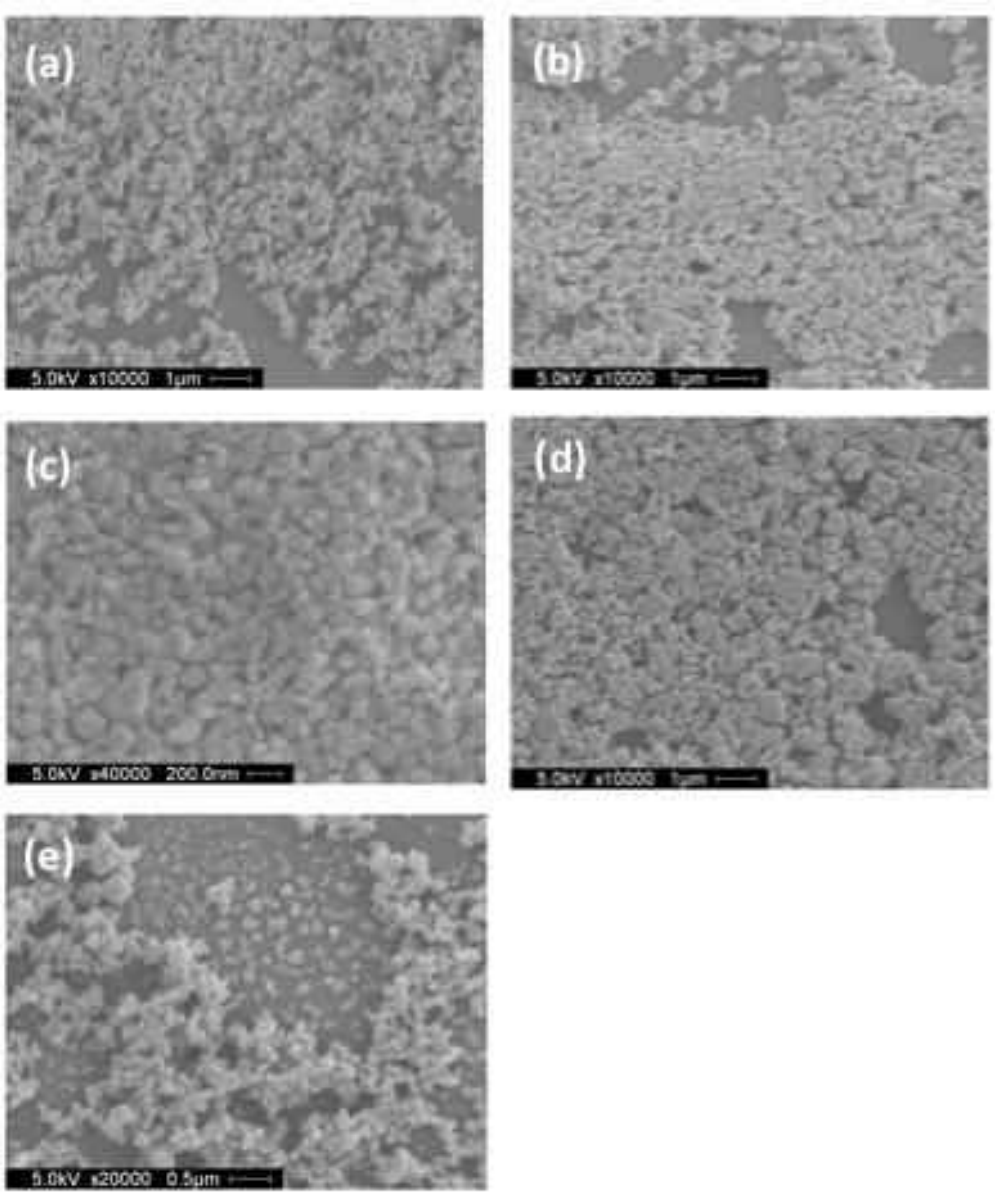

Figure 50: SEM micrographs of 4 g of W powders dispersed in 0.5 % oleic acid and 20 ml of ethanol under an ultrasonic power of 18 watts for (a) 15 min, (b) 30 min. 4 grams of W in 0.8 % and 20 ml of ethanol under an ultrasonic power of 18 watts for (c) 10 min, (d) 20 min, and (e) 30 min.

Figure 51 shows the SEM micrographs of 2 grams of W powders dispersed in 1 % oleic acid and 10 ml of ethanol under an ultrasonic power of 5 watts. The surface of each SEM specimen was rough and had some cavities due to the evaporation of ethanol. The dispersion of W particles was affected by ultrasonic time and 30 minutes led to the smallest particle sizes.

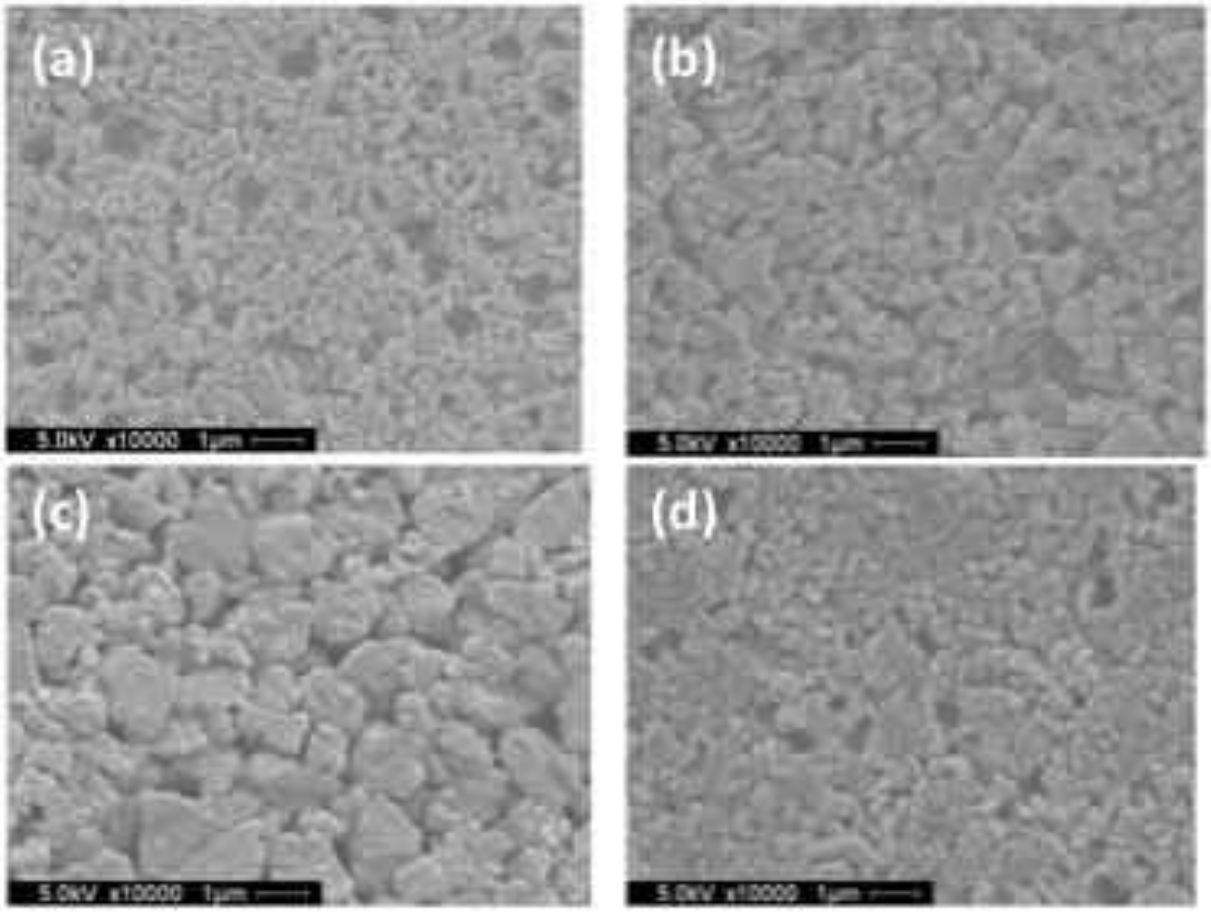

Figure 51: SEM micrographs of 2 grams of W dispersed in 1 % oleic acid and 10 ml of ethanol under an ultrasonic power of 5 watts for (a) 10, (b) 15, (c) 25, and (d) 30 min. (The length of the scale bar is 1 μm.)

Figure 52 shows the SEM micrograph of 2 grams of W powders dispersed in 5 % oleic acid and 10 ml of ethanol. Ultrasonication for 10, 20 and 25 min resulted in similar dispersion with agglomerates sizes of 2 μm. 5 % oleic acid was too high to improve dispersion.

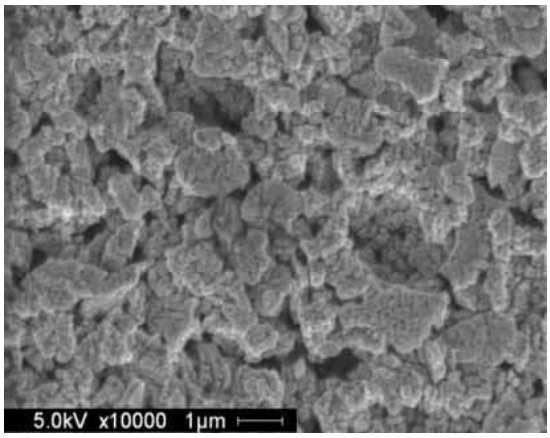

Figure 52: An SEM micrograph of 2 g of W dispersed in 5 % oleic acid and 10 ml of ethanol under an ultrasonic power of 10 watts for 25 min.

4.2.9 W in Fish Oil and Ethanol

Fish oil from Menhaden is one of the most common deflocculants/dispersants and contains more than 20 different types of fatty acids. It is a steric-hindrance deflocculant. 0.01, 0.015, 0.035 and 0.054 gram of FO were separately mixed with 2 grams of W powders and 10 ml of ethanol and the corresponding weight concentrations of FO relative to W were 0.5 %, 0.75 %, 1.75 % and 2.7 %, respectively. Figure 53 shows the SEM micrographs of 2 grams of W powders in 0.5 % FO and 10 ml of ethanol. Agglomerates of sizes of 1-2 µm were observed after ultrasonication for 5 and 20 minutes. Therefore 0.5 % FO was not enough to disperse W powders.

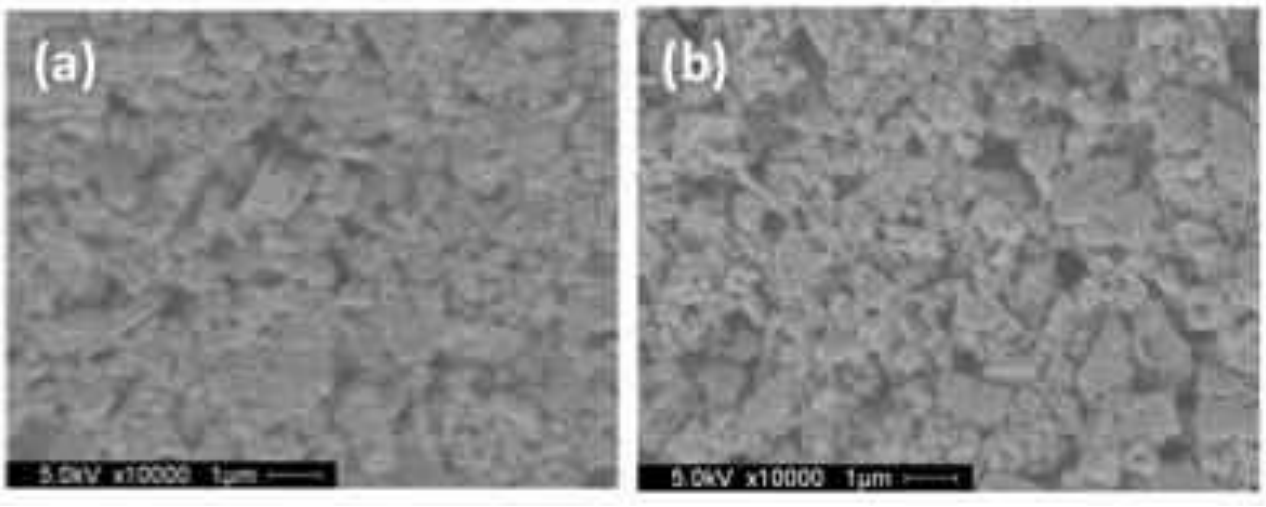

Figure 53: SEM micrographs of 2 g of W powders in 0.5 % FO and 10 ml of ethanol under an ultrasonic power of 13 watts for (a) 5 min, and (b) 20 min.

Figure 54 shows the SEM micrographs of 2 grams of W powders in 0.75 % FO and 10 ml of ethanol. Some cavities were evident because of the evaporation of ethanol. Ultrasonication for 20 minutes resulted in reasonably good dispersion and 10 more minutes did not further improve dispersion.

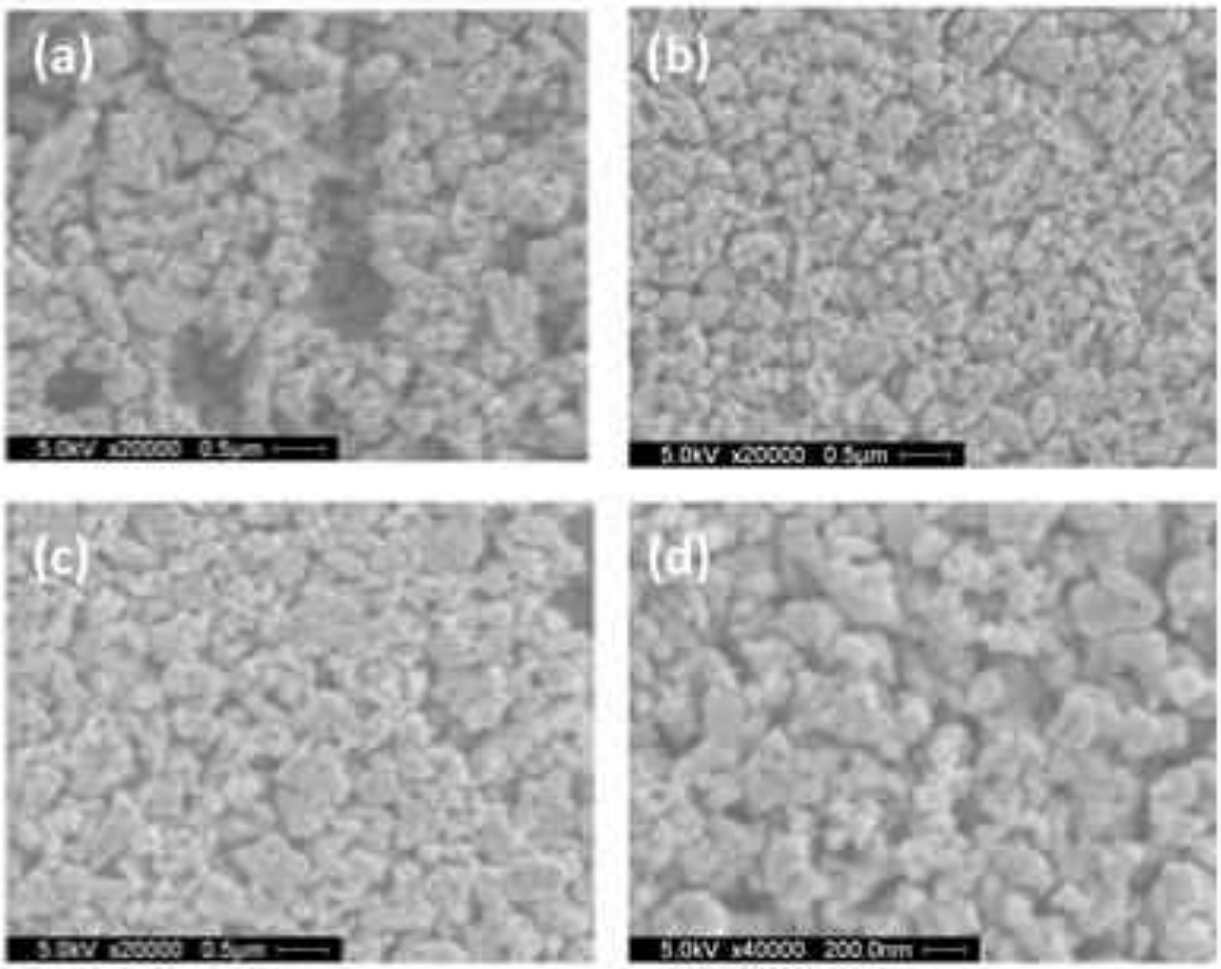

Figure 54: SEM micrographs of 2 grams of W powders in 0.75 % FO and 10 ml of ethanol under an ultrasonic power of 10 watts for (a) 10 min, (b) 20 min, and (c, d) 30 min.

Figure 55 shows the SEM micrographs of 2 grams of W powders in 1.75 % FO and 10 ml of ethanol. After ultrasonication for 10 minutes, some agglomerates with sizes of 1 μm existed. 20 minutes led to significant reduction in the number and sizes of agglomerates and therefore was the optimum ultrasonic time. Dispersion became worse after 25 minutes.

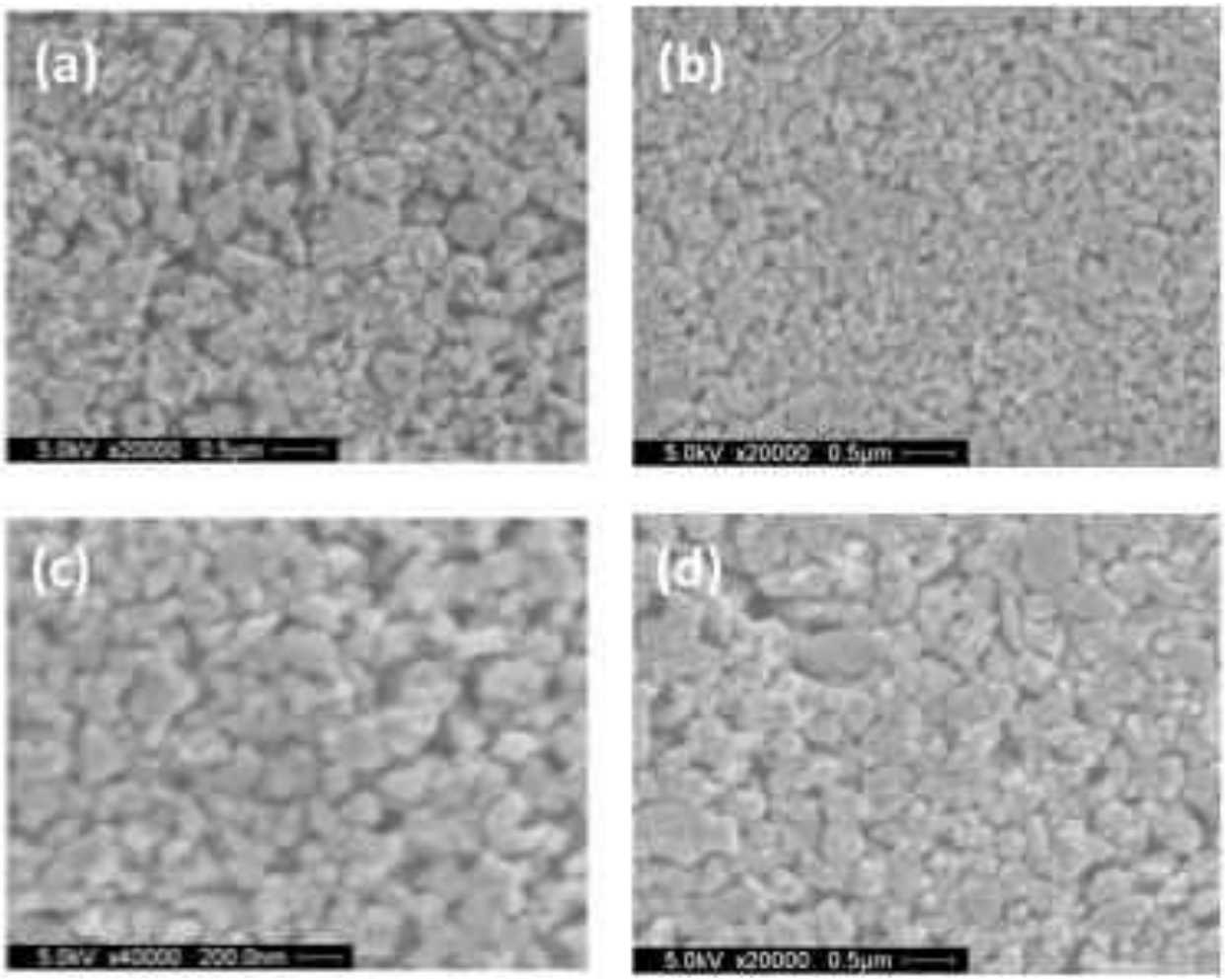

Figure 55: SEM micrographs of 2 grams of W powders in 1.75 % FO and 10 ml of ethanol under an ultrasonic power of 10 watts for (a) 10 min, (b, c) 20 min, and (d) 30 min.

Figure 56 shows the SEM micrographs of 2 grams of W powders in 2.7 % FO and 10 ml of ethanol under a power of 10 watts. Ultrasonication for 20 minutes produced slightly smaller particle sizes than 10 minutes. The dispersion was not good because 2.7 % FO was too high.

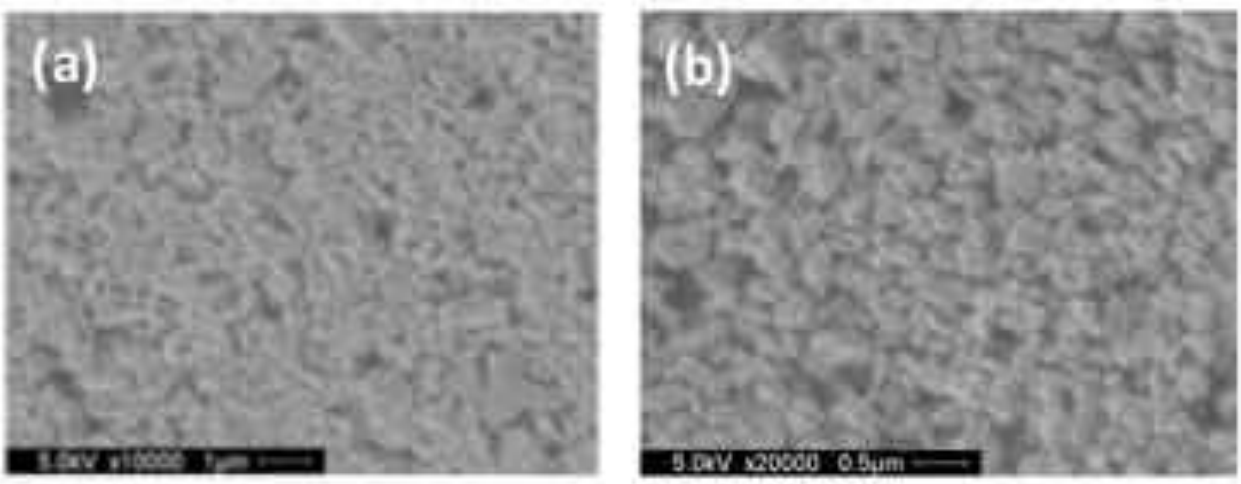

Figure 56: SEM micrographs of 2 grams of W powders in 2.7 % FO and 10 ml of ethanol under an ultrasonic power of 10 watts for (a) 10 min, and (b) 20 min.

In summary, ultrasonication under a power of 10 watts for 20 minutes was sufficient to broken up some agglomerates and resulted in the smaller particle sizes than ultrasonication for 10 minutes. Dispersion did not further improve or was worse after ultrasonication for 30 minutes. The possible reason was that water moisture was absorbed to ethanol, leading to oxidation of W by water. Among all tested FO concentrations, 2 grams of W powders in 1.75 % FO and 10 ml of ethanol under an ultrasonic power of 10 watts for 20 min led to the particle sizes of 100-300 nm.

4.3 Sintered W

4.3.1 Densities of Sintered W

The as received W powders were uniaxially pressed at compaction pressures of 232, 386 and 618 MPa and the green densities were 36%, 38% and 42%, respectively. The compacts were sintered at 900 °C for 2 hours, at 1000 °C for 1 hour and at 1400 °C for 2 hours under atmospheric pressure in argon atmosphere. The fractional theoretical densities of the sintered W pellets increased with increasing compaction pressure and were 0.872, 0.881 and 0.932 as shown in Figure 57.

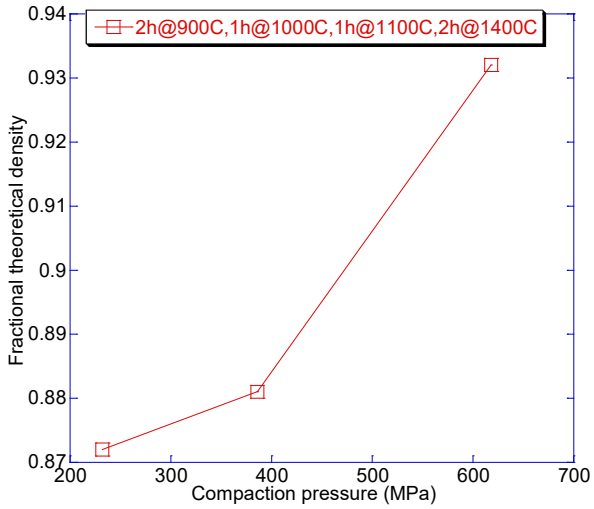

Figure 57: Fractional theoretical densities of the sintered as-received W pellets as a function of uniaxial compaction pressure.

4.3.2 Characterization of Sintered W

The as-received W powders were uniaxially compressed into pellets under compaction pressures of 386 and 618 MPa and cold isostatic pressed into a pellet under a pressure of 350 MPa. The three pellets were sintered at 900 °C for 2 hours, at 1000 °C for 1 hour and at 1400

°C for 2 hours. The fractional theoretical densities were 0.923, 0.943 and 0.922, respectively. The typical SEM micrographs of the cross sections of theses three sintered specimens are presented in Figure 58. The grain sizes of the specimens pressed at 386 MPa and CIP are approximately 1-2 μm. The grain sizes of specimen pressed at 618 MPa are not uniform in the range of 2-4 μm. It is not surprising to see abnormal grain growth due to agglomeration and non-uniform compaction of the as-received powders. The largest grains observed are about 3-4 μm. Another feature is the presence of large pores with sizes up to 1 μm. These large pores are more likely to undergo pore-boundary separation, thus preventing high densities in nanoparticles. Grain growth is inhibited due to grain boundary pinning by pores, but is enhanced after pore-boundary separation [57].

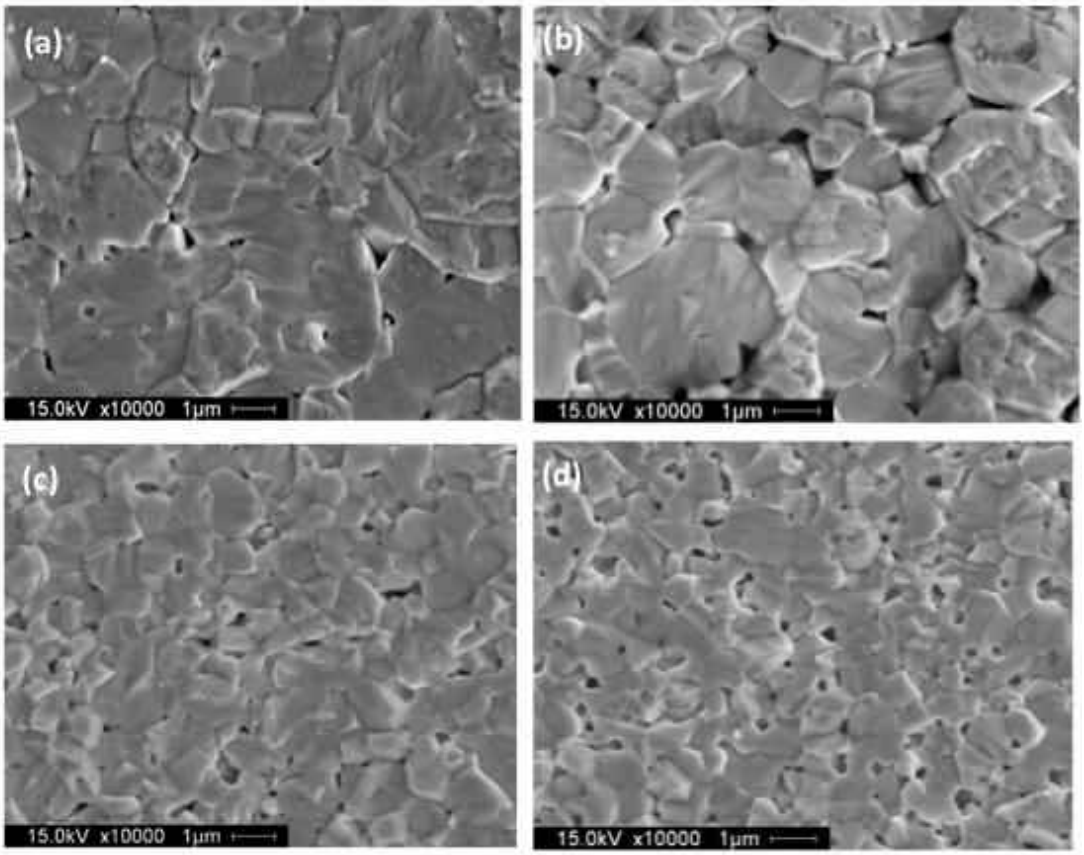

Figure 58: SEM micrographs of the cross sections of the specimens sintered at 900 °C for 2 hours, at 1000 °C for 1 hour and at 1400 °C for 2 hours. (a, b) uniaxially-pressed at 618 MPa, (c) CIP at 350 MPa, and (d) uniaxially-pressed at 386 MPa.

A slip cast was made from a 20 vol.% slip and was cold isostatic pressed at 350 MPa. The green density was 45%. Figure 59 shows the SEM micrographs of the cast cross section. Particles are closely packed. Most agglomerates are broken up and typical particle sizes are less than 400 nm.

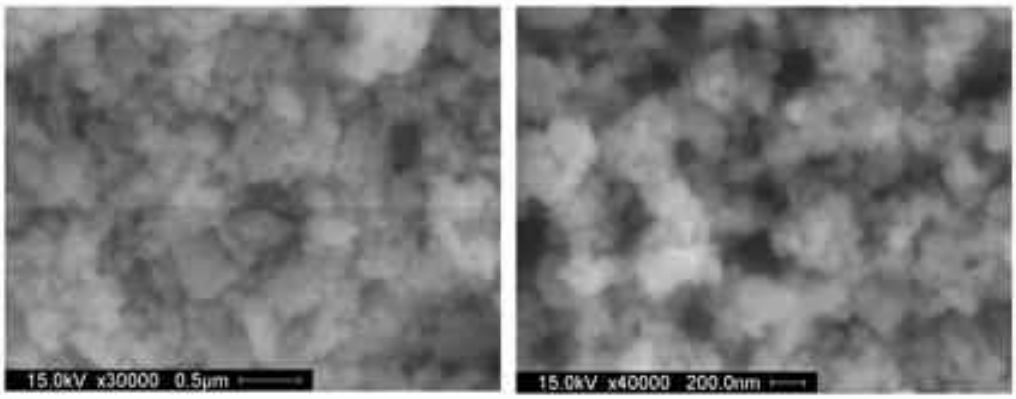

Figure 59: SEM micrographs of a cast cross-section after CIP.

Figure 60 shows the SEM micrographs of the sintered cast cross section. It exhibits a more uniform microstructure with smaller grains and pores (maximum 200 nm) than the sintered dry-pressed specimen. De-agglomeration of the as-received W powders via repeated ultrasonication, washing with water and centrifugation led to a more uniform pore structure, which yielded more uniform and smaller grain sizes after sintering. These small pores have a much better chance to be removed during a post HIP treatment. Suzuki *et* al. [58] have shown that ultrasonication improved particle dispersion in suspensions and led to a homogeneous microstructure of sintered bodies. Hausner [59] has observed higher sinter-ability and better grain uniformity for a slip cast than for dry-pressed powders together with similar mechanical properties. Similar results were observed for slip cast Mo [60].

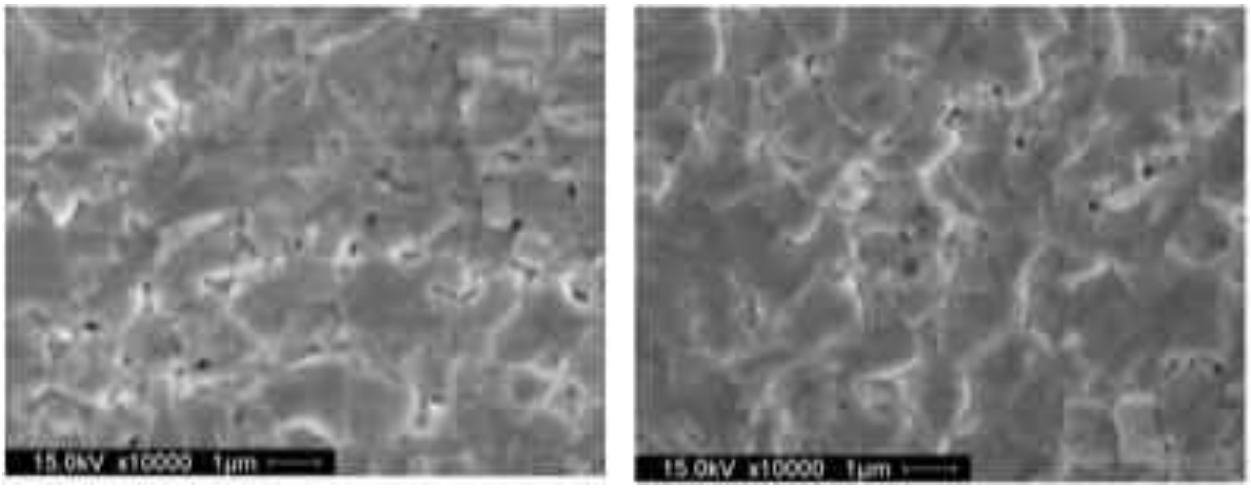

Figure 60: SEM micrographs of the cross section of sintered compacts produced by slip casting followed by CIP. Initial green density was 45 %, and the final density was 90 %.

The sintered cast has a lower final density than the sintered dry-pressed compact. One reason is that the water-washed powders contain more W oxides than the dry-pressed ones. Usually, the slip cast W would be heat treated in a hydrogen atmosphere at 1400°C for 2 hours. The heat treatment reduces W oxide formed during processing of slip to metal. Entrapped air is one reason for defects in slip casting [61]. Some air bubbles may be trapped in the W slurry before slip casting and evolve into pores after slip casting. Air bubbles can be avoided by improving the wetting characteristics of the particles by the liquid and de-airing of the slurry. Adding glycerol to the slurry can remove the trapped air bubbles from the bulk slurry. Glycerol is a well-recognized freeze-casting aid [62].

Another cast was made from a 20 vol.% slip and was cold isostatic pressed at 350 MPa. The compact was sintered at 1400ºC for 2 hours and at 1400ºC for 1 hour in vacuum and the relative sintered density was 87.57 %. The SEM micrographs of the cross section of the sintered

compact are shown in Figure 61.

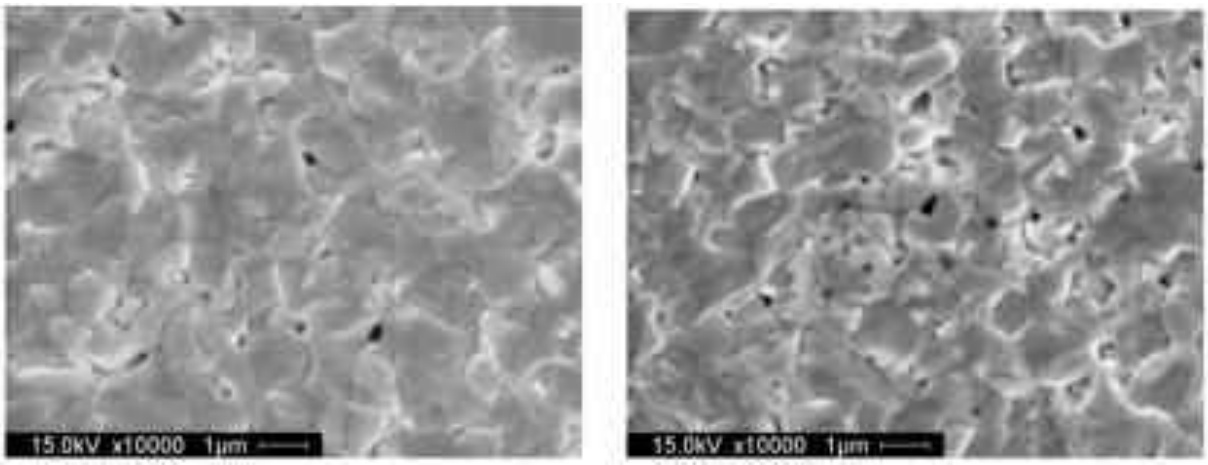

Figure 61: SEM micrographs of the cross section of a sintered W slip cast.

Other advantages of consolidating W powders by slip casting include low cost and unusually-shaped products fabricated. It is difficult to consolidate metal powders into parts with complex shapes by press compaction [63]. W and Mo parts with undercuts and curvatures can be slip cast [64]. The crystal structure of one sintered slip cast was characterized via Riga D/Max XRD shown in Figure 62. The scan rate was 1.5 degree/min. The measured XRD pattern matches well to the published PDF # 00-004-0806 for pure BCC W. The four major peaks from left to right correspond to the (110), (200), (211) and (220) planes of BCC W.

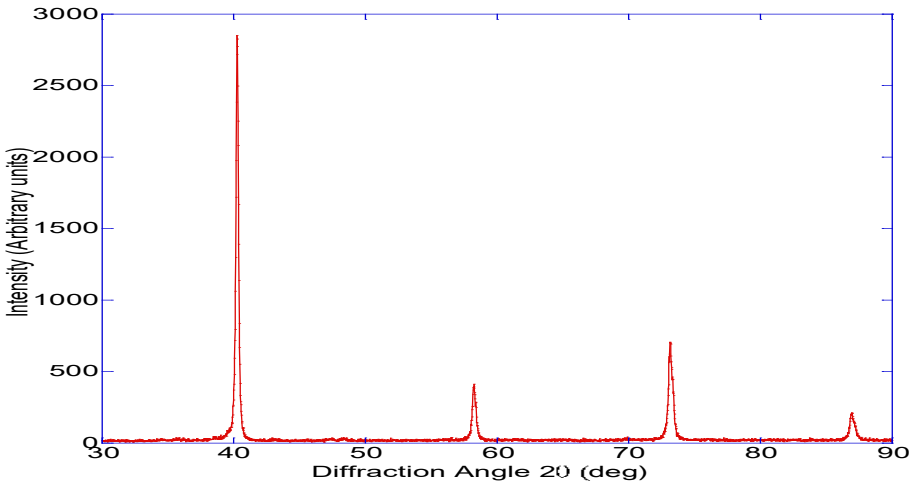

Figure 62: X-ray diffraction diagram of one sintered slip cast (Cu $K\alpha_1$ radiation λ=1.5406 Å)

5. DISCUSSION

5.1 Processing Parameters Affecting De-agglomeration

There are several processing variables controlling de-agglomeration of W nanoparticles, namely the suspension pH and the corresponding zeta potential and viscosity. The W suspension pH should be close to 5 to produce the most negative zeta potential and the lowest viscosity, which leads to the optimum de-agglomeration and castability. Ultrasonication was an effective technique for de-agglomeration of W nanoparticles. Yu Jia *et* al. [65] prepared a well-dispersed nano-ZrO^2 suspension by de-agglomeration of as-received nano-ZrO_2 powders via ultrasonication and centrifugation to remove agglomerated bigger particles. In water, the W suspension pH decreased with longer ultrasonic time and decreased with increasing ultrasonic power after the same ultrasonic time. Repeated ultrasonication, washing with water, and centrifugation gradually increased the suspension pH. During each washing cycle, some soft agglomerates were broken up into smaller particles. Increasing washing cycle decreased the average particle size and increased the suspension pH value. However, it is difficult and time consuming to increase the suspension pH value above 4 by just increasing the washing cycle, especially at high solids loadings. Addition of aqueous TMAH solutions to the W suspension quickly increases the pH value. The suspension is ultrasonicated under a high power for several

hours to de-agglomerate. The suspension pH decreases and viscosity increases with longer ultrasonication time. When the viscosity is too high, W flocs sticks to the probe tip. Another washing cycle removes most acidic W oxides and H^+, hence increases the pH.

5.2 Processing Parameters Controlling the Cast Density

A good slip casting slurry is a well-stabilized and highly concentrated particle suspension. The stability against flocculation gives a dense incompressible consolidated layer, and the high solid content reduces the amount of liquid sucked away by the mold. A well-dispersed slip containing no agglomerates and stabilized by electrostatic or steric repulsion results in a cast with a high packing density and homogenous microstructure.

There are several important processing variables controlling the W slip cast density. One of them is the ultrasonic time for dispersing W powders in water especially in the pH range between 4 and 5.3 where the viscosities are relatively low. The influence of accumulated ultrasonic time under a power higher than 10 watts on the cast density is shown in Figure 63. The density tends to increase with longer ultrasonic time, especially during the initial 5.9 hours because more and more W agglomerates are broken up and the mean diameter of agglomerates decreases after longer ultrasonic treatment. Other researchers observed decreasing mean diameter of agglomerates with longer ultrasonic treatment [66-67]. After 5.9 hours, the effect of ultrasonication is less pronounced because a limiting mean particle size is approached. With

increasing degree of ultrasonication, the suspension viscosity decreases and the dispersion of the particles in the suspension becomes better, leading to a higher green density. Similar effect of ultrasonication on colloidal dispersion of Submicron-sized Al_2O_3 and ZrO_2 powders in pH-controlled suspensions has been observed [68].

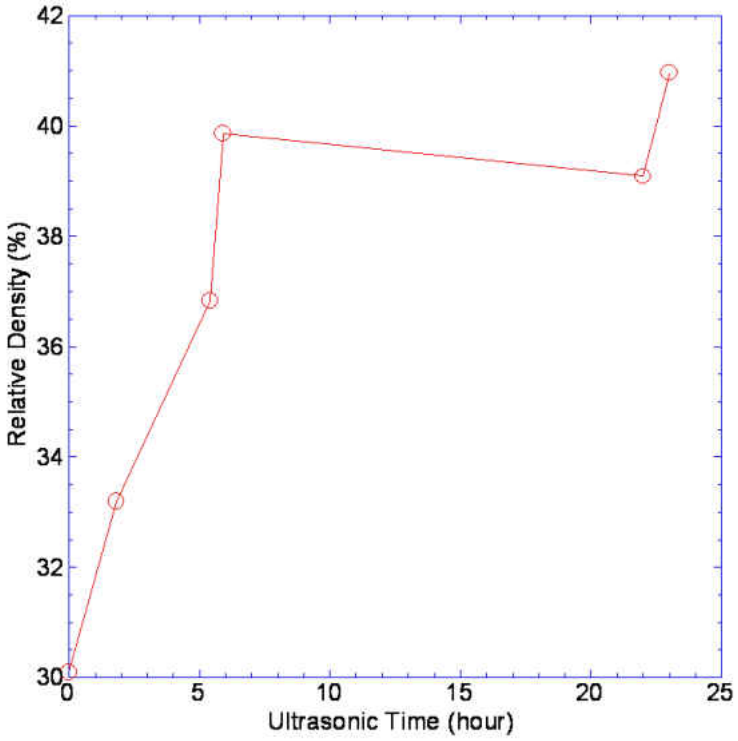

Figure 63: of ultrasonic time on the relative density of W cast.

Magnetic stirring of the W slurry before slip casting causes peptization of W particles and electrostatic charges are built up on the particles' surfaces. A repulsive force then exists between particles, thus stabilizing the slurry. This effect was manifested in the processing of 50 grams of W powders. The slurry without being stirred was slip cast into 9 pellets and the average relative density was 39.09 % as shown in Table 12. The remaining slurry was ultrasonicated for one hour and stirred for 20 minutes using a magnetic stirrer. It was slip cast

into 8 pellets and the average relative density was 40.97 %. Both slurries had a 25 vol.% solids loading.

Table 12: Relative densities of casts with and without magnetic stirring of the slurry before slip casting

Cast #	50 g W without stirring	Remaining 50 g W after stirring
1	39.52 %	40.34 %
2	38.54 %	40.48 %
3	40.98 %	41.17 %
4	40.34 %	40.13 %
5	39.32 %	41.42 %
6	37.62 %	40.89 %
7	36.9 %	41.3 %
8	39.58 %	42.05 %
9	39 %	-
Average density	39.09 %	40.97 %
Standard deviation	1.27 %	0.64 %
Ultrasonic time (hr)	22	23

It is critical to increase the solids loading in the slurry to a level as high as possible. A high solids loading reduces the shrinkage during drying and sintering, and increases the green strength of the sample. Producing a free flowing, high solids slurry requires an overall good understanding of physical and chemical properties of W particles and control of the particle interactions, particle solvent interactions such as wetting and dispersion, slurry rheology and mixing techniques. A high solids loading causes a high viscosity and a low-density slip cast. An intermediate solid loading will give the highest density. It has generally been observed that the green density of a slip cast decreases with a decreasing solids loading in the casting slurry. The main reason for the lower green density is that in a diluted suspension there is more time for the

particles to segregate. A high solids loading significantly hinders the sedimentation and reduces particle segregation. Maximizing the solids loading can diminish the segregation and smaller particles can fill the voids between the larger ones. The suspension pH is important and should be well controlled to obtain high green densities. Otherwise, an inappropriate pH will result in particle flocculation, a high viscosity and a low green density. Chaklader *et* al. [69] prepared stable slips of powder mixtures of tungsten carbide and cobalt by controlling the pH of suspending medium and slip cast dense specimens of powder mixtures, which were sintered without any defects. The slip must have a reasonably low viscosity to flow easily into the cavities of the mold. The slip viscosity increases with higher solids loading. To achieve a high green density, a high solids loading and an acceptable viscosity should be balanced.

Slurries at several solid-loadings with different pH values were cast in plaster molds. At a pH below 3, only low solids loadings such as 15 vol.% could be obtained with acceptable viscosities. Solids loadings above 35 vol.% are difficult because the suspension pH drops quickly as a result of W dissolution and van der Waals attraction dominates over weak electrostatic repulsion due to decreasing mean distance among colloids. The green densities of the slip cast specimens are listed in Table 13. There is a trend that the green density increases with increasing solids loading. The slip cast relative density (44 %) of a 30 vol.% slurry is higher than that of the dry pressed pellet (42 %) under a high pressure of 618 MPa. The green density can be further increased by CIP under a moderate pressure of 350 MPa. For example, the initial slip cast density of a 20 vol.% W slurry with a pH 3.3 is 34.5 %. After CIP, the relative green density is increased to 45 %, which is higher than that of the dry-pressed sample.

This is not surprising as weak flocs exist in the slurry. The weakly flocculated particles cannot move towards each other in the mold. However, they can be pressed under moderate pressures. It is expected that 50 % relative densities can be achieved by slip casting of W slurries of solids loadings higher than 25 vol.% followed by CIP.

Table 13: Relative green densities of slip casts as a function of processing variables

	pH 2.6, 15 vol.%	pH 3.3, 20 vol.%	pH 4.5 25 vol.%	pH 5.1 30 vol.%
Relative green density	30.6 %	34.5 %	41.2 %	43.9 %
Relative green density after CIP at 350 MPa	42 %	45 %	TBD	TBD

Power characteristic is a crucial parameter in influencing the compressibility and the cast packing density. Particle size, particle size distribution and particle morphology are the most important parameters. Tiller *et* al. [70] have studied the effects of particle size, particle shape, and the degree of flocculation of the slurry on the cast packing density. They demonstrated that colloidal effects and particle dispersion are increasingly important with decreasing particle size and irregular particles produce casts with a lower packing density than spherical ones of the same size. The sizes of the as-received W nanopowders range from 30 nm to 1 μm and irregularly-shaped agglomerates exist, which hinders the orderly packing of W particles during slip casting and lowers the green density. The slip cast density will increase if other starting powders with a more spherical morphology are selected. Barta *et* al. [52] have investigated the influence of W particle size distribution on properties of slips and cast

specimens and found blended powders consisting of 50 % coarse, 31 % medium and 19 % fine particles led to the optimum results.

Mechanical vibration at relatively low intensities during slip casting can increase the filtration rates of W slurries and green densities if other conditions are the same. External vibration results in oscillation of colloids around their rest positions and weakens point contacts in the cake, which accelerates water removal. A reduced cast formation time is crucial for increasing productivity and minimizing particle segregation and inhomogeneous microstructure. Application of vibration increases green densities of all solid loadings due to better particle packing and reduction of particle bridging during cake formation. The hydrodynamic vibration cancels out the static friction between adjacent colloids and place them in more energetically favorable positions leading to higher densities [71].

5.3 Comparison of Dispersants

Water, PEI, PAH, Oleic acid and Menhaden fish oil have been used to disperse W nanopowders. Water was most successful in de-agglomeration and increasing the cast green density. Water is cheap and environmentally friendly. The major disadvantage of dispersing W nanoparticles in water is the oxidation of W by water and resultant oxides followed by dissolution of oxides. TMAH solutions were added to the W suspension to increase the pH.

Addition of aqueous PEI solutions to W suspension increased the pH because aqueous PEI solutions have relatively high pH values. For example, the pH of 30 wt.% aqueous PEI (MW 10000) solution was 11. Ultrasonication of W powders in dilute aqueous PEI solutions for several hours did not significantly decrease the suspension pH. For example, the pH values of 4 vol.% W suspensions in 1 % PEI under an ultrasonic power of 6 watts for 5 and 10 hours were 5.94 and 5.86, respectively. PEI worked well for low solids loadings, but was less effective for high solids loadings. For example, 20 grams of W was dispersed in 2 % PEI and the slurry was slip cast into a pellet at 20 vol.% solids loading at a pH 8.76. The cast weighed 2 grams and the green density was 32.5%. Other combinations of solid loadings and PEI concentrations were tried, but the green densities did not exceed 40 %. After de-agglomeration in water via ultrasonication, the slurry was stirred using a magnetic stirrer. The slurry viscosity gradually increased with longer stirring time and resulted in low cast densities. One possible reason was that some hard agglomerates could not be broken up by ultrasonication and PEI was adsorbed onto the surfaces of these agglomerates. Another possible reason was the dissolution of surface W oxides and the resultant loss of previously adsorbed PEI into the solution, leading to the increase in viscosity. If ball milling is utilized to provide homogeneous mixing of high solids loading W powders in PEI and break up agglomerates, better results can be achieved. Ultrasonic horn will stop working for a W suspension with a high solids loading and a high viscosity while ball milling can still mix the viscous suspension. 40 vol.% WC-Co slurry has been prepared by mixing dry WC-Co powder, liquid and PEI in a mill jar [72].

Dispersion of W powders in aqueous PAH was not successful, especially when the solids loading was high. The main reason is that aqueous PAH solutions were acidic and significantly reduced the W suspension pH. When basic solutions such as NaOH were added to the suspension to increase the pH, dispersion became worse.

6. CONCLUSIONS

W nanopowders were characterized. XRD and TEM results showed the bulk of W nanopowders consisted of bcc-W. The surface consisted of WO_3 with traces of WO_2 and WC based on XPS. Irregularly-shaped agglomerates greater than 1 μm in size were observed and the sizes of de-agglomerated particles ranged from 30 to 100 nm.

W nanopowders were de-agglomerated by repeated ultrasonication in water, washing with water, centrifugation and pH adjustment, which reduced the reactivity of W to water. The degree of de-agglomeration and stability of the W suspension increased with increasing cycle of ultrasonication and washing. Increasing the pH value up to 5 led to a more negative zeta potential and a lower viscosity. The pH values of W slurries were adjusted close to 5 using TMAH water solutions to lower the viscosity and to increase the solids loading. The relative densities of slip casts increased with longer ultrasonic time and reached 42 % at a 22 vol.% solids loading after ultrasonication for 23 hours. Small W particles were separated from large ones, and slip cast at a 27.8 vol.% solids loading into pellets with relative densities up to 41.3 % and approximate particle sizes of 100 nanometers. The particle-separated small W slurry exhibited a much lower casting rate than the slurry without particle separation.

Ultrasonication of W nanopowders in 1 wt.% PEI resulted in the optimum dispersion. Ultrasonication at a low power for longer time led to better dispersion. Ultrasonication of 0.5 g of W nanopowders in 10 ml of 0.03 M and 0.04 M PAH and washing with water twice improved the dispersion. Ultrasonication of 2 grams of W nanopowders in 0.5 % oleic acid and 10 ml of ethanol under a power of 10 watts for 25 minutes resulted in optimum dispersion. Ultrasonication of 2 grams of W nanopowders in 1.75 % fish oil and 10 ml of ethanol under a power of 10 watts for 20 minutes led to optimum dispersion. The grains and pores of sintered slip cast compacts were smaller and more uniform than those of sintered dry-pressed compacts. But the sintered slip cast had a lower density than the sintered dry-pressed compact. A better comparative study can be done by using hydrogen sintering followed by HIP.

REFERENCES:

[1]Cai WD, Li Y, Dowding RJ, Mohamad FA, Lavernia EJ. A review of tungsten-based alloys as kinetic energy penetrator materials. Reviews in Particulate Materials 1995;3:71–132.

[2]Cho KC, Woodman RH, Klotz BR, Dowding RJ. Plasma pressure compaction of tungsten powders. Materials and Manufacturing Processes 2004;19(4):619–30.

[3]Cho KC, Woodman RH, Klotz BR, Dowding RJ. Plasma pressure compaction of tungsten powders. Materials and Manufacturing Processes 2004;19(4):619–30.

[4]German RM, Olevsky E. Strength predictions for bulk structures fabricated from nanoscale tungsten powders. International Journal of Refractory Metals & Hard Materials 2005;23:77–84.

[5]Mayo MJ, Hague DC, Chen DJ. Processing nanocrystalline ceramics for applications in superplasticity. Materials Science and Engineering: A 1993;166(1-2):145–59.

[6]Rahaman MN. Ceramic Processing.CRC Press, Taylor & Francis Group; 2007.

[7]Lu K, Kessler CS, Davis RM. Optimization of a nanoparticle suspension for freeze casting. Journal of the American Ceramic Society 2006;89(8):2459–65.

[8]Dorbrovol'skii AG, Dem'yanchuk VG, Tutakov OV. Production of molybdenum parts by slip casting. Soviet Powder Metallurgy and Metal Ceramics 1967;6(8):599–603.

[9]Hernández N, Sánchez-Herencia AJ, Moreno R. Forming of nickel compacts by a colloidal filtration route. Acta Materialia 2005;53:919–25.

[10]Yih YH, Wang CT. Tungsten: sources, metallurgy, properties, and applications. New York: Plenum Press; 1979.

[11]Ryu HJ, Hong SH. Fabrication and properties of mechanically alloyed oxide-dispersed tungsten heavy alloys. Materials Science and Engineering A 2003;363:179–84.

[12]German RM, Ma J. Processing model for tungsten powders and extension to nanoscale size range. Powder Metallurgy 2006;49(1):19–27.

[13]Aoki M, Ring TA, Haggerty JS. Analysis and modeling of ultrasonic dispersion technique. Advanced Ceramic Materials 1987;2(3A):209–12.

[14]Jorge E, Chartier T, Boch P. Ultrasonic Dispersion of Ceramic Powders**.** Journal of the American Ceramic Society 1990;73(8):2552–4.

[15]Sato K, Li J, Kamiya H, Ishigaki T. Ultrasonic dispersion of TiO2 nanoparticles in aqueous suspension. Journal of the American Ceramic Society 2008;91(8):2481–7.

[16]Doktycz SJ, Suslick KS. Interparticle collisions driven by ultrasound. Science 1990; 247(4946):1067–9.

[17]Magness LS,Farrand TG. Proceedings 1990 Army Science Conference 1990 Durham, NC.

[18]Dümmer T, Lasalvia JC, Ravichandran G, Meyers MA. Effect of strain rate on plastic flow and failure in polycrystalline tungsten. Acta Materialia 1998;46(17):6267–90.

[19]Lennon AM, Ramesh KT. The thermoviscoplastic response of polycrystalline tungsten in compression.Materials Science and Engineering A 2000;276(1-2):9–21.

[20]Kim DK, Lee S, Baek WH. Microstructural study of adiabatic shear bands formed by high-speed impact in a tungsten heavy alloy penetrator. Materials Science and Engineering A 1998;249(1-2):197-205.
[21]Kim DK, Lee S**,** Noh JW. Dynamic and quasi-static torsional behavior of tungsten heavy alloy specimens fabricated through sintering, heat-treatment, swaging and aging. Materials Science and Engineering A 1998;247(1-2):285–94.
[22]Bless SJ, Tarcza K, Chau R, Taleff E, Persad C. Dynamic fracture of tungsten heavy alloys. International Journal of Impact Engineering 2006;33(1-12):100–108.
[23]Bose A, German RM. Microstructural refinement of W-Ni-Fe Heavy alloys by alloying additions. Metallurgical and Materials Transactions; A; Physical Metallurgy and Materials Science 1988;19(12):3100–3.
[24]Öveçoglu ML, Özkal B, Suryanarayana C. A comparison of the sintering characteristics of ball-milled and attritor-milled W–Ni–Fe heavy alloy. Journal of Materials Research 1996;11(7):1673–82.
[25]Ryu HJ, Hong SH, Baek WH. Microstructure and mechanical properties of mechanically alloyed and solid-state sintered tungsten heavy alloys.Materials Science and Engineering A 2000;291(1-2):91–6.
[26]Lee KH, Cha SI, Ryu HJ, Hong SH. Effect of two-stage sintering process on microstructure and mechanical properties of ODS tungsten heavy alloy. Materials Science and Engineering:A 2007;458(1-2):323–9.
[27]Wei Q, Ramesh KT, Ma E, Kesckes LJ, R. Dowding RJ, Kazykhanov VU, Valiev RZ, Plastic localization in bulk tungsten with ultrafine microstructure.Applied Physics Letters 2005;86:101907.
[28]Wei Q, Jiao T, Ramesh KT, Ma E, Kecskes LK, Magness L, Dowding RJ, Kazykhanov VU, Valiev RZ. Mechanical behavior and dynamic failure of high-strength ultrafine grained tungsten under uniaxial compression. Acta Materialia 2006;54:77–87.
[29]Wei Q, Ramesh KT, Ma E, Kesckes LJ, R. Dowding RJ, Kazykhanov VU, Valiev RZ, Plastic localization in bulk tungsten with ultrafine microstructure. Applied Physics Letters 2005;86:101907.
[30]Wei Q, Jiao T, Ramesh KT, Ma E, Kecskes LK, Magness L, Dowding RJ, Kazykhanov VU, Valiev RZ. Mechanical behavior and dynamic failure of high-strength ultrafine grained tungsten under uniaxial compression. Acta Materialia 2006;54:77–87
[31]Wei Q, Zhang HT, Schuster BE, Ramesh KT, Valiev RZ, Kecskes LJ,Dowding RJ, Magness L, Cho KC. Microstructure and mechanical properties of super-strong nanocrystalline tungsten processed by high-pressure torsion. Acta Materialia 2006;54:4079–89.
[32]Wei Q, Kecskes L, Jiao T, Hartwig KT, Ramesh KT, Ma E. Adiabatic shear banding in ultrafine-grained Fe processed by severe plastic deformation. Acta Materialia 2004;52: 1859–69.
[33]Ferkel H, Hellmig RJ. Effect of nanopowder deagglomeration on the densities of nanocrystalline ceramic green bodies and their sintering behavior. NanoStructured Materials 1999;11(5):617–22.
[34]Kothari NC. Sintering kinetics in tungsten powder. Journal of the Less-common Metals 1962;140–50.
[35]Kothari NC. Effect of particle size on the sintering kinetics in tungsten powder. Powder

Metallurgy 1964;7(14):251–60.
[36]Jain M, skandan G, Martin K, Kapoor D, Cho KC, Klotz B, Dowding RJ, Agrawai D,Cheng JP.Microwave sintering: A new approach to fine-grain tungsten-II. International Journal of Powder metallurgy 2006;42(2):53–7.
[37]Laarz E,Bergström L.Dispersing WC–Co powders in aqueous media with polyethylenimine. International Journal of Refractory Metals and Hard Materials 2000;18(6)281–86.
[38]Zhang JX, Jiang DL, Tan SH, Gui LH, Ruan ML. Aqueous processing of SiC green sheets I: Dispersant. Journal of Materials Research 2002;17(8):2012–18.
[39]Tang F, Uchikoshi T, Ozawa K, Sakka Y.Effect of polyethylenimine on the dispersion and electrophoretic deposition of nano-sized titania aqueous suspensions.Journal of the European Ceramic Society 2006;26(9):1555–60.
[40]Aoki M, Ring TA, Haggerty JS. Analysis and modeling of ultrasonic dispersion technique. Adv. Ceram. Mater. 1987;2(3A):209–12.
[41]Li W, Chen P, Gu M, Jin Y. Effect of TMAH on rheological behavior of SiC aqueous suspension. Journal of the European Ceramic Society 2004;3679–84.
[42]Rahaman MN. Ceramic Processing.CRC Press, Taylor & Francis Group; 2007
[43]Lassner E. Tungsten properties, chemistry, technology of the element, alloys, and chemical compounds. New York: Kluwer Academic/Plenum Publishers; 1999.
[44]Warren A, Nylund A, Olefjord I. Oxidation of tungsten and tungsten carbide in dry and humid atmospheres. International Journal of Refractory Metals and Hard Materials 1996;14(5-6):345–53.
[45]Lassner E. Tungsten properties, chemistry, technology of the element, alloys, and chemical compounds. New York: Kluwer Academic/Plenum Publishers; 1999
[46]Anik M, Dissolution kinetics of WO3 in acidic solutions. Journal of Applied Electrochemistry 2006;36:603–8.
[47]Anik M, Osseo-Asare K. Effect of pH on the anodic behavior of tungsten. Journal of The Electrochemical Society 2002;149:B224.
[48]Parks GA. The isoelectric points of solid oxides, solid hydroxides, and aqueous hydroxo complex systems. Chemical Reviews 1965;65(2):177–98.
[49]Andersson KM, Bergström L. DLVO interactions of tungsten oxide and cobalt oxide surfaces measured with the colloidal probe technique. Journal of Colloid and Interface Science 2002;246(2):309–315.
[50]Aveston J. Hydrolysis of tungsten (VI): ultracentrifugation, acidity measurements, and Raman spectra of polytungstates. Inorganic Chemistry 1964;3(7):981–6.
[51]Li W, Chen P, Gu M, Jin Y. Effect of TMAH on rheological behavior of SiC aqueous suspension. Journal of the European Ceramic Society 2004;3679–84.
[52]Barta J, Gorni J, The slip casting of tungsten. Planseeberichte fuer Pulvermetallurgie 1965;13(2):90–99.
[53]Olhero SM, Ferreira JMF. Particle segregation phenomena occurring during the slip casting process. Ceramic International 2002;28(4):377-86.
[54]Adcock DS, McDowall IC. The mechanism of filter pressing and slip casting. Journal of the American Ceramic Society 1957;40(10):355–60.
[55]Aksay IA,Schilling CH. Forming of ceramics. Advances in Ceramics, American Ceramic Society 1984; 9: 85–93.
[56]Andersson KM, Bergstrom L. Effect of the cobalt ion and polyethyleneimine adsorption on

the surface forces between tungsten oxide and cobalt oxide in aqueous media. Journal of American Ceramic Society 2002;85(10):2404–08.
[57]Groza JR, Dowding RJ. Nanoparticulate materials densification. NanoStructured Materials 1996;7:749–68.
[58]Suzuki TS, Sakka Y, Nakano K, Hiraga K. Effect of ultrasonication on the microstructure and tensile elongation of zirconia-dispersed alumina ceramics prepared by colloidal processing. Journal of the American Ceramic Society 2001;84(9):2132–4.
[59]Hausner H. Slip casting of metal powders and metal ceramic combinations. Powder Metallurgy. New York: Interscience publishers; 1961.
[60]Pierre PD. Slip casting of metal powders: Molybdenum. Reactive Metals. New York: Interscience publishers; 1959.
[61]Pugh RJ, Bergström L. Surface and colloid chemistry in advanced ceramics processing. New York: Marcel Dekker, Inc.;1994.
[62]Lu K. Microstructural evolution of nanoparticle aqueous colloidal suspensions during freeze casting. Journal of the American Ceramic Society 2007;90(12):3753–58.
[63]Hausner HH, Poster AR. Slip casting technique widens powder metallurgy. Steel 1960; 146(7):120–3.
[64]Hausner HH, Ferriss DP. Metal powder slip castings. Materials and Methods 1956; 43(5):132–134.
[65]Jia Y, Duran C, Hotta Y, Sato K, Watari K. Macroporous ZrO2 ceramics prepared from colloidally stable nanoparticles building blocks and organic templates. Journal of Colloid and Interface Science 2005;291(1):292–5.
[66]Aoki M, Ring TA, Haggerty JS. Analysis and modeling of ultrasonic dispersion technique. Advanced Ceramic Materials 1987;2(3A):209–12.
[67]Liu Y, Yu Z, Zhou S, Wu L. De-agglomeration and dispersion of nano-TiO2 in an Agitator bead mill. Journal of Dispersion Science and Technology 2006;27:983–90.
[68]Suzuki TS, Sakka Y, Nakano K, Hiraga K. Effect of ultrasonication on colloidal dispersion of Al2O3 and ZrO2 powders in pH controlled suspension. Materials Transactions, Japan Institute of Metal 1998;39(6):689-92.
[69]Chaklader ACD, Ganshorn JA. Slip-casting tungsten carbide/cobalt powder mixtures. Powder Metallurgy 1967; 10(19):1–12.
[70]Tiller FM, Tsai CD. Theory of filtration of ceramics: I, slip casting, Journal of the American Ceramic Society 1986;69(12):882–7.
[71]Maleksaeedi S, Paydar MH, Saadat S, Ahmadi H. In situ vibration enhanced pressure slip casting of submicrometer alumina powders. Journal of the European Ceramic Society 2008;28:3059–64.
[72]Laarz E,Bergström L. Dispersing WC–Co powders in aqueous media with polyethylenimine. International Journal of Refractory Metals and Hard Materials 2000;18(6)281–86.